

8-2010

PERFLUOROALKYL PHOSPHONIC AND PHOSPHINIC ACID ELECTROLYTES FOR PROTON EXCHANGE MEMBRANE FUEL CELLS

Mahesha Herath
Clemson University, mbgsu@yahoo.com

Follow this and additional works at: https://tigerprints.clemson.edu/all_dissertations

 Part of the [Analytical Chemistry Commons](#)

Recommended Citation

Herath, Mahesha, "PERFLUOROALKYL PHOSPHONIC AND PHOSPHINIC ACID ELECTROLYTES FOR PROTON EXCHANGE MEMBRANE FUEL CELLS" (2010). *All Dissertations*. 602.
https://tigerprints.clemson.edu/all_dissertations/602

This Dissertation is brought to you for free and open access by the Dissertations at TigerPrints. It has been accepted for inclusion in All Dissertations by an authorized administrator of TigerPrints. For more information, please contact kokeefe@clemson.edu.

PERFLUOROALKYL PHOSPHONIC AND PHOSPHINIC ACID ELECTROLYTES FOR
PROTON EXCHANGE MEMBRANE FUEL CELLS

A Dissertation
Presented to
the Graduate School of
Clemson University

In Partial Fulfillment
of the Requirements for the Degree
Doctor of Philosophy
Chemistry

by
Mahesha Bharatha Herath
August 2010

Accepted by:
Stephen E. Creager, Committee Chair
Darryl D. DesMarteau
George Chumanov
Rhett Smith

ABSTRACT

Perfluorinated sulfonic acid polymers have been considered as the state-of-art membrane materials for proton exchange membrane fuel cells. A major technical issue with these polymers is that they do not function well at temperatures above 80 °C and at low humidities. Therefore, research has been focused on developing PEM materials that can operate independent of hydration requirements. The operation of fuel cells at high temperature (e.g. 120 °C) increases fuel cell system efficiency due to faster electrode kinetics and better CO tolerance. This dissertation will describe a study of proton-transport rates and mechanisms under anhydrous and aqueous conditions using a series of acid model compounds analogous to comb-branch perfluorinated ionomers functionalized with phosphonic, phosphinic, sulfonic and carboxylic acid protogenic groups. Model compounds were synthesized and characterized with respect to proton conductivity, viscosity, proton and anion (conjugate base) self-diffusion coefficients, and Hammett acidity and as a function of increasing perfluoroalkyl chain length. The highest conductivities and also the highest viscosities were typically observed for the phosphonic and phosphinic acid model compounds. The results of the study collectively supported the hypothesis that anhydrous proton transport in the phosphonic and phosphinic acid model compounds occurs primarily by a structure-diffusion, hopping-based mechanism rather than a vehicle mechanism. Further analysis of ionic conductivity and ion self-diffusion rates using the Nernst-Einstein equation reveals that the phosphonic and phosphinic acid model compounds are relatively highly dissociated even under anhydrous conditions. In contrast, sulfonic and carboxylic acid-based systems exhibit relatively low degrees of dissociation under anhydrous conditions. Investigations of these model acids under low hydration levels (3 mols of acid per a mole of acid) indicate that

the proton conductivity of these phosphonic and phosphinic acids can be improved by more than an order of magnitude relative to the water-free conditions. These findings suggest that fluoroalkyl phosphonic and phosphinic acids are good candidates for further development as anhydrous, high temperature proton conductors.

The chapter 5 describes the synthesis, characterization and ion transport of lithium polymer electrolytes that resist concentration polarization. Investigation of the purity of the ionic-melt by HPLC analysis and electrospray ionization mass spectrometry indicated that the ionic-melt is free of non-ionic impurities. The highest ionic conductivity of 7.1×10^{-6} S/cm at 30 °C was obtained for the sample consisting of a lithium salt of an arylfluorosulfonimide anion attached to a polyether oligomer with an ethyleneoxide (EO) to lithium ratio of 12. The conductivity order of various ionic melts having different polyether chain lengths suggests that at higher EO:Li ratios the conductivity of the electrolytes at room temperature is determined in part by the amount of crystallization of the polyether portion of the ionic melt.

The chapter 6 describes the synthesis and characterization of a new room-temperature ionic liquid based on a alkylimidazolium cation and new fluoro anion $[(CF_3)_2PO_2^-]$. Investigation of its thermal stability, viscosity, voltage window, and conductivity suggests that it may be a useful as an electrolyte in batteries.

DEDICATION

This dissertation is dedicated to my late father Tissa, mother Neelamani and brother Gayan who have shown continuous support and were always encouraging me with their best wishes during my vital educational years.

ACKNOWLEDGMENTS

First and foremost, I would like to express the deepest appreciation to my advisor Professor Stephen E. Creager, whose wisdom, knowledge and commitment to the highest standards inspired in me a spirit of adventure in research. Without his guidance and persistent help this dissertation would not have been possible. I also would like to thank Professor Darryl D. DesMarteau, for guiding my research for the past several years and helping me to develop my background in synthetic fluorine chemistry. I would like to thank Dr. George Chumanov, who was always willing to help and give his best suggestions. Special thank goes to Dr. Rhett Smith, who was willing to participate in my final defense committee at the last moment. Many thanks to past and present colleagues, Peter, Ashwin, Hemangi and Jung in Creager group and Drs Olt Geiculescu, Rama Rajgopal, Changqin Lu, Arno Rettenbacher, Lei-Mi Jin, and Iqbal Shariff in DesMarteau group. My research would not have been possible without their helps.

I am also grateful for the financial support from the United States Department of Energy hydrogen program (grant No. DE-FG36-06GO16031). Without their support none of this research could have been accomplished. Additional funding came from the Batteries for Advanced Transportation Technologies (BATT) Program which was supported by the U.S. Department of Energy Office of Vehicle Technologies (OVT).

TABLE OF CONTENTS

	Page
TITLE PAGE	i
ABSTRACT.....	ii
DEDICATION.....	iv
ACKNOWLEDGMENTS	v
LIST OF TABLES	x
LIST OF FIGURES	xi
LIST OF SCHEMES.....	xiv
 CHAPTER	
I. INTRODUCTION TO PROTON CONDUCTORS FOR POLYMER ELECTROLYTE MEMBRANE (PEM) FUEL CELLS	1
Proton Exchange Membrane Fuel Cells	1
Proton Transport Mechanisms	6
Proton Conductors	10
Phosphonic Acid Based Polymer Electrolyte Membranes	14
Polymer Morphology	31
Polarization Curve for Phosphonated Membranes	34
Scope of This Work	35
References.....	37

Table of Contents (Continued)

II.	PERFLUOROALKYL PHOPHONIC AND PHOSPHINIC ACIDS AS PROTON CONDUCTORS FOR ANHYDROUS PROTON EXCHANGE MEMBRANES	42
	Introduction.....	42
	Experimental.....	45
	Results and discussion	52
	Conclusion	65
	Acknowledgements.....	66
	References.....	66
	Supporting Information.....	68
III.	THE EFFECT OF INCREASING THE PERFLUOROALKYL CHAIN LENGTH ON THE PHOSPHONIC AND PHOSPHINIC ACID BASED PROTON CONDUCTORS.....	69
	Introduction.....	69
	Experimental.....	70
	Results and Discussion	73
	Conclusions.....	83
	References.....	83
	Supporting Information.....	84
IV.	PROTON CONDUCTIVITY OF PHOSPHONIC AND PHOSPHINIC ACIDS UNDER LOW HYDRATION	86
	Introduction.....	86
	Experimental.....	87
	Results and Discussion	88
	Conclusions.....	93
	References.....	94
V.	IONIC CONDUCTION IN POLYETHER-BASED LITHIUM ARYLFLUOROSULFONIMIDE IONIC MELT ELECTROLYTES	95
	Introduction.....	95
	Experimental.....	99
	Results and discussion	105
	Conclusions.....	117
	References.....	117

Table of Contents (Continued)

	Page
VI. A NEW ANION FOR ROOM-TEMPERATURE IONIC LIQUIDS	119
Introduction.....	119
Experimental	120
Results and discussion	122
Conclusions.....	129
References.....	129
Supporting Information.....	130
VII. CONCLUSIONS AND OUTLOOK.....	136
APPENDICES	
A. Conductivity Cell	141
B. NMR Spectra for the Phosphonic Acids	142
C. Ionic Melt	148

LIST OF TABLES

Table	Page
1.1 Chemical structures of polymers and their proton conductivity	16
1.2 Comparison of membrane properties for phosphonic acid based membranes by Burton and co-workers.....	20
1.3 Comparison membrane properties for phosphinic acid based membranes.....	23
1.4 Properties of polymers ^{46,55}	25
2.1 Density ρ , Molecular weight MW, Molar concentration C_0 , Viscosity η , and specific conductivity σ of the model acid compounds	53
2.2 Best fit parameters for temperature dependant conductivity and fluidity of model acids	56
2.3 PFG-NMR diffusion coefficients (m^2/s) for the model acids at 20 and 85 °C	60
2.4 Nernst-Einstein calculated conductivity σ_{cal} ($S\text{cm}^{-1}$), experimental conductivity obtained from Arrhenius plot σ_{meas} ($S\text{cm}^{-1}$), percent dissociation $\sigma_{meas}/\sigma_{cal}$ of the model acid compound	61
2.5 Hammett acidities of model acids.....	65
3.1 Density ρ , Molecular weight MW, Molar concentration C_0 , Viscosity η , and specific conductivity σ of the model acid compounds	74
3.2 PFG-NMR diffusion coefficients (m^2/s) for the model acids at 85 °C	81
3.3 Nernst-Einstein calculated conductivity σ_{cal} ($S\text{cm}^{-1}$), experimental conductivity obtained from Arrhenius plot σ_{meas} ($S\text{cm}^{-1}$), percent dissociation $\sigma_{meas}/\sigma_{cal}$ of the model acid compound	82
3.4 Best-fit parameters for temperature-dependent conductivity and fluidity of model acids	85
3.5 Hammett acidities of model acids.....	85

4.1 Diffusion coefficients of acid water mixtures.....	91
5.1 Chemical formula and EO: Li ratio of the ionic melt	106
5.2 DSC results of ionic melts 4b and 6c and pure PEG 5c.....	115
6.1 Physical parameters determined for ionic liquids.....	124
6.2 The best fit parameters for the fluidity data.....	127
6.3 The best fit parameters for conductivity data	127
6.4 The self-diffusion coefficients of cation (D^+ , cm^2s^{-1}) and anion (D^- , cm^2s^{-1}) of the ILs	133

LIST OF FIGURES

Figure	Page
1.1 proton exchange membrane operation principle (Adapted from U. S. Department of Defense Fuel Test and Evaluation Center. "Fuel Cell Basics". http://www.fctec.com/fctec_howworks.asp)	2
1.2 Transport of gases, protons and electrons in a PEM fuel cell ¹¹	5
1.3 Electrochemical reactions that takes place at the anode and cathode	6
1.4 Schematic of the vehicle type transport mechanism of the proton ¹⁵	7
1.5 Schematic of the Grotthuss type transport mechanism of the proton ¹⁵	8
1.6 Schematics of proton transfer by <i>ab-initio</i> MD simulation from ref 11. Only the protonic charge is displaced during the rapid interchange between the Eigen and Zundel forms ^{19,20} by rearrangement of only covalent and hydrogen bonds.	9
1.7 Comparative conductivity plot of selected proton conductors adapted from Kreuer 2005 for PEM fuel cells. Drawn in blue are approximate data extracted from graphs in reference ²¹	10
1.8 Temperature dependence of the DC conductivity of the ethylphosphonic acid ⁴⁸ functionalized membrane (degree of modification 12%) doped with H ₃ PO ₄ of various strengths	30
1.9 Experimental SEM (left panel) and AFM (right panel) images of the copolymer in scheme 1.13 above ⁶⁸	33
1.10 polarization data comparing the phosphonic acid-basaed ionomer of A- phosphonated poly(trifluorostyrene) (IEC = 7.7 meq/ g) , C3- phosphonated poly(trifluorostyrene) (IEC =	

5 meq/g) ⁵⁴	35
2.1 (left) The schematic of the stainless steel conductivity apparatus where (A) Vacuum / gas inlet / outlet,(B) Impedance analyzer, (C) Pressure gauge (Mcmaster), (D) Thermocouple (Omega, J-type), (E) Cell holder, (F) Liquid electrolyte (acid or/and water), (G) PEEK cell body of the conductivity cell, (H) Platinized platinum rod electrodes, (I) Pressure equalization hole (very narrow), (J) Heating tape for temperature control(Omega).	50
2.2 (top) The anhydrous conductivity data as a function of temperature (bottom) Fluidity vs temperature studies for the model compounds 1-4.....	54
2.3 The Walden plot of the model compounds	57
2.4 ³¹ P NMR spectrum of neat (CF ₃) ₂ PO ₂ H compound locked with an external lock solvent....	68
3.1 (top) anhydrous conductivity data as a function of temperature (bottom) fluidity vs temperature studies for the model compounds 1-3 compared with their short chain analogs	76
3.2 (top) conductivity data as a function of F/H ratio (bottom) fluidity vs. F/H ratio; for all the short and longer chain model compounds	77
3.3 Walden plot for the model acids	78
4.2 Addition of water to perfluoromethyl phosphonic acid.....	89
4.2 Addition of water to perfluorosulfonic acid.....	89
4.3 Addition of water to bistrifluoromethylphosphonic acid.....	92
4.4 Addition of water to perfluorobutylphosphonic acid.....	92
5.1 Two different architectures of ionic melts based on lithium salts linked to polyether	98
5.2 HPLC chromatograms for (top) starting polyethylene glycol CH ₃ O(CH ₂ CH ₂ O) _{11.8} H. (bottom) product ionic melt CH ₃ O(CH ₂ CH ₂ O) _{11.8} -C ₆ H ₄ -SO ₂ N(Li)SO ₂ CF ₃ . Absence of a	

peak near 3.5 minutes in the bottom spectrum indicates the product is free of starting material.	108
5.3 Electrospray mass ionization spectra (top) of starting polyethylene glycol $\text{CH}_3\text{O}(\text{CH}_2\text{CH}_2\text{O})_{11.8}\text{H}$. (bottom) Product ionic melt $\text{CH}_3\text{O}(\text{CH}_2\text{CH}_2\text{O})_{11.8}\text{-C}_6\text{H}_4\text{-SO}_2\text{N}(\text{Li})\text{SO}_2\text{CF}_3$. The most abundant peak, 517 Da of top spectra corresponds to the protonated structure $[\text{CH}_3\text{O}(\text{CH}_2\text{CH}_2\text{O})_{11}\text{H-H}]^+$. The most abundant peak, 804 Da of bottom spectra corresponds to the protonated structure $[\text{CH}_3\text{O}(\text{CH}_2\text{CH}_2\text{O})_{11}\text{C}_6\text{H}_4\text{SO}_2\text{NHSO}_2\text{CF}_3\text{-H}]^+$	110
5.4 Temperature dependence of the conductivity of polyether-linker-salt ionic melts, compounds 4a -4c.....	113
5.5 Temperature dependence of conductivity of salt-linker-polyether-linker-salt ionic melts, compounds 6a -6c.	114
5.6 DSC traces obtained for ionic melts 4b and 6c and pure PEG 5c.....	115
6.1 TGA results for $[\text{BMIM}][(\text{CF}_3)_2\text{PO}_2]$ and $[\text{BMIM}][\text{TFSI}]$	124
6.2 Fluidity data for $[\text{BMIM}][(\text{CF}_3)_2\text{PO}_2]$ in comparison with $[\text{BMIM}][\text{TFSI}]$	126
6.3 Ionic conductivity of data for $[\text{BMIM}][(\text{CF}_3)_2\text{SO}_2\text{N}]$ in comparison $[\text{BMIM}][(\text{CF}_3)_2\text{PO}_2]$ conductivity values.	127
6.4 Cyclic voltammetry of neat $[\text{BMIM}][(\text{CF}_3)_2\text{PO}_2]$ and neat $[\text{BMIM}][\text{TFSI}]$ at 23 °C , on a platinum electrode, with a platinum counter electrode and Ag/Ag+ pseudo reference electrode with a sweep rate of 100mV/s.	128
6.5 FT-IR spectrum of the $[\text{BMIM}][(\text{CF}_3)_2\text{PO}_2]$ ionic liquid	130
6.6 FT-IR spectrum of the $[\text{BMIM}][\text{TFSI}]$	131

6.7	FT-IR spectrum of the [BMIM][(CF ₃) ₂ PO ₂] ionic liquid obtained under vacuum conditions. Note the absence of the –OH stretch that appears at 3200-3500 cm ⁻¹ that appeared in Figure 6.5.....	131
6.8	DSC spectrum of the [BMIM][(CF ₃) ₂ PO ₂] ionic liquid	132
6.9	EDX spectrum of the the [BMIM][(CF ₃) ₂ PO ₂] ionic liquid. The two K _α lines centered at 1.5 kv shows the where a peak for Br is expected	132
6.10	FT-IR spectra of [BMIM]Br	134
6.11	FT-IR spectra of (CF ₃) ₂ PO ₂ K	134

LIST OF SCHEMES

Scheme	Page
1.1 (a) Chemical structure of a perfluorinated sulfonic acid membrane, where x is between 6 and 13 and y is 1 for Nafion [®] ⁸ (b) Chemical structure of perfluorinated sulfonimide membrane. ⁹	3
1.2 Molecular structure of the Nafion (left) by dupont inc. and perfluorophosphonic acid polymer (right) prepared by Burton and co-workers.	19
1.3 Monomers that were used in the co-polymerization with TFE in the preparation of perfluorophosphonic acid polymers by Burton and co-workers.....	20
1.4 Perfluoro phosphinic acid polymers synthesized by DesMartau and co-workers according to ref. [41]	22
1.5 Synthesis of phosphonic acid group containing polymer by polycondensation ⁴⁴	24
1.6 Synthesis of fluorinated poly (aryl ether) with a phosphonic group ^{45,46}	26
1.7 The chemical structures of high performance fibers ^{47,58}	27
1.8 Catalytic phosphorylation of brominated polysulfone high performance polymer tris(trimethylsilyl) phosphite (TMSP) by the nickel-catalyzed Arbuzov reaction and subsequent methanolysis ⁴⁷	28
1.9 Phosphonic acid functionalized PBI synthesis	29
1.10 PVPA/PBI networks via polymerization/crosslinking technique ⁴⁸	31
1.11 Block copolymer of poly(vinylbenzylphosphonic acid) and poly(ether-ether-ketone) ⁶⁸	33
2.1 Chemical structure of model acids. 1-trifluoromethyl-phosphonic acid, 2-bistrifluoromethyl-phosphinic acid, 3-trifluoromethyl-sulfonic acid, 4-trifluoroacetic acid	45

2.2 Synthesis of trifluoromethylphosphonic acid	46
2.3 Synthesis of bis(trifluoromethyl)phosphonic acid	48
3.1 The chemical structures of model acids. 1-perfluorobutyl sulphonic acid 2-perfluorobutyl phosphonic acid, 3-bisperfluorobutyl phosphinic acid	70
3.2 Synthesis of n-perfluorobutyl phosphonic acid	71
3.3 Synthesis of bisperfluorobutyl phosphinic acid.....	72
5.1 Synthesis of sulfonimide salts.....	100
5.2 Synthesis of ionic melts	102
6.1 chemical structures of (top) [BMIM] [(CF ₃) ₂ PO ₂] and (bottom) [BMIM][TFSI]	120

CHAPTER ONE

PROTON CONDUCTORS FOR FUEL CELLS

Proton Exchange Membrane Fuel Cells (PEMFCs)

Fuel cells have emerged in the last decade as one of the most promising new technologies for meeting energy needs in the twenty-first century. A fuel cell is an electrochemical device that converts chemical energy into electrical energy without combustion. Since the invention of fuel cell by Sir William Grove by 1839, a variety of fuel cells have been developed. The most common classification of fuel cells is on the basis of the type of electrolyte used in the cells. There are presently six major types of fuel cell technologies currently under development and commercialization. They are (1) proton exchange membrane fuel cell (PEMFC), (2) alkaline fuel cell (AFC), (3) phosphoric acid fuel cell (PAFC), (4) molten carbonate fuel cell (MCFC), (5) solid oxide fuel cell (SOFC) and (6) direct methanol fuel cell (DMFC).

For vehicles, proton exchange membrane fuel cells are the most practical design. Figure 1.1 is a cross-sectional view of the basic design of a PEMFC. It consists of proton exchange membrane which is a solid polymer electrolyte sandwiched between two electrode layers (anode and cathode).

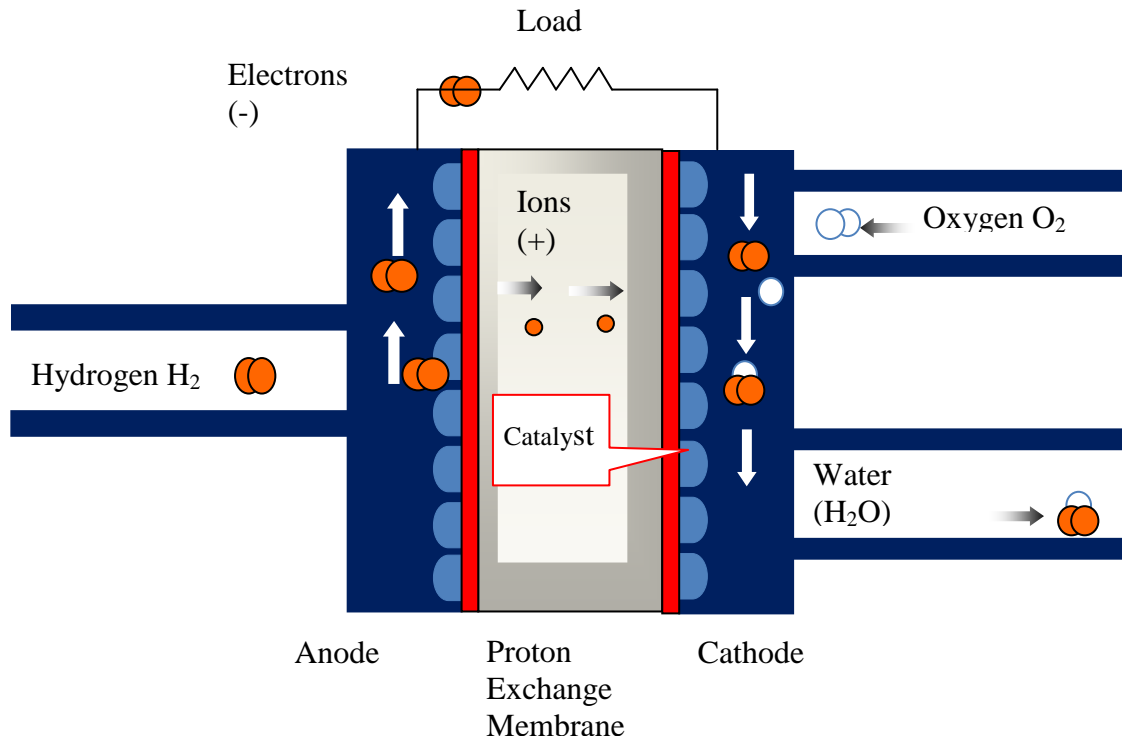
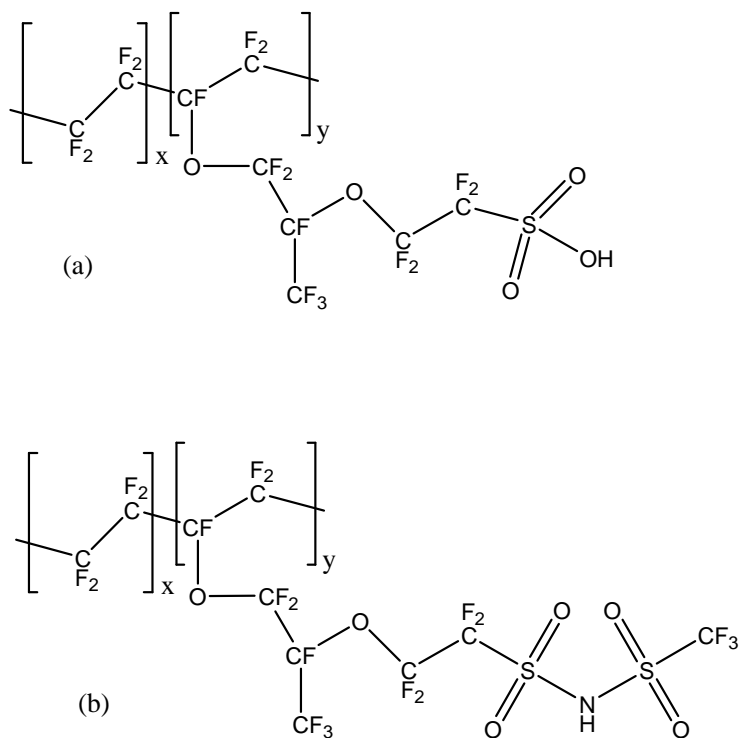


Figure 1.1 Proton exchange membrane Fuel cell operation principle (Adapted from U. S. Department of Defense Fuel Test and Evaluation Center. "Fuel Cell Basics". http://www.fctec.com/fctec_howworks.asp)

Proton Exchange Membrane: PEM fuel cells use a solid polymer membrane as the electrolyte. Ideally this proton exchange membrane should be an ion conductor, an electronic insulator, impermeable gas barrier and possess good mechanical strength. During the last two decades, the standard materials used for PEM have been perfluorinated copolymers containing

sulfonic acid groups.¹⁻⁷ The most well-known is the Nafion[®] family manufactured by E. I. du pont de Nemours and Company. Its chemical formula is given in Scheme 1.1.



Scheme 1.1 (a) Chemical structure of a perfluorinated sulfonic acid membrane, where x is between 6 and 13 and y is 1 for Nafion[®] (b) Chemical structure of perfluorinated sulfonimide membrane.⁹

Sulfonic acid based Nafion[®] has a proton conductivity of around 0.1 Scm^{-1} . The water uptake of Nafion at 100% relative humidity is about 30% by weight. The internal pore sizes of Nafion is about 2 nm.

Scheme 1.1 (b) shows a sulfonimide ionomer reported by DesMarteau and coworkers⁹ that has structural similarity to the Nafion. This sulfonimide ionomer exhibited comparable proton conductivity as that of Nafion and was found to depend on humidity as the Nafion. The sulfonimide membrane showed a higher water uptake compared to Nafion suggesting that it may possess high degree of porous channels. Experimental studies on the acidity of sulfonimide group in the gas phase suggest that sulfonimide group is more acidic than sulfonic acid. Therefore the high degree of porous channels in sulfonimide ionomer could be a result of its higher acidity. It was also found that compared to Nafion the sulfonimide membranes exhibit a higher thermal stability and have a higher capacity to promote the conversion of H₂ and O₂ gases to ions and electrons when used in the catalyst layers of MEA.

Anode and Cathode : A PEMFC electrode is a composite porous structure consisting of carbon, metal catalyst and proton-conducting polymer (e.g., Nafion). So far the best catalyst used in the electrodes is platinum and/or a platinum alloy such PtRu, PtRh, or PtNi . Typically an electrode consist of 0.1 to 1 mg/cm² catalyst loading impregnated on Vulcan XC-72-carbon support placed on top of hydrophobic carbon paper as a backing layer.¹⁰ The catalyst particles are highly interconnected to the proton exchange membrane by strings of polymer electrolyte binder ionomers. The catalyst surface facilitate the formation ions and electrons from the reactant gases. This 3-phase interphase is shown Figure 1.2. Therefore for the optimal performance of the PEM fuel cell utilization of all the catalyst particles to form a 3-phase interphase is important. Typically perfluorinated sulfonic acid ionomers such as Nafion are used as these binders. Gas diffusion layers allow direct and uniform access of the fuel and oxidant to the porous electrodes.

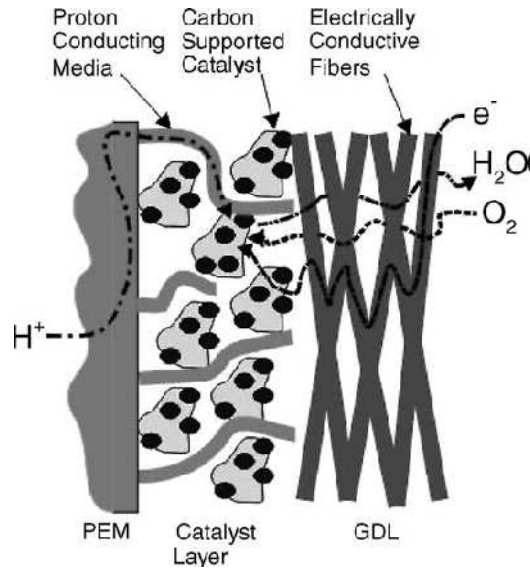


Figure 1.2 Transport of gases, protons and electrons in a PEM fuel cell¹¹

The fuel for the PEMFC is hydrogen and the charge carrier is hydrogen ion. As hydrogen flows into the fuel cell anode, platinum catalyst particles of the anode facilitate separation of the hydrogen gas into protons and electrons. The proton exchange membrane in the center allows only the protons to pass through the membrane towards the cathode. Since the electrons cannot pass through this membrane, they flow as an electric current through the external circuit, which provides electric power to the vehicle. As oxygen flows into the cathode region, platinum particles at the cathode cause the oxygen, protons, and electrons to combine, producing water and heat. Figure 1.2 shows the electrochemical reactions that takes place at the anode and cathode catalyst layer, respectively.

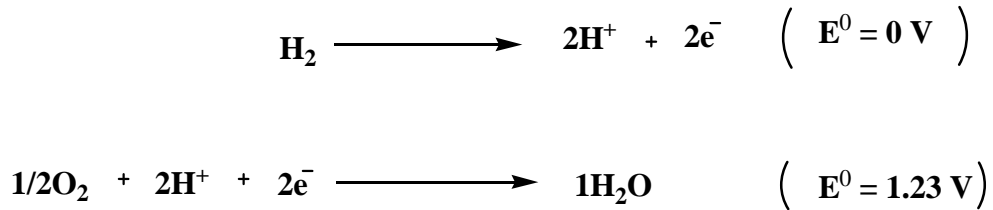


Figure 1.3 Electrochemical reactions that takes place at the anode and cathode

At present the operation of PEMFC is limited to 80 °C. The operation of fuel cells at high temperature (for ex. 120 °C) increases fuel cell systems efficiency due to faster electrode kinetics and better CO tolerance. The commonly used commercially available perfluorinated sulfonic acid based proton exchange membranes, however do not function well at temperatures above 80 °C. This observation has been attributed to the change in proton transport mechanism occurring at low hydration levels in these polymers.

Proton Transport Mechanisms

Proton transport in aqueous solutions is believed to occur by two competing transport mechanisms.^{12,13} These two mechanisms are known as vehicle mechanism and Grotthuss mechanism.

Vehicle mechanism : This mechanism relies on a physical transport of a vehicle to move the proton (see Figure 1.3). For example water can carry the proton as H_3O^+ or as a proton aggregate such as H_5O_2^+ or H_9O_4^+ and similarly a vehicle such as NH_3 can carry the proton as NH_4^+ ion through the aqueous environment, in a process similar to normal molecular diffusion. The cooperative counter diffusion of the unprotonated vehicles allows the net transport of

protons. Hence, the self diffusion coefficient of the unprotonated vehicle and protons are similar.

13,14

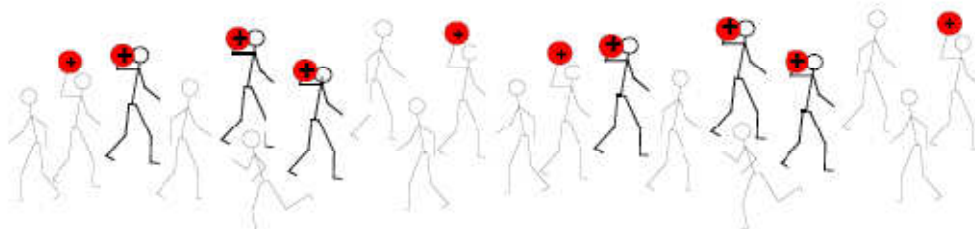


Figure 1.4 Schematic of the vehicle type transport mechanism of the proton ¹⁵

Grotthuss mechanism: First proposed by Grotthuss, ¹⁶ also described as structure diffusion, transport of the proton occurs by handing it off from one hydrogen bonding site to the another by inter-converting weak hydrogen bonds into strong covalent bonds and vice versa (see Figure 1.4). When Grotthuss mechanism occurs, the proton is transported faster than it could be by molecular diffusion of a proton carrying vehicle molecule. This is because the net proton movement is uncoupled from self-diffusion of its mass. ¹⁰ Therefore the measurement of self diffusion rates of protons can be used as a criterion to conclusively show structural diffusion.

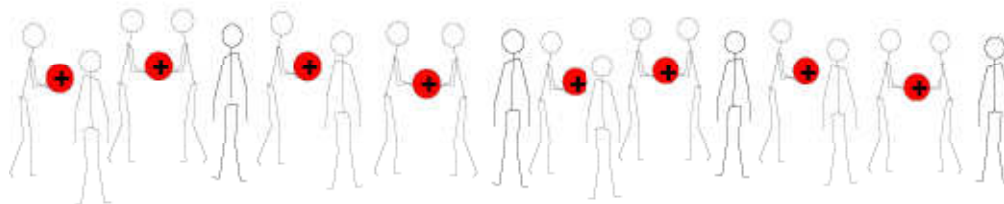
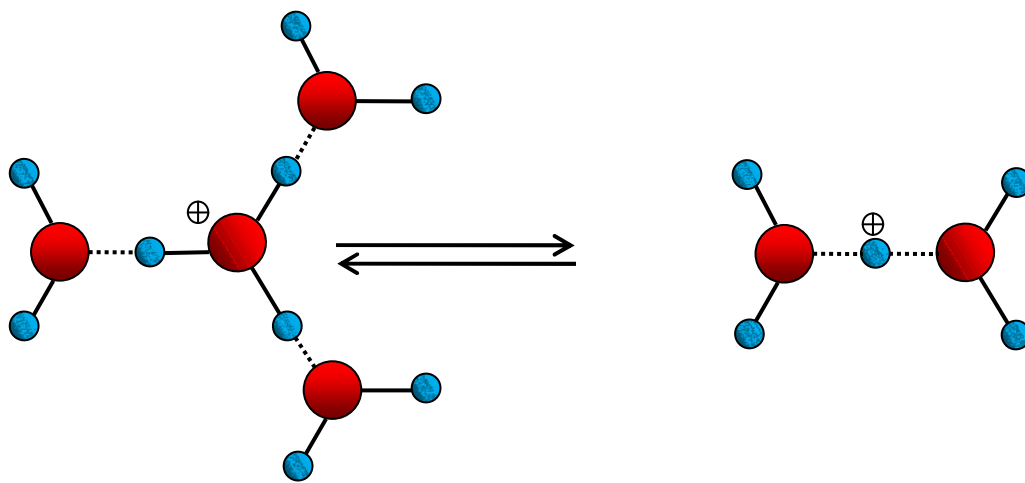


Figure 1.5 Schematic of the Grotthuss type transport mechanism of the proton ¹⁵

The quantitative work of Agmon,¹⁶ Kreuer¹² and the recent *ab initio* molecular dynamics simulations of the Tuckerman¹⁷ have provided a clear understanding of this mechanism in bulk water. *Ab initio* molecular dynamic calculations ^{13,18} of an excess proton in water show that when the proton gets solvated in water it can form one of the two limiting aggregated proton structures: a Zundel (H_5O_2^+) or Eigen (H_9O_4^+) ion. These two structures have a lower energy state than a hydronium ion (H_3O^+). When the proton is transported through the medium, the proton diffuses by converting itself from one limiting structure to the other by inter-converting weak hydrogen bonds to covalent bonds and vice versa (see Figure 1.5).



“Eigen” - ion

“Zundel”- ion

Figure 1.6 Schematics of proton transfer by *ab-initio* MD simulation from ref 11. Only the protonic charge is displaced during the rapid interchange between the Eigen and Zundel forms^{19,20} by rearrangement of only covalent and hydrogen bonds.

Proton Conductors

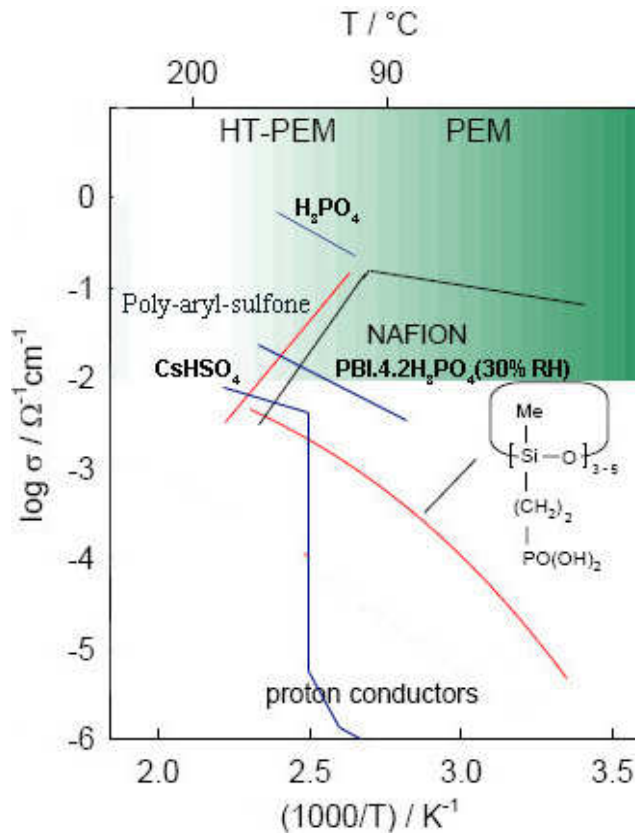


Figure 1.7 Comparative conductivity plot of selected proton conductors adapted from Kreuer 2005 for PEM fuel cells. Drawn in blue are approximate data extracted from graphs in reference ²¹.

Based on the above described proton transport mechanisms the proton conductors suitable for PEM fuel cells can be divided into two major categories as follows.

Water-containing systems: (optimum temperature $< 100\text{ }^\circ\text{C}$)

- 1) Hydrated acidic polymers based on sulfonic acid group (ex: Nafion, S-PBI, S-PEEK)
- 2) Hydrated acidic polymers based on sulfonamide group
- 3) Heteropolyacid hydrates (ex: $\text{H}_4\text{SiW}_{12}\text{O}_{40} \cdot 28\text{H}_2\text{O}$)
- 4) Xerogels or hydrated particles (ex: $\text{SnO}_2 \cdot n\text{H}_2\text{O}$)

Water-free systems : (optimum operational temperature 100 – 200 °C)

- 1) Oxo acids (ex: H_3PO_4)
- 2) Salts of oxo acids (ex : CsHSO_4)
- 3) PBI- H_3PO_4 adducts
- 4) Heterocycle-based systems (imidazole and imidazole-based systems)

A more comprehensive review on water-based and water-free proton conductors can be found in review articles by Norby²², Kreuer^{12,21}, and Phair²³. The most commonly used sample system for each category is discussed below.

Hydrated acidic polymers: Water-containing systems can be discussed in terms of hydrated acidic polymers based on sulfonic acid group. These types of polymers have been the industry standard for fuel cell materials for decades. To keep a high proton conductivity above 100 °C, the water-based systems need to be hydrated. This can be done only when the systems are pressurized above ambient pressure to ensure the availability of liquid water. This complicates the fuel cell structure and produces the risk of explosion. As shown in Figure 1.6, above 100 °C the conductivity of Nafion and Nafion-like polymers (ex. Poly-aryl-sulfone) starts to decrease. This observation has been described as due to the dominant proton transport mechanism at low hydration levels. Nafion-like water-based systems are thought to transport the protons through two main mechanisms. These are 1. Vehicle mechanism and 2. Grotthuss mechanism/Proton hopping as described earlier. At high water content in Nafion like membranes, the most prevalent mechanism is Grotthuss mechanism. However, at low water content vehicle mechanism governs the proton conductivity.

For elevated operation (above 100 °C), a polymer membrane that does not depend on the presence of water for their performance is thought to be ideal. Such membranes are thought to

achieve a high proton conductivity by the transport of the proton by the Grotthuss mechanism. Examples of commonly studied water-free systems that display this mechanism to transport the protons are, H_3PO_4 and heterocycles like imidazole, benzimidazoles.

Phosphoric acid: Concentrated phosphoric acid has remarkably high proton conductivity despite its high viscosity. For example molten phosphoric acid shows a conductivity of 0.1 S cm^{-1} at 298 K at a viscosity of 100 cp in contrast to water which has a viscosity of 1.00 cps at 293 K. The conductivity of 99% H_2SO_4 ²⁴ at 294.6 K is 0.0305 S cm^{-1} . The experimentally observed very high conductivity for the molten phosphoric acid^{25,26} could not be explained by way of the regular hydrodynamic movement of ions through a viscous medium as described by the Stokes–Einstein equation (1.1).^{27,28} (and Nernst-Einstein relation).

$$D = \frac{k_B T}{\xi} \quad \text{Equation 1.1}$$

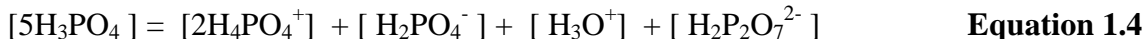
In equation 1.1, ξ is the friction coefficient and D is the diffusion coefficient. k_B is the Boltzmann constant and T is temperature. For the simple case of a spherical particle with an effective hydrodynamic radius r in a solution of viscosity η , the friction coefficient is given by Equation 1.2.

$$\xi = 4 \pi \eta r \quad \text{Equation 1.2}$$

Just as the Stokes-Einstein equation gives the relation between the transport of viscous flow (η) and transport of matter (D), the Nernst-Einstein relation (Equation 1.3) gives the connection between the diffusion (D) and conductivity (σ).

$$\sigma = \frac{q^2 \eta D}{k_B T} \quad \text{Equation 1.3}$$

In this equation, σ is the conductivity, q is charge. It was also found that phosphoric acid can self dissociate to generate charge carriers as follows.



In this equation, $[\text{H}_3\text{PO}_4] = 16.8 \text{ M}$, $[\text{H}_4\text{PO}_4^+] = 0.89 \text{ M}$, $[\text{H}_2\text{PO}_4^-] = 0.43 \text{ M}$, and $[\text{H}_3\text{O}^+] = [\text{H}_2\text{P}_2\text{O}_7^{2-}] = 0.46 \text{ M}$ at 311 K ²⁹

Given its high conductivity despite its high viscosity, it was inferred that molten phosphoric acid transport the proton through structure diffusion. ²⁹

Another experimental observation that supports this hypothesis is the temperature dependency of the Walden product $(\sigma\eta)$ ^{30,31} of the phosphoric acid. The Walden rule states that for a solution that shows Stokesian migration the product of the viscosity and conductivity of a solution $(\sigma\eta)$ ³² is a constant and independent of the temperature. The temperature dependence of the Walden product for phosphoric acid is a deviation from this rule and therefore led the authors in those studies to conclude that this was due to structure diffusion/proton hopping mechanism. Comparison of the self-diffusion data for the proton and for the anion of the phosphoric acid by the Pulsed Field Gradient Nuclear Magnetic Resonance (PFG NMR) experiments ³³, is also another experimental observation that confirms the structure diffusion/proton hopping occurs in phosphoric acid. It can be visualized that similar to the Zundel and Eigen ions does with water molecules the self dissociated charge carriers setup a hydrogen bonded network with the neutral phosphoric acid molecules and then transport the proton through this network by intermolecular H-bond breaking and forming mechanism.

Heterocycles: It has been shown that similar to phosphoric acid, different heterocycles such as imidazole³⁴⁻⁴⁰ and benzimidazoles also have the ability to transport the proton by structure diffusion at low hydration levels at temperatures above 100 °C. Unlike phosphoric acid these materials have the capability to be incorporated into the polymer to make fuel cell proton exchange membrane materials.

Phosphonic Acid Based Polymer Electrolyte Membranes

As it has been demonstrated in phosphoric acid and heterocycles, which are conductive even when completely dry due to self-ionization and proton hopping, it was hoped that replacement of the sulfonic acid group in Nafion and Nafion-like hydrated acidic polymers with a phosphonic or imidazole group would provide better conductivity under low RH conditions. This section will review the progress in synthetic approaches of obtaining phosphonic acid based membranes and discussion of the proton-conducting properties in comparison with sulfonic acid functionalized polymer such as Nafion.

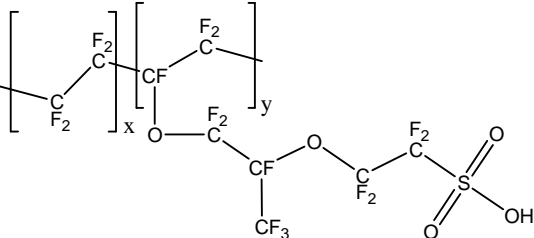
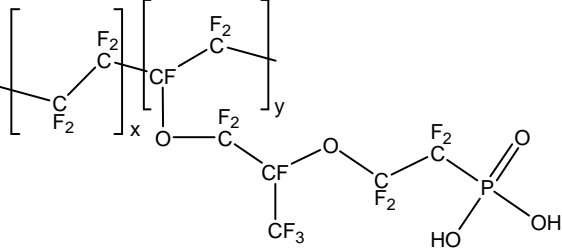
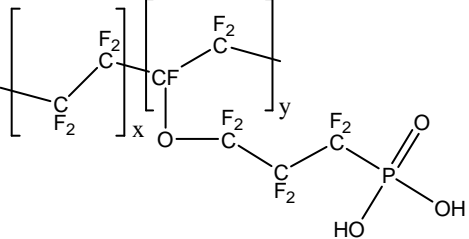
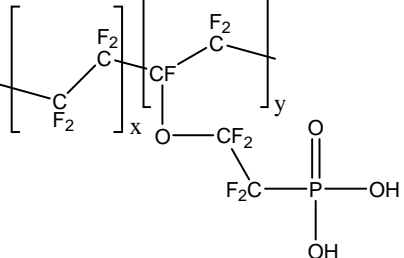
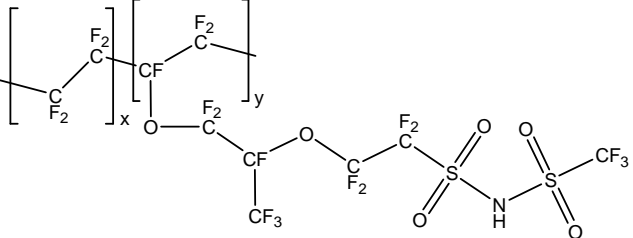
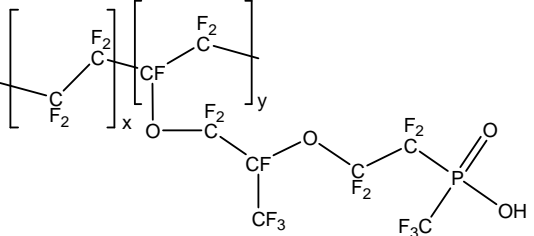
Nafion membranes are considered the benchmark of the polymer electrolyte membranes. The suitability of a membrane for PEM application is considered by comparing its 1) proton conductivity 2) ion exchange capacity (IEC) value 3) water content 4) thermal and chemical stability against the values reported for Nafion membrane. The ion exchange capacity (IEC) is defined as the amount of charged species present per gram of dry polymer. The ion exchange capacity of a proton exchange membranes are frequently expressed by equivalent weight. The equivalent weight (EW) is the gram weight of acid-form-membrane needed to neutralize 1 mol of sodium hydroxide. In other words this is 1000 times the reciprocal of the ion exchange capacity in milligram equivalents per gram dry membrane. The proton conductivity of Nafion or

Nafion like polymer membranes (i.e ionomers based on sulfonic acid functionality) are influenced by the amount of water content absorbed. The water content is determined from both water uptake amount and by the hydration number. The hydration number is defined as the number of water molecules per acid unit. The hydration number (λ) is calculated from water uptake and ion exchange capacity of the membrane.

$$\text{Water Uptake (\%)} = [(W_{\text{wet}} - W_{\text{dry}}) / W_{\text{dry}}] \times 100 \quad \text{Equation 1.5}$$

$$\text{Hydration number } \lambda = 1000 \times [(W_{\text{wet}} - W_{\text{dry}}) / W_{\text{dry}}] / (18 \times IEC) \quad \text{Equation 1.6}$$

Table 1.1 Chemical structures of polymers and their proton conductivity

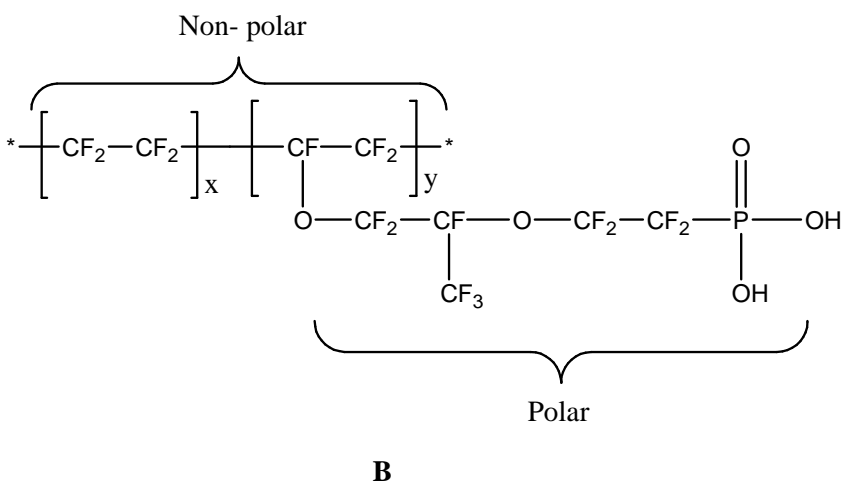
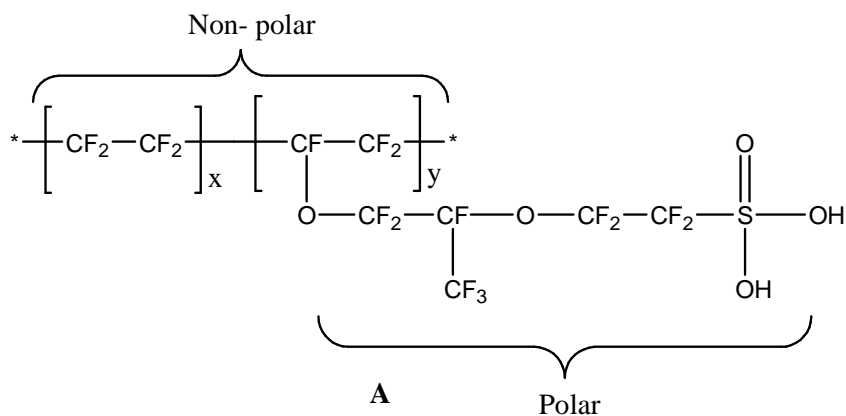
Polymer	Chemical structure	Conductivity (Scm ⁻¹)(°C) (comment)	References
Nafion		0.1 (80)(fully hydrated)	8
Nafion analog of Phosphonic acid		0.006 (80) (fully hydrated)	41
		0.076 (80) (fully hydrated)	41
		0.069 (80) (fully hydrated)	41
Nafion analog of Sulfonimide		0.1(80) (fully hydrated)	9,42
Nafion analog of phosphinic acid		0.1 (80) (fully hydrated)	43

		0.02 (80) (fully hydrated)	43
Poly(aryl-ether)-sulfone		2.9×10^{-5} (80)(fully hydrated)	44
		6.0×10^{-3} (80)(95% RH)	45,46
Poly(aryl-ether)-sulfone		N/A	47
PBI-Phosphonic acid + H ₃ PO ₄		5×10^{-3} (RT)	48

Fluorinated membranes: For decades most of the polymers reported as suitable for use in the PEMFCs were appear to be some structural variations of Nafion. All these different types of

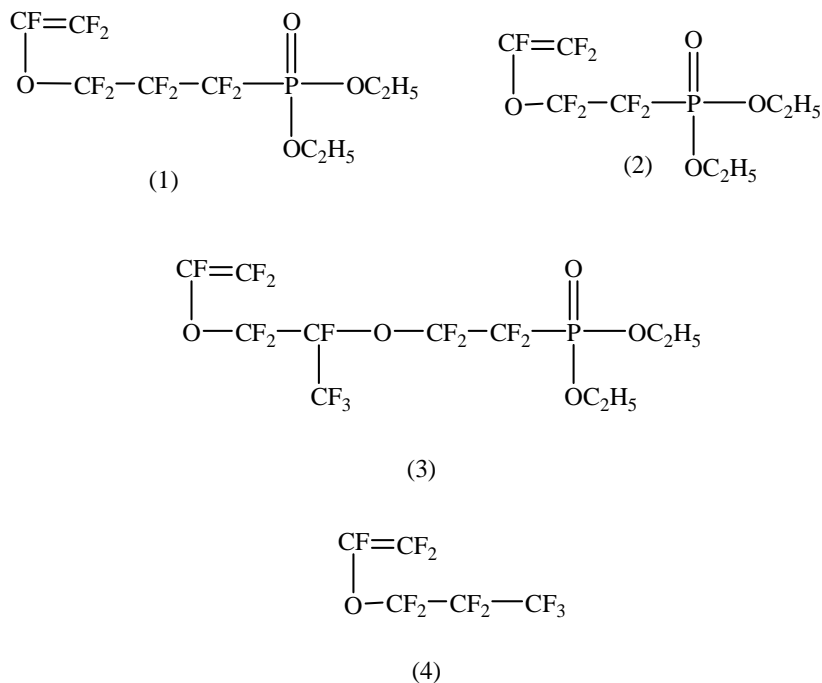
polymers were functionalized with sulfonic acid group as the protogenic group. This was primarily because sulfonic acid group is very acidic compared to other possible protogenic groups such as phosphonic, carboxylic imidazole etc. and also because of the numerous easy ways available for introducing a sulfonic acid group to a polymer compared other protogenic groups.⁴⁹⁻⁵²

Burton and co-workers prepared the first perfluorinated phosphonated polymer⁴¹ that has a structural similarity to Nafion. Scheme 1.2 below shows that Nafion is a perfluorinated copolymer consisting of a nonpolar tetrafluoroethylene backbone and a polar perfluorosulfonic vinyl ether pendant groups.



Scheme 1.2 Molecular structure of the Nafion (left) by dupont inc. and perfluorophosphonic acid polymer (right) prepared by Burton and co-workers.

Co-polymers of TFE (tetrafluoroethylene) with the functional monomers shown in Scheme 1.3 were co-polymerized via redox initiated emulsion polymerization. The hydrolysis of the esters has been found to be difficult. The polymers have been refluxed more than 10 days in HCl/glacial acetic acid mixtures. The membranes of the polymers have been prepared by compression molding.



Scheme 1.3 monomers that were used in the co-polymerization with TFE in the preparation of perfluorophosphonic acid polymers by Burton and co-workers

Table 1.2 Comparison of membrane properties for phosphonic acid based membranes by Burton and co-workers

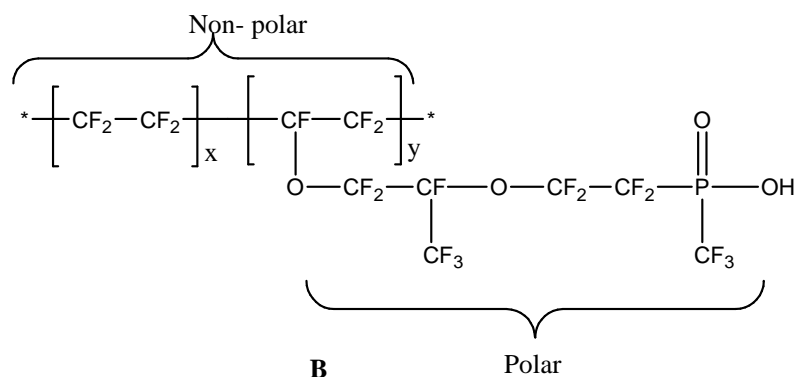
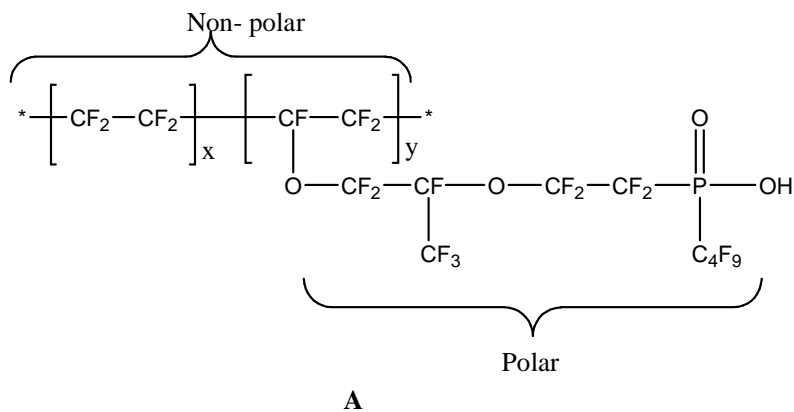
Monomer	IEC of acid film (meq g ⁻¹)	Water absorption (%) ^a	Proton conductivity (Scm ⁻¹) ^b
1, TFE	2.8	22	0.076
2, TFE	2.7	21	0.069
3, TFE	3	54	0.006
Nafion	-	30	0.07-0.08

^a Measured after boiling in deionized water for 4h
^b Measured at 80 °C under saturated water vapor

The highest IEC capacity was shown by the copolymer made with monomer 3 and TFE polymerization. This polymer has a chemical structure analogous to the structure of Nafion. This copolymer was expected to have the highest proton conductivity because of the higher IEC value. The higher the IEC value, higher the density of acid groups present in the polymer.

However, its much lower proton conductivity observed was thought to be due to poor micro phase separation of hydrophilic and hydrophobic phases, during the compression molding of the polymer. The micro-phase separation of phosphonic acid membranes is further discussed in a separate section below.

DesMarteau and coworkers⁴³ have synthesized perfluorinated polymer membranes functionalized with a phosphinic acid group (see scheme 1.4). The phosphinic acid based ionomers were synthesized by copolymerization of the sodium salt of the trifluoro vinyl ether phosphinic acid monomers with tetrafluoroethylene using emulsion polymerization technique. Then acidification of the sodium salt form of the ionomers gave the desired polymers in the respective phosphinic acid form. The chemical structures of the ionomers are shown in Scheme 1.4 below.



Scheme 1.4 Perfluoro phosphinic acid polymers synthesized by DesMartau and co-workers according to ref. [41]

Thermogravimetric analysis has shown that the prepared ionomers of structures **A** and **B** by DesMartau and co-workers⁴³ are thermally stable to up to 400 °C while their corresponding monomers decompose at just above 250 °C. The membrane properties are listed in Table 1.2. Proton conductivity data acquired for both structures show that their conductivities at 100 % RH are significantly lower for membranes based on structure A, but structure B showed a proton conductivity similar to Nafion 112 under fully hydrated conditions. However, the conductivities under anhydrous conditions were not reported for these membranes.

Table 1.3 Comparison membrane properties for phosphonic acid based membranes

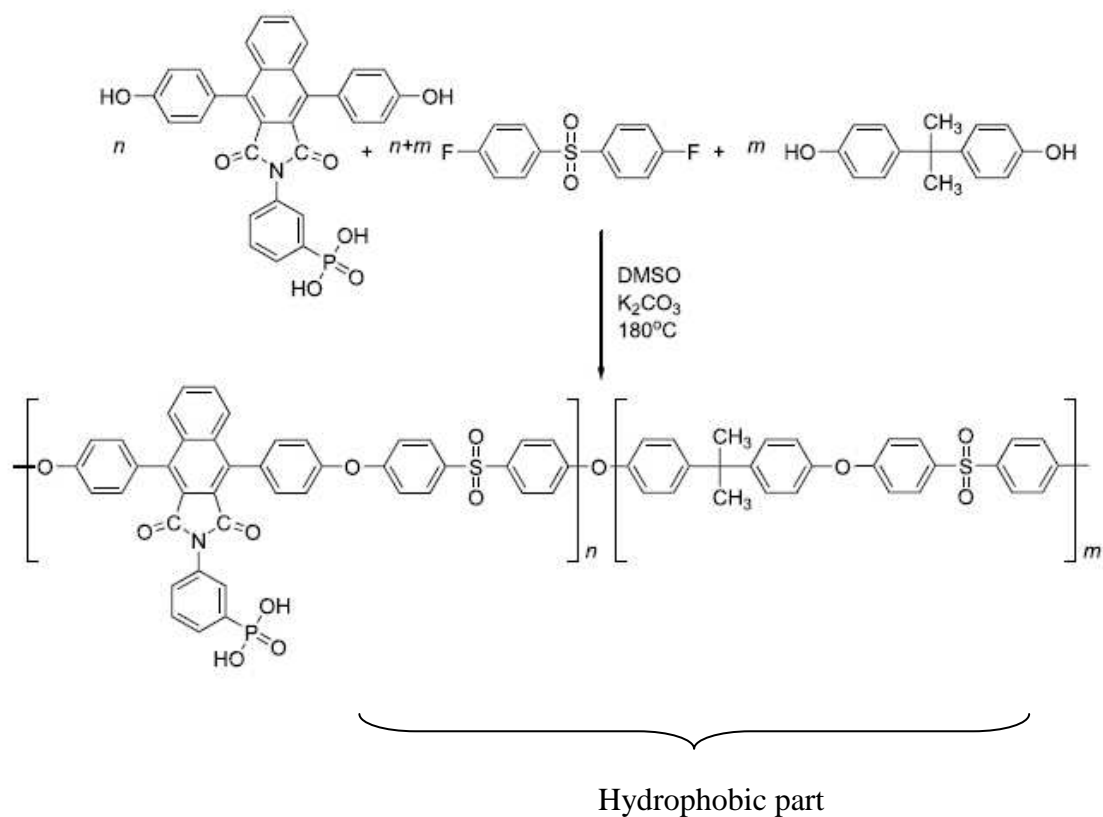
Membrane	EW (g/mol)	IEC (mequi/g)	Water uptake (%)	Conductivity 25 °C (Scm ⁻¹)	Conductivity 80 °C(Scm ⁻¹)	Conductivity 120 °C(Scm ⁻¹)
A1	750	1.33	124	0.026	0.025	0.046
A2	1250	0.8	16	0.006	0.018	0.013
A3	1000	1	74	0.014	0.021	0.035
B	1100	0.9	N/A	0.044	0.122	0.124

A1, A2, A3 have the same chemical structure as of A with different EWs

Other examples for fluorinated phosphonic acid membranes are work by Yamabe et al. and Stone and co-workers. Yamabe et al also prepared structurally similar tetrafluoroethylene copolymerized pendant phosphonic acid polymers.⁵³ Stone and co-workers prepared copolymers based on phosphonic acid functionalized α,β,β -trifluorostyrene by free radical polymerization. These polymers have a perfluorinated backbone and pendant phosphonic acid functionalized phenyl group.⁵⁴

Non-fluorinated polymers: The main types of nonfluorinated phosphorous-containing proton-conducting polymers reported in literature are phosphorylated polyethers, polysulfones, polybenzimidazoles, and polyphosphazenes prepared on the basis of phosphonic acid functionalized monomers or by phosphorylation of existing polymers.

Meng et. al has prepared the poly(arylene ethers) containing phosphonic acid groups from the polycondensation reaction of *bis*-phenol (mixed with *bis*-phenol A) and 4,4'-difluorodiphenyl sulfone.^{44,55} Polymers synthesized by polycondensation reactions give high molecular weight polymers. This will give excellent mechanical properties and high resistance to hydrolysis. Poly(arylene ether sulfone)s groups impart high thermal stability and high Tgs. The synthetic route is shown in scheme 1.5 below.



Scheme 1.5 Synthesis of phosphonic acid group containing polymer by polycondensation⁴⁴

Poly(arylene ethers) copolymers were synthesized by a one pot polycondensation method with various composition of hydrophobic to hydrophilic parts. The high viscosity η values in Table 1.3 indicate the polymers were obtained in high molecular weights. The polymers were soluble in LiOH solution. The film was cast from that solution and then acidified back to the acid form. The cast films of the polymer were tough and ductile except for the polymer with n % = 100.

Table 1.4 Properties of polymers^{46,55}

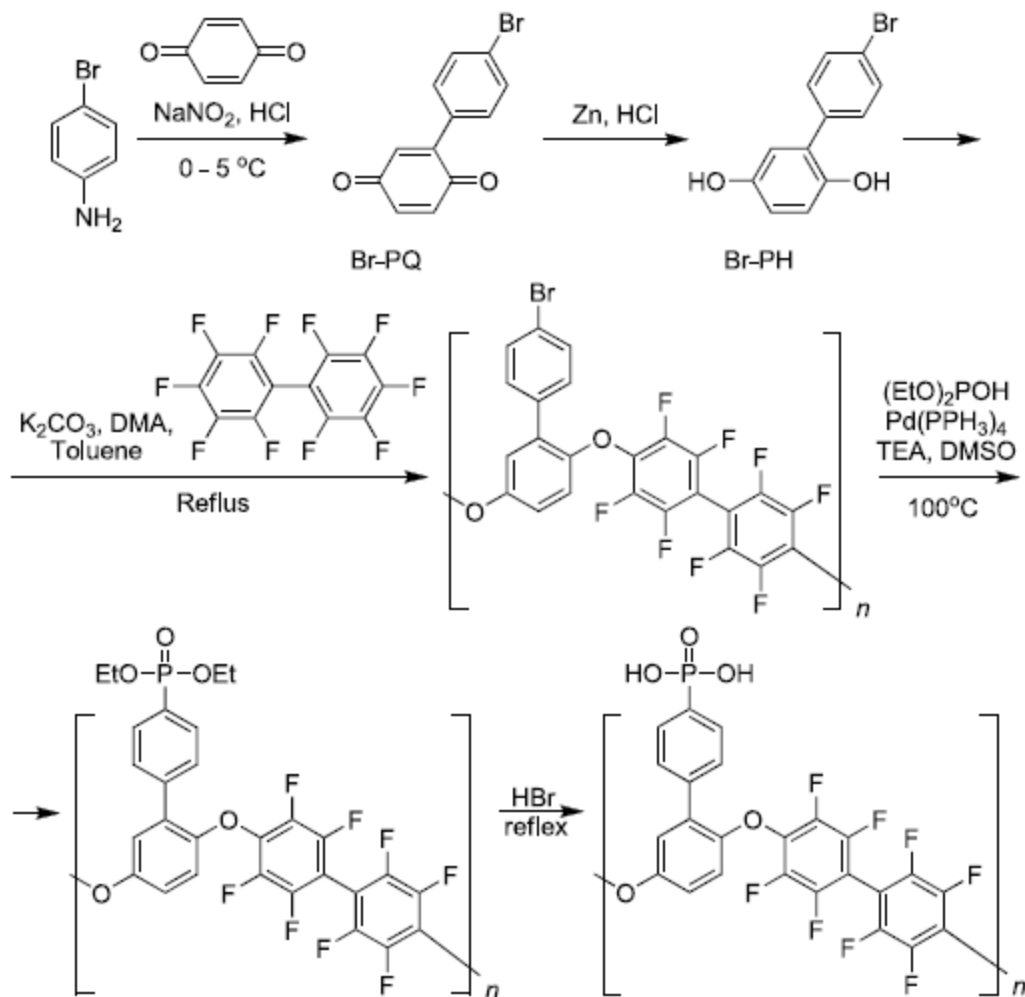
n%	m%	viscosity	EM ^a	Water ^b Absorption	T _g (°C)	TGA _{onset} (°C)	TGA _{5%}	Proton conductivity (10 ⁶ Scm ⁻¹)
25	75	0.67	518	3.2	254	289.8	502.4	6.78
50	50	0.60	596	4.7	277	245.7	498.0	29.6
75	25	0.54	673	6.4	315	229.1	480.5	18.6
100	0	0.43	750	7.5	ND	194.2	476.1	13.2

^a EM-equivalent molecular weights that are defined as the equivalent weight per phosphonic acid group

^b Water absorption in hot water (12 hours)

The proton conductivity was highest for the copolymer of (n % : m% = 50 :50) . But its conductivity is still three orders of magnitude lower than that of Nafion (10⁻² Scm⁻¹ under moisture). However, the authors did not observe any increase in conductivity when the n % content of the phosphonic acid monomer is increased. The conductivity was observed to decrease by a factor of two. And this is attributed to the increase in Tg value.

Holdcroft and co-workers have shown that by replacing the rigid dicarboxylic imide structure with the attached phosphonic acid group (see scheme 1.5) in the above discussed poly(aryl ether) polymer with a more flexible arylphosphonic acid group⁴⁵ (see scheme 1.6) that most of the desired polymer properties for PEM applications can be improved. The phosphonic acid group has been introduced based on a previously reported successful conversion of phenyl bromine group using a palladium catalyst.^{56,57}

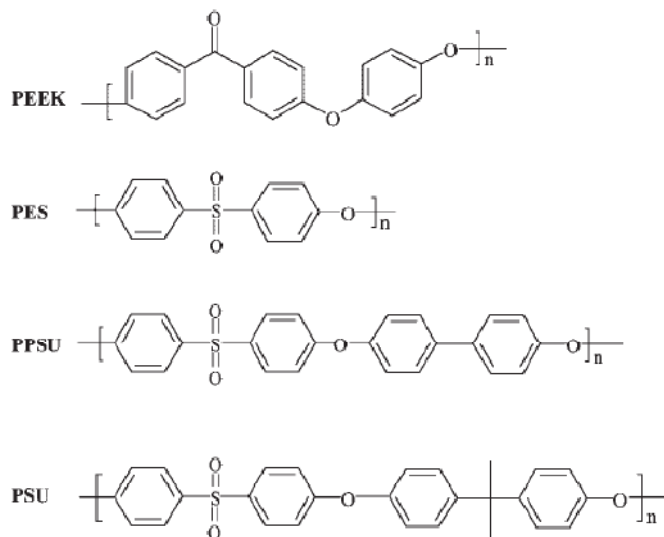


Scheme 1.6 Synthesis of fluorinated poly (aryl ether) with a phosphonic group^{45,46}

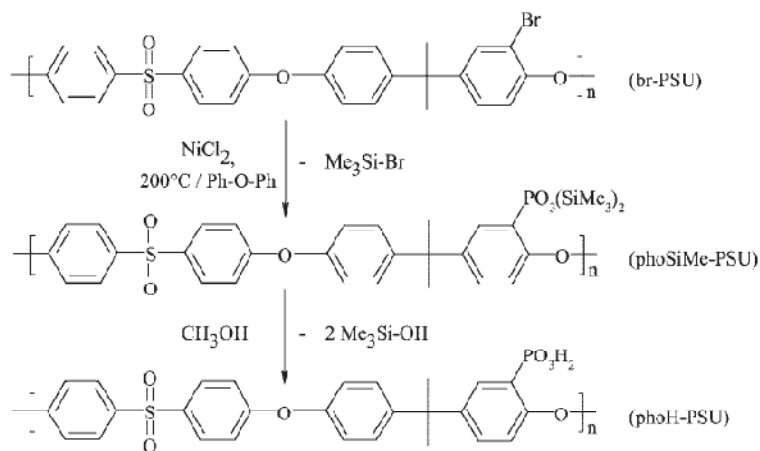
The polymer has good solubility. It is soluble in DMA, DMF, DMSO, and N-MP . It has high thermal stability and good tensile strength. The main chain decomposition does not start until the temperatures are higher than $400\text{ }^\circ\text{C}$. Proton conductivity has been tested as a function of temperature and relative humidity. The proton conductivity is less than that of Nafion but at room temperature a conductivity value of $2.6 \times 10^{-3}\text{ S/cm}$ has been measured in water. At 95% relative humidity and at $80\text{ }^\circ\text{C}$, the proton conductivity has reached $6.0 \times 10^{-3}\text{ S/cm}$. At lower

humidity's at 120 °C , the measured conductivity values are very low, at 45% relative humidity a value of 2.9×10^{-6} S/cm and at 25% relative humidity 2.0×10^{-6} S/cm. The lower degree of phosphonation has been indicated as the cause of the lower conductivities.

Another common method explored for the synthesis of phosphonated PEM polymers is the phosphorylation of the existing high performance polymers. The chemical structure of some of the high performance polymers is shown in Scheme 1.7. Such structures have been shown to impart good swelling resistance at elevated temperatures. An example of a phosphorylation of a polymer is shown in scheme 1.8.

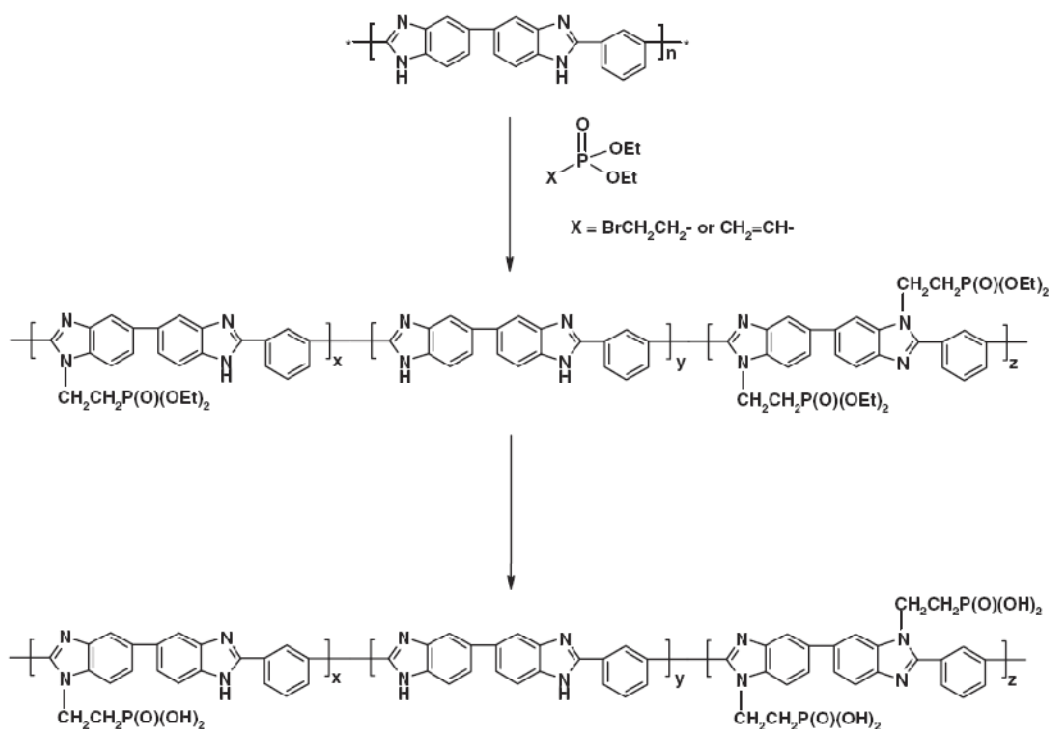


Scheme 1.7 The chemical structures of high performance fibers^{47,58}



Scheme 1.8 Catalytic phosphonylation of brominated polysulfone high performance polymer tris(trimethylsilyl) phosphite (TMSP) by the nickel-catalyzed Arbuzov reaction and subsequent methanolysis⁴⁷

Ethylphosphorylated polybenzimidazole polymer synthesis as a polymer electrolyte membrane has been reported.^{48,59} The scheme 1.9 show the synthetic details for the polymer in reference.⁴⁸



Scheme 1.9 Phosphonic acid functionalized PBI synthesis

The ethylphosphonic acid ester was introduced by N-alkylation of the PBI. Then the ester was hydrolyzed to produce the acid. Membranes were prepared by casting of solutions of 19% modified ethyl phosphonic acid-grafted PBI in DMAc using Petri dishes. The thickness and size of the membranes has been varied by controlling the volume of solution according to the diameter of the dishes. The degree of functionalization of the polymer has been calculated using the distinct proton signals coming from $-P-CH_2-$ and $-N-CH_2-$ group. The 12% phosphonic acid functionalized membrane was then doped with different concentrations of phosphoric acid and the proton conductivity was measured. The conductivity data are shown in Figure 1.7.

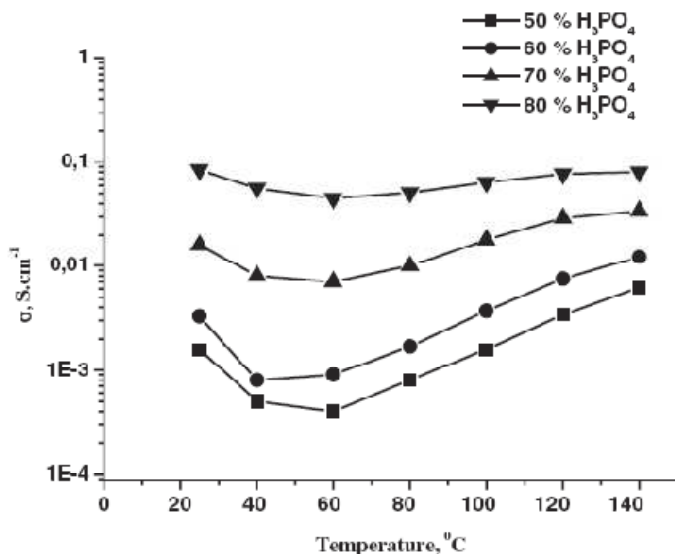
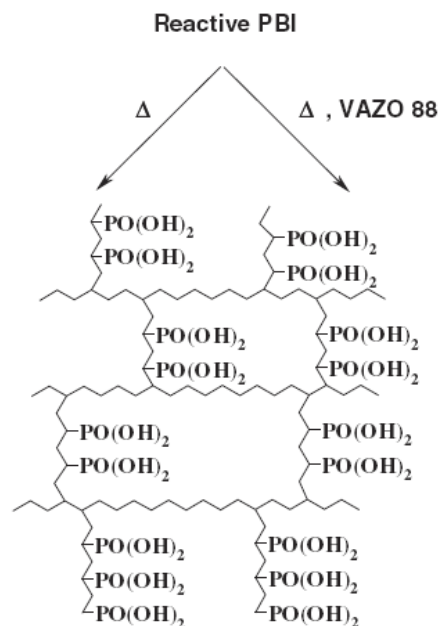


Figure 1.8 Temperature dependence of the DC conductivity of the ethylphosphonic acid⁴⁸ functionalized membrane (degree of modification 12%) doped with H₃PO₄ of various strengths

Figure 1.7 shows that the conductivity values of the doped membranes are very high compared to Nafion which reach up to 0.1 S cm⁻¹ at 80 °C when 100% humidified. M.H. Litt and coworkers first described the successful application of phosphoric acid doped PBI based membranes in PEMFCs.⁶⁰⁻⁶² The PBI polymers described in these applications have a maximum doping concentration of 50%. They show a conductivity of 5 × 10⁻³ S cm⁻¹ at room temperature. At a temperature of 190 °C the conductivity reaches a value of 4 × 10⁻² S cm⁻¹.⁶⁰⁻⁶⁴

The main disadvantage of this type of phosphoric acid doped membranes is that the phosphoric acid can get washed away with water. The authors in this paper have prepared polyvinyl grafted PBI membranes as a solution to this problem. The scheme 1.10 shows the attempted synthesis of this polyvinyl phosphonic acid grafted polymer.



Scheme 1.10 PVPA/PBI networks via polymerization/crosslinking technique⁴⁸

Grafting has been done using two different methods. The two methods are (1) thermally induced polymerization and (2) polymerization in the presence of radical initiator. Use of the azobiscyclohexanenitrile (VAZO 88) radical initiator produced polymer networks that had 10-12 vinyl phosphonic acid units per benzimidazole ring. This was the membrane that later determined to show the highest degree of grafting. Under anhydrous conditions a maximum proton conductivity of $2.8 \times 10^{-2} \text{ Scm}^{-1}$ was observed at 160°C for this membrane. At 20°C this membranes conductivity was observed to be near $1.0 \times 10^{-3} \text{ S cm}^{-1}$. This membrane had IEC value of 1.4 meq g^{-1} . The proton conduction mechanism in these membranes is thought to occur by structure diffusion mechanism.

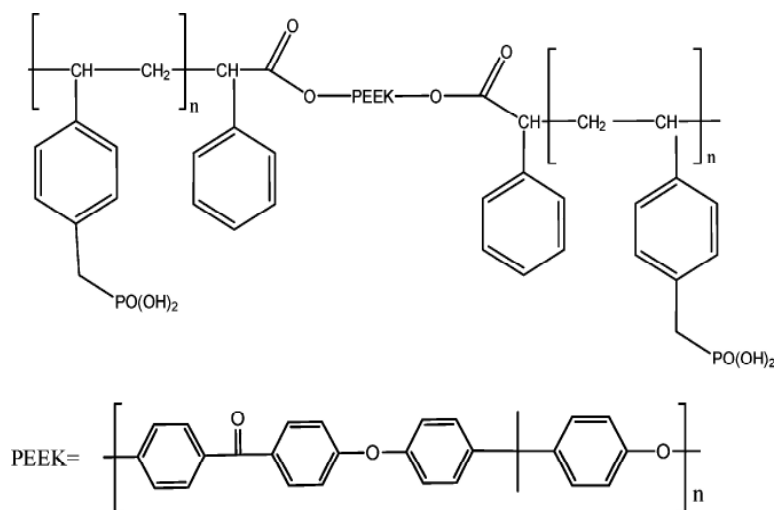
Polymer morphology

In addition to the chemical structure and the type of protogenic group, controlling the microstructure of the polymer electrolyte membranes is also considered very important to

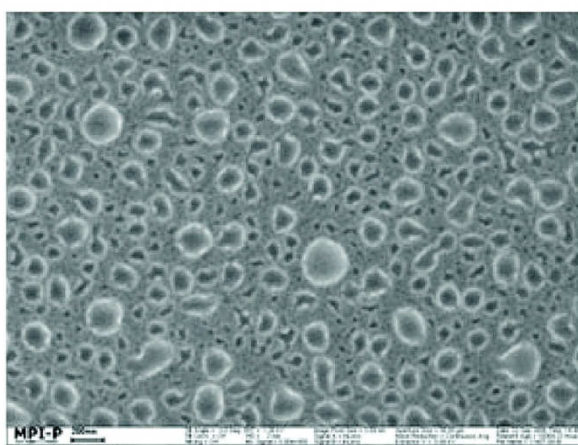
achieve optimum proton conductivity. For example, it has been observed that proton conductivity of the proton electrolyte membrane “Nafion” decreases by several orders of magnitude when it is dissolved and recasted as a membrane.⁶⁵

The high proton conductivity and its high mechanical strength of Nafion membranes is due to the nano-scale phase separated structure. Based on the Cluster-Network Model, a model proposed to explain the morphology of Nafion structure, Nafion membranes consists of clusters of sulfonic acids units held within a fluorocarbon rich continuous phase.⁶⁶ These clusters make a continuous network of channels after water uptake increasing the proton conductivity. A report by Wu and Weiss showed⁶⁷ that based a dynamic mechanical analysis (DMA) data of a styrene-vinyl phosphonic acid based ionomer and a corresponding sulfonic acid based ionomer that the tendency for microphase separation of phosphonic acid ionomer is greater compared to the sulfonic acid based ionomer. As mentioned in the section on Fluorinated Polymers, the poor conductivity of the Nafion analog of phosphonic acid prepared by Burton and co-workers, based on differential scanning calorimetry experiments, it was explained as due to the poor cluster formation of acidic groups during the compression molding.

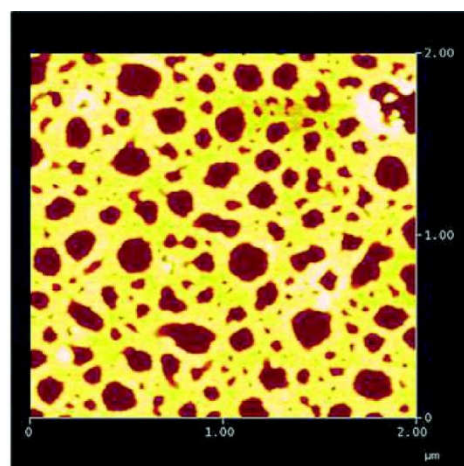
A phase percolated non-fluorinated Block copolymer of poly(vinylbenzylphosphonic acid) and poly(ether-ther-ketone) (PEEK) that can be expected to have a high proton conductivity has been reported by Roy et al.⁶⁸ The chemical structure of the copolymer is shown below in Scheme 1.11.



Scheme 1.11 Block copolymer of poly(vinylbenzylphosphonic acid) and poly(ether-ether-ketone)⁶⁸



2nm



2 μm

Figure 1.9 Experimental SEM (left panel) and AFM (right panel) images of the copolymer in scheme 1.13 above⁶⁸

The nano-phase separated structure of this copolymer as obtained from the scanning electron microscopy (SEM) and atomic force microscopy (AFM) is shown in Figure 1.8 above. The PEEK blocks can be seen as aggregated small clusters dispersed in a percolated phase of poly(vinylbenzylphosphonic acid). The morphology is good for proton conductivity. However its proton conductivity is yet to be reported.

The morphologies of the different polymers results in different proton conductivities and mechanical strength. The morphology will depend on the volume fractions of the hydrophilic and hydrophobic fractions of the polymers used and the copolymer architecture. In addition to the electron microscopic techniques, small angle x-ray and neutron scattering studies have also been used to study the morphology of PEM membranes.

Polarization Curve for Phosphonated Membranes

In an ideal fuel cell the cell voltage is independent of the current drawn. However, practically due to the different types of irreversible processes such as activation polarization losses, ohmic losses, mass transport losses and losses due to fuel crossover causes the cell voltage to decrease. The theoretically calculated cell voltage for a PEM fuel cell is 1.229 V. The following figure compares the polarization curves of two phosphonated poly(trifluorostyrene) membranes of different IEC values with the Nafion membrane. It appears that under operational fuel cell conditions that performance of a phosphonated poly(trifluorostyrene) polymer is slightly lower than that of Nafion.

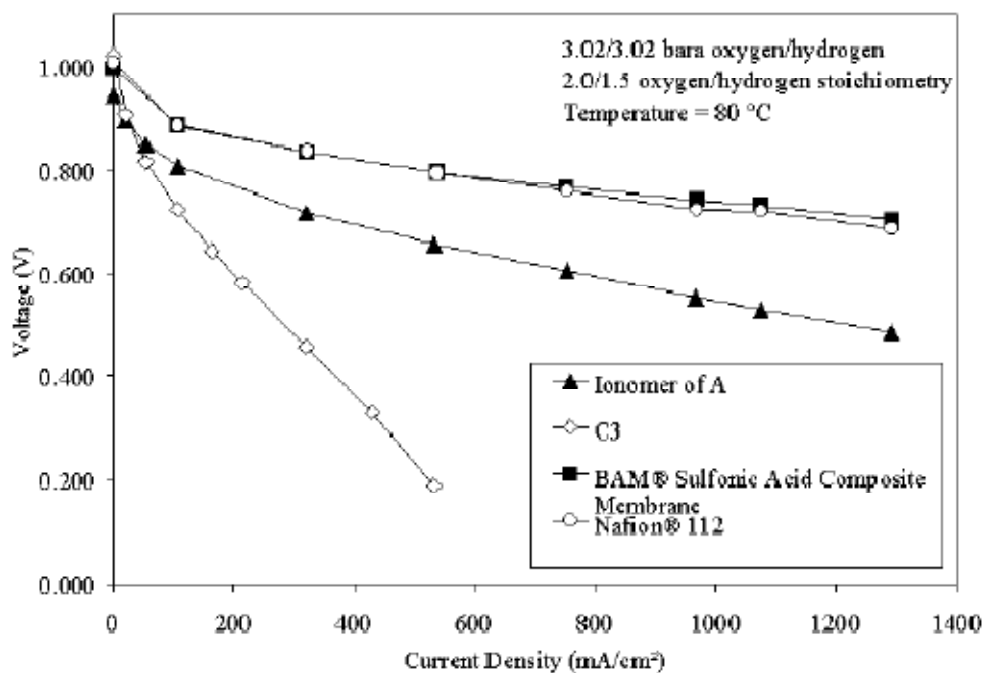


Figure 1.10 polarization data comparing the phosphonic acid-based ionomer of A-phosphonated poly(trifluorostyrene) (IEC = 7.7 meq/g), C3-phosphonated poly(trifluorostyrene) (IEC = 5 meq/g)⁵⁴

Scope of This Work

Literature discussed in the previous section shows that synthesis of phosphonic acid based polymers has been achieved with difficulty but in many different ways. This shows that C-P bond can be made as successfully as C-S bond seen in sulfonic acid polymers. Most of the phosphonic acid based polymers show comparable IEC values, similar water uptake and in some cases even higher thermal and chemical stabilities compared to sulfonic acid based polymers. Some of the phosphonic acid based membranes exhibit comparable ionic conductivities to that of sulfonic acid based membranes when fully hydrated, however under low relative humidity conditions some of the phosphonic acid membranes were a lot worse than sulfonic acid

membranes. Therefore to help guide design and synthesize better fluorinated polymeric materials that can function under low hydration conditions I undertook a comparative study based on perfluoroalkyl model compounds functionalized with commonly used protogenic groups, most notably, phosphonic and phosphinic acids. These are the most comprehensive studies to date of fluoroalkylated phosphonic and phosphinic acids as proton conductors. This dissertation describes my work with these model compounds.

Chapter 2 of this dissertation focuses on four acid model compounds that have chemical structures analogous to comb-branch perfluorinated ionomers functionalized with phosphonic, phosphinic, sulfonic and carboxylic acid protogenic groups. The chapter describes synthesis and characterization of these different acid model compounds with respect to molecular properties such as proton conductivity, viscosity, proton and anion (conjugate base) self-diffusion coefficients, and Hammett acidity to identify suitability of each protogenic group for use in the construction of anhydrous polymeric materials. In chapter 3, the selected protogenic groups were further investigated for the same molecular properties as a function of increasing perfluoroalkyl chain length. Synthesis of some of the longer chain perfluoroalkyl phosphonic and phosphinic acids are also described. The literature indicates that ionomers with side chains terminated with a protogenic groups such as sulfonic acid, exhibit different macroscopic properties, in terms of proton conductivity, membrane morphology and hydrolytic stability^{69,70} depending on the length of the side-chain that was used to construct them. Chapter 4 discusses a comparison of the proton conductivity as a function of hydration for the phosphonic, phosphinic and sulfonic acid model compounds.

The work in Chapter 5 was performed during the first two years at Clemson University when I worked in the Batteries for Advanced Transportation Technologies (BATT) Program which was supported by the U.S. Department of Energy Office of Vehicle Technologies (OVT) to help develop high-performance rechargeable batteries for use in electric vehicles (EVs) and hybrid-electric vehicles (HEVs). This chapter describes the synthesis, characterization and ion transport of lithium polymer electrolytes that can provide rechargeable lithium batteries with high power/ high rate capabilities by overcoming concentration polarization.

Chapter 6 describes the synthesis and characterization of a new air and water stable perfluorinated anion for room temperature ionic liquids.

References

- (1) Brandon, N.;Skinner, S.;Steele, B. *Annu. Rev. Mater. Res.* **2003**, 33, 183-213.
- (2) Kerres, J. *J. Membr. Sci.* **2001**, 185, 3-27.
- (3) Kreuer, K.D. *J. Membr. Sci.* **2001**, 185, 29-39.
- (4) Rikukawa, M.;Sanui, K. *Prog. Polym. Sci.* **2000**, 25, 1463-1502.
- (5) Roziere, J.;Jones, D. *Annu. Rev. Mater. Res.* **2003**, 33, 503-555.
- (6) Rusanov, A. *Russ. Chem. Rev.* **2002**, 71, 761.
- (7) Savadogo, O. *J. New Mater. Electrochem. Syst.* **1998**, 1, 47.
- (8) Zhao, T.;Kreuer, K.;Van Nguyen, T. *Advances in Fuel Cells*; Elsevier Oxford, **2007**.
- (9) Sumner, J.J.;Creager, S.E.;Ma, J.J.;DesMarteau, D.D. *J. Electrochem. Soc.* **1998**, 145, 107-110.
- (10) Krewer, U.;Yoon, H.;Kim, H. *J. Power Sources* **2008**, 175, 760-772.

- (11) Litster, S.;McLean, G. *J. Power Sources* **2004**, 130, 61-76.
- (12) Kreuer, K.D. *Chem. Mater.* **1996**, 8, 610-641.
- (13) Kreuer, K.D. *Solid State Ionics* **2000**, 136, 149-160.
- (14) Zawodzinski, T.;Neeman, M.;Sillerud, L.;Gottesfeld, S. *J. Phys. Chem.* **1991**, 95, 6040-6044.
- (15) Kreuer, K.D.;Rabenau, A.;Weppner, W. *Angew. Chem., Int. Ed. Engl.* **1982**, 21, 208-209.
- (16) Agmon, N. *Chem. Phys. Lett.* **1995**, 244, 456-462.
- (17) Tuckerman, M.;Marx, D.;Klein, M.;Parrinello, M. *Science* **1997**, 275, 817-820.
- (18) Marx, D.;Tuckerman, M.;Hutter, J.;Parrinello, M. *Nature* **1999**, 397, 601-604.
- (19) Wicke, E.;Eigen, M.;Ackermann, T. *Z. Phys. Chem.* **1954**, 1, 340.
- (20) Zundel, G.;Metzger, H. *Z. Phys. Chem.* **1968**, 58, 225-&.
- (21) Kreuer, K.D.;Paddison, S.J.;Spohr, E.;Schuster, M. *Chem. Rev.* **2004**, 104, 4637-4678.
- (22) Norby, T. *Solid State Ionics* **1999**, 125, 1-11.
- (23) Phair, J.W.;Badwal, S.P.S. *Ionics* **2006**, 12, 103-115.
- (24) Darling, H.E. *J. Chem. Eng. Data* **1964**, 9, 421-6.
- (25) Greenwood, N.N.;Thompson, A. *J. Chem. Soc.* **1959**, 3485.
- (26) Munson, R.;Lazarus, M. *J. Phys. Chem.* **1967**, 71, 3242-&.
- (27) Ratner, M.A. *Polymer Electrolyte Review*; Elsevier New York, **1987**.
- (28) Tyrrell, H.J.V. *Diffusion in Liquids: A Theoretical and Experimental Study*; Butterworth London, **1984**.
- (29) Munson, R.A. *J. Phys. Chem.* **1964**, 68, 3374-7.
- (30) Chin, D.;Chang, H. *J. Appl. Electrochem.* **1989**, 19, 95-99.
- (31) Peled, E.;Brand, M.;Gileadi, E. *J. Electrochem. Soc.* **1981**, 128, 1697-1704.

- (32) Smedley, S.I. In *The Interpretation of Ionic Conductivity in Liquids*; Plenum: New York, 1980.
- (33) Dippel, T.;Kreuer, K.;Lassegues, J.;Rodriguez, D. *Solid State Ionics* **1993**, 61, 41-46.
- (34) Herz, H.;Kreuer, K.;Maier, J.;Scharfenberger, G.;Schuster, M.;Meyer, W. *Electrochim. Acta* **2003**, 48, 2165-2171.
- (35) Kreuer, K.D.;Fuchs, A.;Ise, M.;Spaeth, M.;Maier, J. *Electrochim. Acta* **1998**, 43, 1281-1288.
- (36) Persson, J.;Jannasch, P. *Chem. Mater.* **2003**, 15, 3044-3045.
- (37) Schuster, M.E.;Meyer, W.H. *Annu. Rev. Mater. Res.* **2003**, 33, 233-261.
- (38) Schuster, M.F.H.;Meyer, W.H.;Schuster, M.;Kreuer, K.D. *Chem. Mater.* **2004**, 16, 329-337.
- (39) Schuster, M.;Meyer, W.H.;Wegner, G.;Herz, H.G.;Ise, M.;Schuster, M.;Kreuer, K.D.;Maier, J. *Solid State Ionics* **2001**, 145, 85-92.
- (40) Schuster, M.;Rager, T.;Noda, A.;Kreuer, K.D.;Maier, J. *Fuel Cells* **2005**, 5, 355-365.
- (41) Kotov, S.V.;Pedersen, S.D.;Qiu, W.;Qiu, Z.-M.;Burton, D.J. *J. Fluorine Chem.* **1997**, 82, 13-19.
- (42) Desmarteau, D.D.;Martin, C.W.;Ford, L.A.;Xie, Y. *Sulfonated perfluorovinyl functional monomers* US patent 6268532 **2001**.
- (43) Jin, L.-M.;Creager, S.;DesMarteau, D. *Prepr. Symp. - Am. Chem. Soc., Div. Fuel Chem.* **2008**, 53, 777-779.
- (44) Meng, Y.Z.;Tjong, S.C.;Hay, A.S.;Wang, S.J. *J. Polym. Sci., Part A: Polym. Chem.* **2001**, 39, 3218-3226.

- (45) Liu, B.;Robertson, G.P.;Guiver, M.D.;Shi, Z.;Navessin, T.;Holdcroft, S. *Macromol. Rapid Commun.* **2006**, 27, 1411-1417.
- (46) Scherer, G.G.;Editor Fuel cells II. [In: Adv. Polym. Sci., 2008; 216], **2008**.
- (47) Bock, T.;Muelhaupt, R.;Moehwald, H. *Macromol. Rapid Commun.* **2006**, 27, 2065-2071.
- (48) Sukumar, P.R.;Wu, W.;Markova, D.;Uensal, O.;Klapper, M.;Muellen, K. *Macromol. Chem. Phys.* **2007**, 208, 2258-2267.
- (49) Harrison, W.L.;Hickner, M.A.;Kim, Y.S.;McGrath, J.E. *Fuel Cells* **2005**, 5, 201-212.
- (50) Iojoiu, C.;Marechal, M.;Chabert, F.;Sanchez, J.Y. *Fuel Cells* **2005**, 5, 344-354.
- (51) Jannasch, P. *Fuel Cells* **2005**, 5, 248-260.
- (52) Kerres, J.A. *Fuel Cells* **2005**, 5, 230-247.
- (53) Yamabe, M.;Akiyama, K.;Akatsuka, Y.;Kato, M. *Eur. Polym. J.* **2000**, 36, 1035-1041.
- (54) Stone, C.;Daynard, T.S.;Hu, L.Q.;Mah, C.;Steck, A.E. *J. New Mater. Electrochem. Syst.* **2000**, 3, 43-50.
- (55) Meng, Y.Z.;Tjong, S.C.;Hay, A.S.;Wang, S.J. *Eur. Polym. J.* **2003**, 39, 627-631.
- (56) Jakoby, K.;Peinemann, K.V.;Nunes, S.P. *Macromol. Chem. Phys.* **2003**, 204, 61-67.
- (57) Miyatake, K.;Hay, A.S. *J. Polym. Sci., Part A: Polym. Chem.* **2001**, 39, 3770-3779.
- (58) Bock, T.;Moehwald, H.;Muelhaupt, R. *Macromol. Chem. Phys.* **2007**, 208, 1324-1340.
- (59) Zawodzinski, T.A., Jr.;Derouin, C.;Radzinski, S.;Sherman, R.J.;Smith, V.T.;Springer, T.E.;Gottesfeld, S. *J. Electrochem. Soc.* **1993**, 140, 1041-7.
- (60) Aharoni, S.M.;Litt, M.H. *J. Polymer Sci. Polymer Chem. Ed.* **1974**, 12, 639-50.
- (61) Fontanella, J.J.;Wintersgill, M.C.;Wainright, J.S.;Savinell, R.F.;Litt, M. *Electrochim. Acta* **1998**, 43, 1289-1294.

- (62) Wainright, J.S.; Wang, J.T.; Weng, D.; Savinell, R.F.; Litt, M. *J. Electrochem. Soc.* **1995**, 142, L121-L123.
- (63) Mecerreyes, D.; Grande, H.; Miguel, O.; Ochoteco, E.; Marcilla, R.; Cantero, I. *Chem. Mater.* **2004**, 16, 604-607.
- (64) Xing, B.; Savadogo, O. *J. New Mater. Electrochem. Syst.* **1999**, 2, 95-101.
- (65) Zaluski, C.; Xu, G. *Macromolecules* **1994**, 27, 6750-6754.
- (66) Yang, Y.; Holdcroft, S. *Fuel Cells* **2005**, 5, 171-186.
- (67) Wu, Q.; Weiss, R.A. *J. Polym. Sci., Part B: Polym. Phys.* **2004**, 42, 3628-3641.
- (68) Roy, S.; Markova, D.; Kumar, A.; Klapper, M.; Muller-Plathe, F. *Macromolecules* **2009**, 42, 841-848.
- (69) Arico, A.S.; Baglio, V.; Di Blasi, A.; Antonucci, V.; Cirillo, L.; Ghilmi, A.; Arcella, V. *Desalination* **2006**, 199, 271-273.
- (70) Miyatake, K.; Yasuda, T.; Hirai, M.; Nanasawa, M.; Watanabe, M. *J. Polym. Sci., Part A: Polym. Chem.* **2007**, 45, 157-163.

CHAPTER TWO

PERFLUOROALKYL PHOSPHONIC AND PHOSPHINIC ACIDS AS PROTON CONDUCTORS FOR ANHYDROUS PROTON EXCHANGE MEMBRANES

Introduction

The work presented in this chapter is being published in ChemPhysChem (Copyright 2010). The citation for this manuscript is:

Mahesha B. Herath, Stephen E. Creager*^[a], Alex Kitaygorodskiy and Darryl D. DesMarteau
Perfluoroalkyl phosphonic and phosphinic acids as proton conductors for anhydrous proton exchange membranes, ChemPhysChem (2010) accepted.

In recent years there has been intense interest in developing proton exchange membrane fuel cells (PEMFCs) that operate at 120 °C and above. High-temperature operation increases power output due to faster electrode kinetics and greater CO tolerance, and it diminishes the need for active cell cooling. Perfluorinated ionomeric membranes such as Nafion® (a perfluorosulfonic acid ionomer) are widely used as electrolytes in PEM fuel cells due to their excellent stability, high ionic conductivity and good mechanical strength. For Nafion-like polymers the conductivity is usually high provided that high relative humidity (RH) is maintained. Above 100 °C, pressurized operation is required to maintain the required RH for high proton conductivity. For example a water vapor pressure of 2-3 atm is required at 120 °C to maintain the same conductivity as at 80 °C at 1 atm under water-saturated conditions. As PEMFC technology has evolved, a need has emerged for devices which operate at high temperature without humidification. A new generation of proton conducting materials that exclusively transport

protons in low-humidity conditions (possibly including anhydrous) when operating at high temperatures is needed.

The ionic conductivity of Nafion and related sulfonated ionomer membranes is due to dissociated protons of the fluoroalkyl sulfonic acid groups attached to side chains of the polymer. When exposed to water, the hydrophilic domains of the polymer merge and form a continuous acid-rich aqueous phase. The sulfonic acid groups dissociate and release protons which are then transported by a combination of two transport mechanisms described as (1) vehicular mechanism¹ and (2) proton hopping / structure diffusion mechanism². In the vehicular mechanism the proton is transported as a complex with a carrier molecule such as H₂O [e.g. H₃O⁺] across the continuous aqueous phase. At high degree of hydration in Nafion-like polymers, due to the continuous nature and the high number of hydrogen bonds within the aqueous phase, structure diffusion becomes the predominant proton-transport mechanism and proton mobility is high.³ However at low water content, discontinuities in the water phase and charge effects of -SO₃⁻ groups cause a decrease in hydrogen bond formation leading to lower proton mobility, particularly long-range mobility. Quasi-elastic neutron scattering (QNS) experiments confirm that the poor ionic conductivity at low hydration in vehicle mechanism is a result of the loss of long-range (> 10nm) proton mobility.⁴

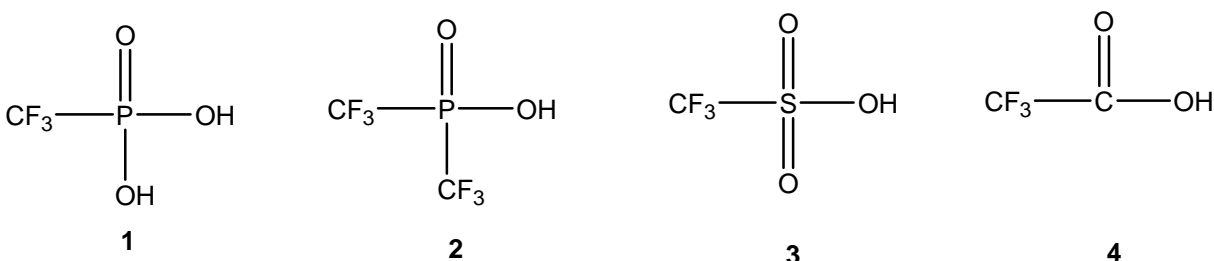
Many alternative polymer systems have been considered for circumventing the limitations of Nafion and related ionomers in PEM fuel cells. It is hoped that replacement of the sulfonic acid group in perfluorinated ionomers with a derivative of an oxoacid such as carboxylic or phosphonic acid as the protogenic group might provide better conductivity under low RH conditions, as has been demonstrated in particular with phosphoric acid itself which is fairly conductive even when completely dry due to self-ionization coupled with proton hopping.⁵

Kreuer and co-workers reported⁶ in a comparative model study that heptyl-phosphonic acid exhibited the highest proton conductivity of all the model compounds studied in the anhydrous state above 100 °C. It was thought that this comparatively high ionic conductivity of an alkyl phosphonic acid could reflect its capacity to transport protons by a structure-diffusion / Grotthuss hopping mechanism involving a hydrogen-bonded network of self-dissociated proton donor and acceptor ion pairs. The structure-diffusion / Grotthuss-hopping mechanism² involves the displacement of a proton charge from a donor to an acceptor through a system of hydrogen bonds without significantly moving the mass of the proton as seen with the vehicle mechanism. The proton transport in dilute aqueous HCl is an example of this observation.⁷ Kreuer's study also showed that heptyl-phosphonic acid has greater thermal and electrochemical stability than other model acids (for example heptyl-sulfonic acid). This finding indicates that alkyl-phosphonic acids may be more suitable than sulfonic acids for use in fuel-cell applications.

Burton and co-workers were the first to report preparation of perfluorinated phosphonated ionomers⁸ having structural similarity to Nafion and related ionomers. Synthesis was accomplished successfully but membrane formation was difficult and conductivity values were not reported. Other fluorinated⁹ and non-fluorinated¹⁰⁻¹³ phosphonic-acid-functionalized ionomers have also been prepared, however membranes prepared from these ionomers all exhibit a low concentration of phosphonic acid groups and thus they have low water uptake and low proton conductivity.

The present study is directed at investigating proton transport rates and mechanisms at a molecular level using a series of four model compounds analogous to perfluorinated ionomers functionalized with fluoroalkyl phosphonic, phosphinic, sulfonic and carboxylic acids as protogenic groups. Structures for the four model compounds are shown in Scheme 2.1. They

are as follows: **(1)** trifluoromethyl-phosphonic acid; **(2)** bis(trifluoromethyl)-phosphinic acid; **(3)** trifluoromethyl sulfonic acid; and **(4)** trifluoroacetic acid. These compounds were investigated for molecular properties such as ion diffusivity, acidity and viscosity that are expected to influence ionic conductivity. These model acids provide the highest possible volumetric acid concentration for each type of acid group. Therefore each measured anhydrous proton conductivity may be considered to define an upper limit for the anhydrous proton conductivity of its analogous ionomer.

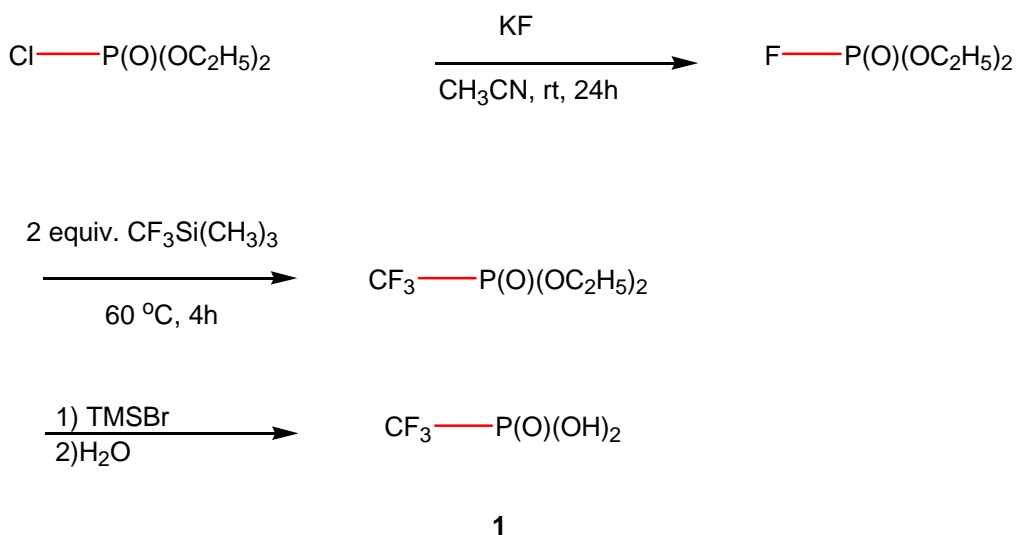


Scheme 2.1 Chemical structure of model acids. **1**-trifluoromethyl-phosphonic acid, **2**-bistrifluoromethyl-phosphinic acid, **3**-trifluoromethyl-sulfonic acid, **4**-trifluoroacetic acid

Experimental

Materials and reagents: Unless otherwise noted, starting materials were obtained from commercial suppliers and used without further purification. Acetonitrile was dried by storing over KOH overnight and distilling from P₂O₅. Trifluoromethyl sulfonic acid (Alfa easer 98+ %) and trifluoroacetic acid (Fluka ≥ 99.5%) were obtained from commercial suppliers and used without further purification. ¹H, ¹⁹F, and ³¹P NMR spectra were recorded on a NMR instrument

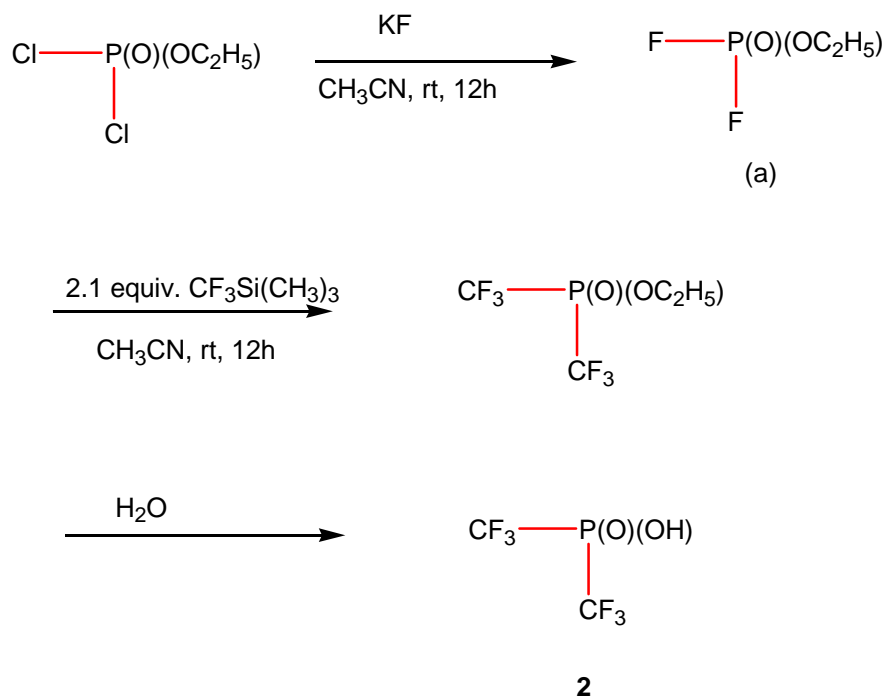
at 300.3, 282.2, and 121.5 MHz respectively, using CD₃CN as the solvent except where noted. In some cases spectra were acquired on neat samples.



Scheme 2.2 Synthesis of trifluoromethylphosphonic acid

Synthesis of trifluoromethyl phosphonic acid (1) Under a nitrogen atmosphere, a dry 100 mL round-bottomed flask was charged with dry KF (2 g, 34.4 mmol) and 20 mL of dry acetonitrile, followed by diethylchlorophosphate (4 mL, 19.4 mmol) via syringe. The reaction was stirred at room temperature for 12 h monitoring the disappearance of the peak corresponding to diethylchlorophosphate in ³¹P NMR and appearance of new peaks for diethylfluorophosphate as the only product in ¹⁹F and ³¹P NMR spectra. After completion, the solution was loaded into a syringe and a Whatman PVDF filter (0.2 μm) was attached. The solution was syringed into a separate flask held under a nitrogen atmosphere. Acetonitrile was

removed under reduced pressure. A small amount of dry P_2O_5 was added to the remaining solution and stirred briefly, then this solution was subjected to vacuum distillation to isolate a colorless liquid (2.3g). The NMR spectrum for this liquid agrees with the literature spectrum reported for diethylfluorophosphate¹⁴ (see below). This liquid (2 g, 12.8 mmol) was then reacted with trifluoromethyltrimethylsilane (3.6 g, 25.6 mmol) in the presence of KF (0.020 g, 3.4 mmol) under an argon atmosphere at 60 °C for 4 h. After removing the excess trifluoromethyltrimethylsilane reagent by rotary evaporation, the crude product was distilled to isolate the diethyl trifluoromethylphosphonate. This ester was mixed with excess bromotrimethylsilane (4.1 g, 26.9 mol) dissolved in dichloromethane (5 ml) and stirred at room temperature overnight monitoring the disappearance of diethyl trifluoromethylphosphonate and appearance of silylated ester by ^{31}P NMR (at -20 ppm). After reaction completion, the silylated ester was hydrolyzed with water (10 mL) to give the phosphonic acid product. The water was evaporated using rotary evaporator and the crude product was dried at 85 °C under dynamic vacuum for 24 h and sublimed to yield 1.63 g (85%) of white crystalline solid. 1H NMR (300.3 MHz, CD_3CN): 11.2 (br, 2H, PO_3H_2). ^{19}F NMR (282.2 MHz, CD_3CN): - 74.4 (d, $^3J_{FCP} = 121.5$ Hz). ^{31}P NMR (121.5 MHz, CD_3CN): -3.0 (q, $^3J_{PCF} = 120.8$ Hz). Diethyldifluorophosphate: 1H NMR (300.3 MHz, CD_3CN): 1.2 (t, 3H, CH_3). 3.4 (q, 2H, CH_2) ^{19}F NMR (282.2 MHz, CD_3CN): - 81.3 (d, $J_{FCP} = 965.1$ Hz). ^{31}P NMR (121.5 MHz, CD_3CN): -7.7 (d, $J_{PCF} = 972$ Hz).



Scheme 2.3 Synthesis of bis(trifluoromethyl)phosphonic acid

Synthesis of bis(trifluoromethyl) phosphinic acid (2): Under a nitrogen atmosphere, a dry 100 mL round-bottomed flask was charged with dry KF (6 g, 103 mmol) and 20 mL of dry acetonitrile, followed by ethyldichlorophosphate (3.5 mL, 15.6 mmol) via syringe. The reaction was stirred at room temperature for 12 h, by monitoring as described above. Formation of ethyldifluorophosphate¹⁵ is indicated in ¹⁹F NMR by a doublet centered at -84.7ppm and triplet centered at -21.3ppm in ³¹P NMR. Reaction of ethyldifluorophosphate with trifluoromethyl trimethyl silane also proceeds as described above. Hydrolysis of the resulting ethyl ester was accomplished simply by adding 5 mL of DI water to the reactions mixture followed by stirring for 30 min. Freshly prepared silver oxide (2.3 g, 18.4 mmol) was then added slowly to the aqueous solution and the mixture was stirred at room temperature for 12 h. The solution was filtered from the excess silver oxide and water was removed under reduced pressure to give the

brown colored silver salt of the organic acid. The silver salt was further dried at 50 °C under dynamic vacuum for 48 h and finally distilled over conc. H₂SO₄ to yield 2.7 g (88%) of colorless oil which is the final phosphonic acid product. ¹H NMR (300.3 MHz, CD₃CN): 11.8 (br, 2H, PO₃H₂). ¹⁹F NMR (282.7 MHz, CD₃CN): - 73.8 (d, 6F, (CF₃)₂, J_{FCP} = 107.4 Hz). ³¹P NMR (121.5 MHz, CD₃CN): -3.0 (septet, J_{PCF} = 106.9 Hz).

Proton conductivity measurements: Ionic conductivity measurements for model acids were carried out inside of a pressurized conductivity apparatus constructed from a 316 stainless steel. A schematic of the apparatus is shown in Figure 2.1. The apparatus temperature was controlled using a heating tape with an Omega CNi3244-C24 temperature controller, and the temperature was measured by a thermocouple inside the chamber.

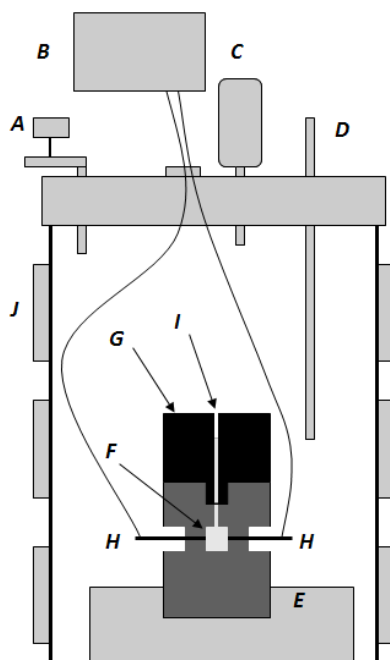


Figure 2.1(left) The schematic of the stainless steel conductivity apparatus where (A) Vacuum / gas inlet / outlet,(B) Impedance analyzer, (C) Pressure gauge (Mcmaster), (D) Thermocouple (Omega, J-type), (E) Cell holder, (F) Liquid electrolyte (acid or/and water), (G) PEEK cell body of the conductivity cell, (H) Platinized platinum rod electrodes, (I) Pressure equalization hole (very narrow), (J) Heating tape for temperature control(Omega).

The conductivity cell used to determine conductivities of neat acids is also shown in Figure 2.1. The cell was fabricated from PEEK and has an internal volume of 25 μL and the two Pt electrodes have contact areas of $2.0 \times 10^{-3} \text{ cm}^2$ each. The cell used to study trifluoromethyl sulfonic acid was similar but was fabricated using a Teflon perfluoroalkoxy (PFA) material.

The conductivity cell was calibrated with standard 0.01 and 0.1 M KCl solutions. Cell constants were determined to be 14.2 cm^{-1} for the PEEK cell and 14.8 cm^{-1} for the PFA cell. Conductivity experiments were conducted with the respective neat acids after the conductivity apparatus was pressurized with N_2 gas to 50 psi. The AC impedance as a function of temperature

was measured over a frequency range from 20 kHz down to 0.01 Hz with a Solartron model 1254 frequency response analyzer in combination with a S11286 electrochemical interface. The temperature was lowered in 10°C decrements from 120 °C down to 50°C and cell was allowed to equilibrate for at least 10mins before each measurement. The process was repeated 2 times after cooling the system to room temperature at the end of each trial. From the Nyquist plots obtained from data, the intercept of the straight line with the real axis gave the impedance associated with ionic conductivity which was then calculated by dividing the impedance from the Nyquist plot by the cell constant.

Viscosity measurements: Viscosities for model compounds were measured using a set of manufacturer-calibrated Cannon-Manning Semi-Micro Extra Low Charge capillary viscometers. The viscometers were thoroughly cleaned before each use. The viscometer was immersed in a silicone oil bath for variable-temperature measurements and the temperature was measured with an accuracy of 0.1 K. The viscosity was calculated from the average of 2-3 runs. The data agreed to within $\pm 5\%$.

Density measurements: Densities of the model compounds were determined by measuring the weight of a 1mL volume dispensed by an Eppendorf micropipette. This procedure was repeated 4 times and the average of the data was used to calculate the density.

PFG NMR studies: Pulsed-field-gradient nuclear magnetic resonance (PFG NMR) experiments were performed on a Bruker avance 300 spectrometer with 5 mm $^{13}\text{C}/^{19}\text{F}/^{31}\text{P}-^1\text{H}$ QNP z-gradient liquid probes at 300.13 MHz for ^1H , 282.7 MHz for ^{19}F at 20 and 85 °C. Temperatures were regulated by a BVT3000 temperature controller and calibrated against ethylene glycol. Samples were neat acids and the experiments were performed without deuterium lock and without sample rotation. The stimulated echo sequence using one spoil gradient

(step1s from the Bruker library) was used in pseudo-two-dimensional mode with constant diffusion time and a linearly ramped gradient from 5 to 95% of maximum power in 16 increments. Diffusion time Δ was kept constant at 100 ms and gradient pulse length δ was optimized for each sample, nucleus, and temperature using the one-dimensional variant of the pulse sequence step1s1d. The data were processed in pseudo-two-dimensional mode then analyzed using SimFit included with Bruker (v 3.5), fitting the signal integration (area) to gradient strength.

Acidity Determination by NMR: Hammett acidity (H_0) of all the model compounds was determined based on the method developed by Farcasiu and Ghenciu. It is based on the ^{13}C NMR spectroscopy chemical shift difference ($\delta\Delta$) between the C_α and C_β carbon atoms of mesityl oxide which increases with increasing protonation at the carbonyl oxygen. Three different concentrations of mesityl oxide (where $[x]=$ % molar concentration of mesityl oxide) solutions were prepared by mixing $[x]=$ 2%, 4% and 8% mole percent of mesityl oxide with neat acid. Then variation (y_i) of $\delta\Delta$ is graphed with the corresponding change (x_i) in concentration $[x]$. The data points (y_i, x_i) were fitted to a straight line $y = ax + b$. The straight line has a negative slope with decreasing $\delta\Delta$ values with increasing $[x]$. The H_0 for the acid was determined as the the H_0 value that corresponds to the intercept value b in the mesityl oxides calibration plot of H_0 vs $\delta\Delta$ found in references by Farcasiu and Ghenciu^{16,17}.

Results and Discussion

Table 2.1 presents a summary of select data on the four model acids studied in this work. C_0 represents the molar concentration of molecular acids calculated using the measured density and calculated molar mass for each acid. Viscosity and conductivity values at 25 °C are part of larger

data sets, discussed below, acquired from ambient temperature to 120 °C (except for CF₃COOH for which data were acquired only up to 70 °C for viscosity and 90 °C for conductivity).

Table 2.1 Density ρ , Molecular weight MW, Molar concentration C_0 , Viscosity η , and specific conductivity σ of the model acid compounds

	ρ (g cm ⁻³)	MW (g equiv ⁻¹)	C_0 (moles cm ⁻³)	η at 25 °C (cP)	σ at 25 °C (S cm ⁻³)
CF ₃ PO ₃ H ₂	1.85	150	1.23x10 ⁻²	----	---
(CF ₃) ₂ PO ₂ H	1.75	202	8.66x10 ⁻³	69	1.60x10 ⁻²
CF ₃ SO ₃ H ^[a]	1.70	150	1.13x10 ⁻²	4.0	6.60x10 ⁻²
CF ₃ COOH ^[b]	1.48	114	1.30x10 ⁻²	0.94	2.50x10 ⁻⁵

[a] Literature value for viscosity is 2.97 cP, and conductivity is 6.0 x 10⁻³ S cm⁻¹; Milne et

Ionic Conductivity and Fluidity: Ion transport and viscous flow have long been believed to be closely correlated processes in electrolytes. One clue to this correlation is the similarity that is commonly observed in Arrhenius activation energies for ionic conductivity and fluidity (inverse of viscosity) in dilute aqueous salt solutions. Dilute aqueous solutions of sodium chlorate¹⁹, sodium silicate²⁰ and sodium octanoate²¹ are elegant examples of this observation. This similarity is thought to reflect the fact that ion transport in such solutions is dominated by the vehicle mechanism, whereby ionic charge carriers move independently of each other in response to application of an electric field with transport rates ultimately set by a balance between electrostatic and viscous drag forces. Temperature dependencies (and particularly, activation energies) of conductivity and fluidity are expected to be similar because both are really variations of the viscous transport.

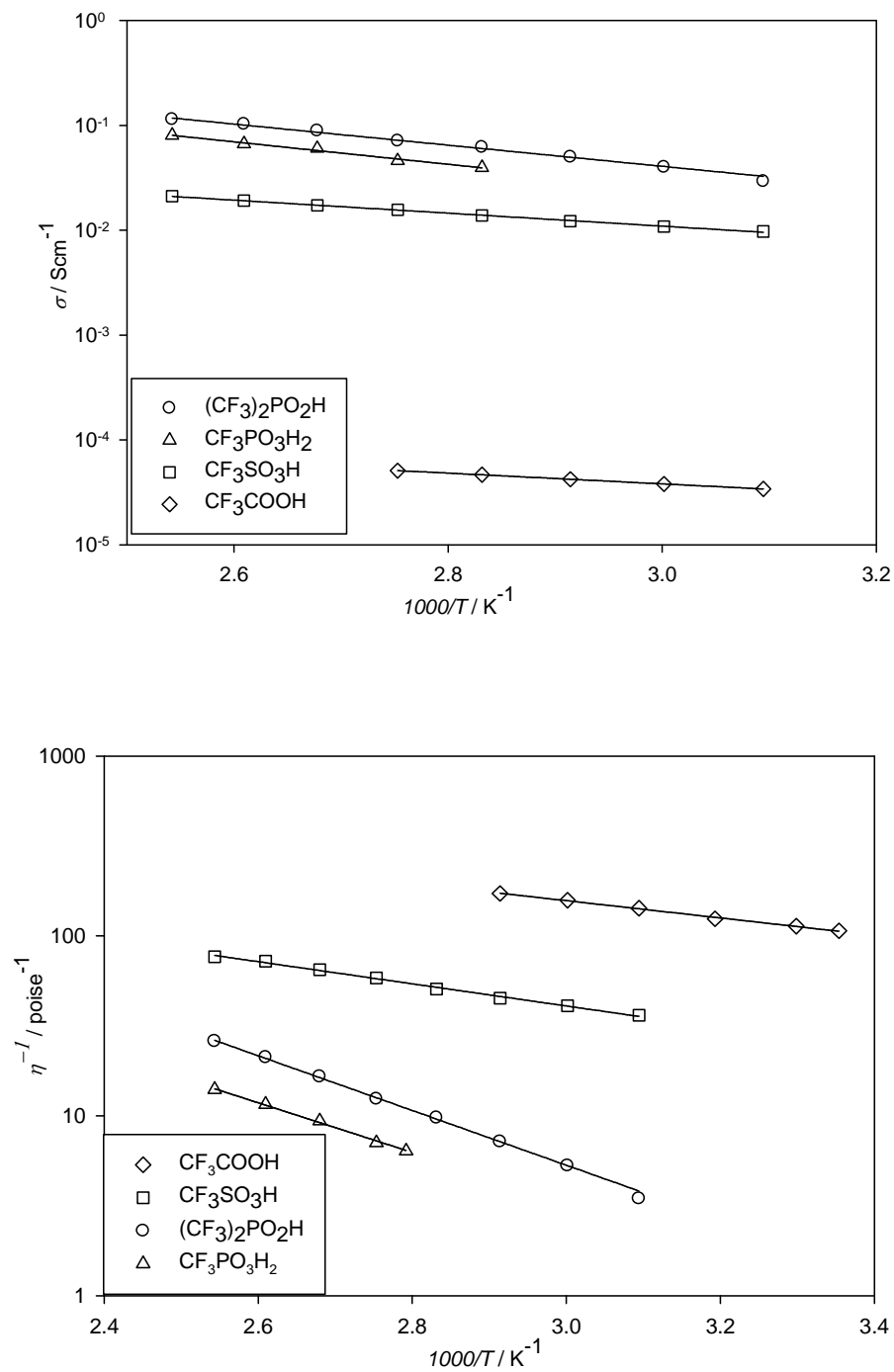


Figure 2.2 (top) The anhydrous conductivity data as a function of temperature (bottom) Fluidity vs temperature studies for the model compounds **1-4**

With this idea in mind, we sought to examine the temperature dependence of ionic conductivity and fluidity for our slate of model compounds. The results are presented in Figure 2.2 as Arrhenius plots of $\log(\text{conductivity})$ (top) and $\log(\text{fluidity})$ (bottom) versus inverse temperature. Several observations are immediately apparent. First, the decrease in conductivity over all temperatures follows the order $(\text{CF}_3)_2\text{PO}_2\text{H} > \text{CF}_3\text{PO}_3\text{H}_2 > \text{CF}_3\text{SO}_3\text{H} > \text{CF}_3\text{COOH}$. The two phosphorous-based acids have the highest anhydrous conductivities, higher even than neat triflic acid. The decrease in fluidity of the model compounds follows almost the opposite order; $\text{CF}_3\text{COOH} > \text{CF}_3\text{SO}_3\text{H} > (\text{CF}_3)_2\text{PO}_2\text{H} > \text{CF}_3\text{PO}_3\text{H}_2$. In general then, higher conductivities are associated with more viscous samples, which is opposite to the expectation from a simple vehicle model of ion conduction whereby charge carriers behave independently and their transport is limited by viscous drag. This situation is reminiscent of the situation in H_3PO_4 , which is also a highly viscous liquid with extraordinary ionic conductivity, which is due to the fact that 98% of the conductivity in H_3PO_4 is by structure diffusion.⁵

It is instructive to fit these data to Arrhenius relationships to obtain activation parameters. Both ionic conductivity and fluidity as a function of temperature follow *Arrhenius* behavior. The Arrhenius equations for conductivity and fluidity are given by equations 2.1 and 2.2 below.

$$\sigma = \sigma_0 \exp(-E_a^\sigma / RT) \quad \text{Equation 2.1}$$

$$\frac{1}{\eta} = \frac{1}{\eta_0} \exp(-E_a^\eta / RT) \quad \text{Equation 2.2}$$

In these equations σ and η are the conductivity and viscosity respectively, σ_0 and η_0 are constants associated with conductivity and viscosity, E_a^σ and E_a^η are activation energies for conductivity and fluidity, R is the universal gas constant, and T is temperature in degrees Kelvin. Best-fit parameters obtained from linear fitting for the conductivity and fluidity Arrhenius plots are listed in Table 2.2

Table 2.2 Best fit parameters for temperature dependant conductivity and fluidity of model acids

	σ_0 (S cm^{-1})	E_a^σ (kJ mol $^{-1}$)	η_0 (poise)	E_a^η (kJ mol $^{-1}$)
(CF $_3$) $_2$ PO $_2$ H	42.6	19.3	5.15×10^{-6}	29.0
CF $_3$ PO $_3$ H $_2$	42.3	20.5	2.2×10^{-5}	26.4
CF $_3$ SO $_3$ H	0.78	11.9	3.48×10^{-4}	11.8
CF $_3$ COOH	1.3×10^{-3}	9.8	2.2×10^{-4}	9.2

The close agreement between activation energies for conductivity and fluidity for trifluoroacetic and trifluoromethyl-sulfonic acids suggests that their conduction mechanism might be similar to the ion conduction mechanism in dilute aqueous salt solutions, namely, a vehicle mechanism involving transport of charge carriers by their motion in a viscous fluid, impeded by viscous drag. The lack of agreement between activation energies for conductivity and fluidity for the other two model acids (the two phosphorous-based acids) suggests that their ion conduction mechanism may not be simple vehicle-based ion transport. We believe that structure diffusion, i.e. proton hopping, is an important mode of proton transport in these acids, as discussed in more detail below.

Walden Plots : Another approach for considering the coupling between conductivity and fluidity in electrolytes is through the use of a Walden plot.²²⁻²⁴ This approach is based upon the classical

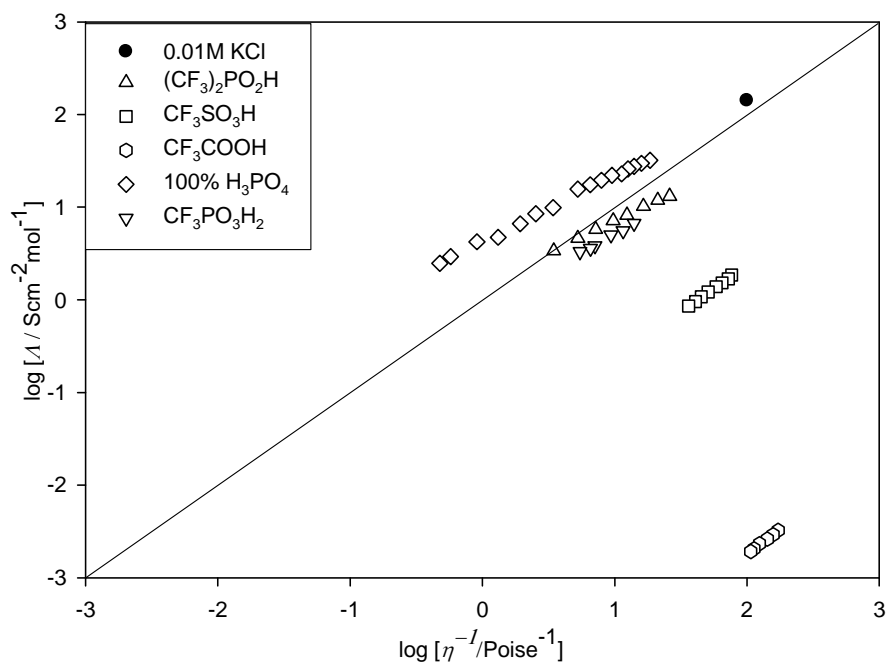


Figure 2.3 The Walden plot of the model compounds

Walden rule which states that for a fully dissociated, ideal electrolyte, the product of the limiting molar conductivity and the viscosity should be constant. The Walden plot is a log-log plot of limiting molar conductivity vs. fluidity. For a given electrolyte, the different points on the Walden plot usually correspond to viscosities and conductivities recorded at different temperatures. In such a case, a straight line in the Walden plot with a slope of unity indicates that the activation energies for viscosity and conductivity are similar. The position of the ideal Walden line may be estimated by forcing a line of slope unity through an experimental point that

closely approximates an ideal, fully dissociated electrolyte. In the plot in Figure 2, that point corresponds to aqueous 0.01 M KCl.

Molar conductivity is calculated from $\Lambda = \sigma_{\text{imp}}/C_0$ where σ_{imp} is the experimental conductivity and C_0 is the concentration of the model acid ($C_0 = \rho / M_w$ in mol cm⁻³ where ρ is the density M_w is the molecular weight of the model acid).

Figure 2.3 presents a series of Walden plots using data acquired at variable temperatures for the four model acid electrolytes studied in this work. The Walden lines of trifluoromethylsulfonic and trifluoroacetic acids lie well below the ideal Walden line. This finding probably indicates that these acids are not fully dissociated under anhydrous conditions, such that the molar concentration of charge carriers is much less than expected from the molar concentration of acid groups. Both lines display slopes near unity, which reflects the fact that the temperature dependencies of conductivity and fluidity are similar (i.e., they have similar activation energies). Thus, even though the conductivities in these acids are low, it is likely that they follow a vehicle mechanism for ion transport because they have the same activation energies for conductivity and fluidity.

The slope of a Walden plot for an electrolyte in which ionic conductivity is decoupled from fluidity or when the percent dissociation is a function of temperature, is often expected to be different from unity.²⁵ In many cases the ion transport mechanism is based on a structure-diffusion, Grotthuss-like hopping mechanism. As noted in the introduction, well-known system that behaves in this way is neat phosphoric acid.²⁶ In a situation like this, activation energy for conductivity is lower than that for fluidity because the movement of the ions is independent of viscous flow and follows a path that is more favorable energetically than viscous flow. Therefore the slope of the Walden plot will be less than unity.²⁴ Analysis of the Walden plot data presented

in Figure 2.3 for neat phosphoric acid (replotted from literature data taken from Chin and Chan²⁶) shows that it has a slope of 0.67 which reflects the fact that the activation energy for conductivity is lower than the activation energy for viscous flow. These results are consistent with the often-quoted idea that proton transport in neat phosphoric acid is based upon the Grotthuss mechanism of proton structure diffusion^{7,26}.

Walden plots for trifluoromethyl-phosphonic acid and bis(trifluoromethyl)-phosphinic acid lie relatively close to the ideal Walden line with slopes of 0.74 and 0.67 respectively. The slopes are approximately similar to the slope for neat phosphoric acid, and assuming that their ion populations do not change much as it is assumed with phosphoric acid, this reflects the fact that the ratio of activation energies for conductivity and fluidity are all less than one, and are similar for all three acids. The fact that these plots all lie close to the ideal Walden line could be interpreted to mean that these two phosphorous based acids behave as ideal electrolytes, for which ion concentrations are similar to the acid concentration (i.e. the acids are highly dissociated) and ion transport is by the vehicle mechanism. This view is however probably not exactly correct since if it were the case, then the Walden slope would be unity and activation energies for conductivity and fluidity would be similar.

Pulsed Field Gradient Nuclear Magnetic Resonance Spectroscopy Studies: Pulsed-field-gradient nuclear-magnetic-resonance (PFG- NMR) spectroscopy can provide information on the rate and mechanism of proton and conjugate base transport in acidic electrolytes. For example, Kreuer and coworkers showed that by measuring self-diffusion coefficients for all of the mobile ionic species of an acid system (e. g. for phosphoric acid by comparing proton (D_H) and anion (D_P) diffusion coefficient values) by PFG NMR the two transport mechanisms (vehicle and

Table 2.3 PFG-NMR diffusion coefficients (m^2/s) for the model acids at 20 and 85 °C

compound	At 20 °C			At 85 °C		
	$10^{10}D_{\text{H}}$	$10^{10}D_{\text{F}}$	$D_{\text{H}}/D_{\text{F}}$	$10^{10}D_{\text{H}}$	$10^{10}D_{\text{F}}$	$D_{\text{H}}/D_{\text{F}}$
$\text{CF}_3\text{PO}(\text{OH})_2$	[a]	[a]	[a]	1.12	4.98×10^{-1}	2.25
$(\text{CF}_3)_2\text{PO}(\text{OH})$	2.64	1.11	2.37	9.47	5.99	1.58
$\text{CF}_3\text{SO}_3\text{H}$	3.36	3.31	1.02	10.8	10.7	1.00
CF_3COOH	12.7	12.17	1.00	33.0	33.0	1.00

[a] This compound was a solid at room temperature

structure diffusion) can be differentiated.^{5,7} If the predominant proton transport mechanism is vehicle diffusion then the proton diffusion coefficient (D_{H}) will be similar to the conjugate base diffusion coefficient (D_{F}), i.e., $D_{\text{H}}/D_{\text{F}} = 1$. If however the predominant proton transport mechanism is Grotthuss-like proton hopping / structure diffusion then the proton diffusion coefficient will be significantly greater than the conjugate base diffusion coefficient, i.e. $D_{\text{H}}/D_{\text{F}} > 1$.

PFG-NMR experiments were performed at 20 °C and 85 °C on all four model acids. The self-diffusion coefficients for the proton and the perfluorinated anion (i.e. the conjugate base of the model acid) for all four model acids are listed in Table 2.3. The order of the decreasing anion diffusion coefficients (D_{F}) rates is consistent with the order of the decreasing fluidity trend observed for the model compounds, with the lowest diffusion coefficients belonging to the trifluoromethyl-phosphonic acid and bis(trifluoromethyl)-phosphinic acid which have the highest viscosities. This is an expected result if anion diffusion occurs by a vehicle mechanism. However, comparison of $D_{\text{H}}/D_{\text{F}}$ ratios for the model compounds shows that they all do not have

the same value; in particular, trifluoromethyl-phosphonic acid and bis(trifluoromethyl)-phosphinic acid both have $D_H/D_F > 1$ suggesting that proton transport is decoupled from perfluorinated anion transport in these acids. This finding also suggests that these two acids must have undergone a considerable degree of self-dissociation at the measured temperatures to allow for decoupled proton and anion transport. Faster proton diffusion also supports the idea that the Grotthuss mechanism is most likely the prevailing proton transport mechanism in these two acids. In contrast, the trifluoroacetic and trifluoromethyl-sulfonic acids show almost the same diffusion coefficient for the anion and proton (ie. $D_H/D_F = 1$). This finding is consistent with the idea that these two acids may have not undergone a considerable degree of dissociation, and the dominant ion transport mechanism is based on vehicular motion.

Table 2.4 Nernst-Einstein calculated conductivity σ_{cal} (Scm^{-1}), experimental conductivity obtained from Arrhenius plot σ_{meas} (Scm^{-1}), percent dissociation $\sigma_{meas}/\sigma_{cal}$ of the model acid compound

compound	At 20 °C			At 85 °C		
	σ_{nmr}	σ_{imp}	H_R	σ_{nmr}	σ_{imp}	H_R
$\text{CF}_3\text{PO}(\text{OH})_2$	[a]	[a]	[a]	6.25×10^{-2}	4.33×10^{-2}	1.4
$(\text{CF}_3)_2\text{PO}(\text{OH})$	1.24×10^{-1}	1.98×10^{-2}	6.2	4.13×10^{-1}	6.53×10^{-2}	6.3
$\text{CF}_3\text{SO}_3\text{H}$	2.89×10^{-1}	6.10×10^{-3}	38.7	7.62×10^{-1}	1.47×10^{-2}	51.8
CF_3COOH	1.21	2.34×10^{-5}	$4.2 \times 10^{+4}$	2.68	4.87×10^{-5}	5.5×10^4

[a] This compound was a solid at room temperature

Nernst-Einstein Relation and Haven ratio: The Nernst-Einstein equation relates the conductivity of an electrolyte to the concentration and diffusion coefficients of charge carriers. As shown in Equation 3 below, the Nernst-Einstein equation may be used to calculate the total conductivity expected from the self-diffusion coefficients of protons and anions obtained from PFG-NMR experiments

$$\sigma_{\text{nmr}} = \frac{z^2 F^2}{RT} C_0 [D_{\text{H}} + D_{\text{F}}] \quad \text{Equation 2.3}$$

In this equation, σ_{nmr} is the total ionic conductivity expected from self-diffusion coefficients, C_0 denotes the molar concentration of the acid (given by density / MW, mol cm⁻³), D_{F} and D_{H} are the diffusion coefficients of the conjugate base and proton in the model acids, z is the valence of the ions which in this case is 1, and F , R and T have their usual meaning. In many cases the ionic conductivity measured experimentally using impedance spectroscopy (σ_{imp}) is significantly lower than the σ_{nmr} value estimated using Equation 2.3. This difference is due to at least three factors. First, neutral species (i.e. un-dissociated acids or ion pairs) diffuse but they contribute little or not at all to σ_{imp} . Second, neutral species can diffuse faster than ionic species due to their lack of charge and lower solvated size. Third, at high ion concentrations ion motion becomes correlated due to ion-ion interactions that fall short of formal ion pairing but still contribute to reducing ion mobilities. All of these factors contribute to measured conductivities being lower than expected from measured diffusivities.

When ionic species are bound the diffusion process becomes highly correlated to avoid energetically unfavorable charge separation. These correlations are expressed by the Haven ratio $H_{\text{R}} = D_{\text{nmr}}/D_{\sigma}$ ²⁷. Here $D_{\text{nmr}} = D_{\text{H}} + D_{\text{F}}$, the sum of experimentally determined self-diffusivities of D_{H} and D_{F} given in Table 2.3, and D_{σ} is a self-diffusivity calculated as $D_{\sigma} = RT\sigma_{\text{imp}}/F^2C_0$. Using

equation 2.3 and D_{σ} as described above, the Haven ratio may also be written as a ratio of the conductivity calculated from PFG-NMR to the experimental conductivity as determined by impedance spectroscopy. Haven ratios calculated in this way are given in Table 2.4 for the model acids studied in this work. A Haven ratio near unity (1.4) was found for $\text{CF}_3\text{PO}_3\text{H}_2$, values near 6 were found for $(\text{CF}_3)_2\text{PO}_2\text{H}$, values near 50 were found for $\text{CF}_3\text{SO}_3\text{H}$, and very high values (above 10^4) were found for CF_3COOH . For the latter two acids the high Haven ratios almost certainly reflect a relatively low degree of dissociation of the acids and a correspondingly low concentration of charge carriers, perhaps coupled with a slightly higher diffusivity for the neutral species than for the charged species due to their different sizes. Effects of ion-ion correlations are likely to be lower in this case because ion concentrations are relatively low. For the phosphorous acids the variations of Haven ratios from unity are probably dominated by a combination of incomplete dissociation and ion-ion interactions. Without independent information on the degree of dissociation, which is not available for these acids, it is impossible to say how much of the decrease in experimental conductivity is due to incomplete dissociation vs. ion-ion correlations.

It is instructive to compare these Haven ratios with values for other phosphorous-based acids. Haven ratios for H_3PO_4 have been reported to vary between 1.5 and 1.7⁵ and values for H_3PO_3 vary between 2.5 and 3.0²⁸. These values are reasonably close to those for the fluoroalkylated phosphorous-based acids studied in this work. Significantly, in all cases the ratios for the phosphonic acids were lower than those for the phosphinic acids, which suggest that the degree of dissociation of the phosphonic acids is probably higher than that for the phosphinic acids.

Hammett acidities of the model compounds: Finally, we have measured acid strengths for the four model acids to learn about the relationship between simple acid strength and anhydrous ionic conductivity. Hammett acidity is a measure of acid strength of a concentrated acid, usually in the absence of water. The Hammett acidity function, H_0 , is defined as follows:

$$H_0 = pK_a - \log[BH^+]/[B]$$

Equation 2.4

In this equation BH^+ and B are the protonated and unprotonated forms of an indicator base, and pK_a is taken as at the standard state in water. Mesityl oxide was used as the indicator in this study as described by Farcasiu and Ghenciu.^{16,17} The method describes that the ^{13}C NMR chemical shift difference ($\Delta\delta$) between the C_α and C_β carbon atoms of mesityl oxide increases with increasing degree of protonation and a graph of ($\Delta\delta$) vs concentration of mesityl oxide has a linear form. From this graph the y-axis intercept of the chemical shift difference ($\Delta\delta^0$) was taken as the value that corresponds to the H_0 value of the acid. The calibration curve of ($\Delta\delta^0$) vs H_0 presented by Farcasiu and Ghenciu was then used to establish the H_0 values for the model acids investigated in this paper. Hammett acidity values found for all the model acids are presented in Table 2.5.

Table 2.5 Hammett acidities of model acids

compound	Hammett Acidity(Exp.)	Hammett Acidity(Lit.)
CF ₃ COOH	-3.03	-3.03 ^{16,17}
CF ₃ PO ₃ H ₂	-7.10	
(CF ₃) ₂ PO ₂ H	-7.95	
CF ₃ SO ₃ H	-13.70	-14.6 ^{17,29}

The more negative values of H_0 correspond to a higher acidity of the compound. Therefore in Table 5, the weakest acid is trifluoroacetic acid and strongest acid is trifluoromethyl-sulfonic acid. Our experimentally obtained values for these two acids are in relatively good agreement with values reported in the literature. The two perfluorinated phosphonic and phosphinic acid model compounds have intermediate acid strength on this scale and they are slightly more acidic than phosphoric acid which has a Hammett acidity of -6.25 .¹⁶ This finding is consistent with the expected action of perfluoroalkyl substituents which are electron withdrawing and should stabilize conjugate bases thereby increasing acid strength. Thus, it appears that no direct correlation can be drawn between the acidity of the model compounds and their anhydrous ionic conductivity.

Conclusion

Perfluoroalkyl phosphonic and phosphinic acids provide high conductivity under anhydrous conditions despite their low fluidity. Both of these acid types display a high degree of self-dissociation. Proton conduction in the two phosphorous-based acids occurs by a Grotthuss-like proton hopping mechanism. Perfluoroalkyl sulfonic and carboxylic acids do not dissociate

considerably under anhydrous conditions and show relatively low anhydrous ionic conductivity. Perfluoroalkylated phosphonic and phosphinic acids exhibit Hammett acidity intermediate between that of perfluorinated sulfonic and carboxylic acids with no apparent correlation between conductivity and acidity.

Acknowledgements

This work was funded by the United States Department of Energy (US DOE) hydrogen program grant number DE-FG36-06GO16031.

Keywords: Proton conductors · Fluoroalkyl Acid· Activation Energies · Grotthuss mechanism· Vehicle mechanism

References

- (1) Kreuer, K.D.;Rabenau, A.;Weppner, W. *Angew. Chem., Int. Ed. Engl.* **1982**, 21, 208-209.
- (2) Colomban, P. *Chemistry of Solid State Materials: Proton Conductors*; Cambridge University Press, **1992**.
- (3) Kreuer, K.D.;Paddison, S.J.;Spohr, E.;Schuster, M. *Chem. Rev.* **2004**, 104, 4637-4678.
- (4) Perrin, J.C.;Lyonnard, S.;Volino, F. *J. Phys. Chem. C* **2007**, 111, 3393-3404.
- (5) Dippel, T.;Kreuer, K.D.;Lassègues, J.C.;Rodriguez, D. *Solid State Ionics* **1993**, 61, 41-46.
- (6) Schuster, M.;Rager, T.;Noda, A.;Kreuer, K.D.;Maier, J. *Fuel Cells* **2005**, 5, 355-365.
- (7) Dippel, T.;Kreuer, K.D. *Solid State Ionics* **1991**, 46, 3-9.

- (8) Kotov, S.V.;Pedersen, S.D.;Qiu, W.;Qiu, Z.-M.;Burton, D.J. *J. Fluorine Chem.* **1997**, 82, 13-19.
- (9) Kato, M.;Akiyama, K.;Yamabe, M. *Reports Res. Lab. Asahi Glass Co. Ltd* **1983**, 33, 135.
- (10) Allcock, H.R.;Hofmann, M.A.;Ambler, C.M.;Lvov, S.N.;Zhou, X.Y.;Chalkova, E.;Weston, J. *J. Membr. Sci.* **2002**, 201, 47-54.
- (11) Jakoby, K.;Peinemann, K.V.;Nunes, S.P. *Macromol. Chem. Phys.* **2003**, 204, 61-67.
- (12) Lafitte, B.;Jannasch, P. *Adv. Funct. Mater.* **2007**, 17, 2823-2834.
- (13) Lafitte, B.;Jannasch, P. *J. Polym. Sci., Part A: Polym. Chem.* **2007**, 45, 269-283.
- (14) Schmutzler, R. *Chem. Ber.* **1965**, 98, 552-6.
- (15) Farooq, O. *J. Chem. Soc., Perkin Trans. 1* **1998**, 839-840.
- (16) Farcasiu, D.;Ghenciu, A. *J. Am. Chem. Soc.* **1993**, 115, 10901-10908.
- (17) Farcasiu, D.;Ghenciu, A. *Prog. Nucl. Magn. Reson. Spectrosc.* **1996**, 29, 129-168.
- (18) Corkum, R.;Milne, J. *Can. J. Chem.* **1978**, 56, 1832-5.
- (19) Campbell, A.N.;Kartzmark, E.M.;Oliver, B.G. *Can. J. Chem.* **1966**, 44, 925-34.
- (20) Ukihashi, H. *Bull. Chem. Soc. Jpn.* **1957**, 30, 470-6.
- (21) Campbell, A.N.;Kartzmark, E.M.;Lakshminarayanan, G.R. *Can. J. Chem.* **1962**, 40, 839-44.
- (22) Angell, C.A.;Byrne, N.;Belieres, J.-P. *Acc. Chem. Res.* **2007**, 40, 1228-1236.
- (23) Xu, W.;Cooper, E.I.;Angell, C.A. *J. Phys. Chem. B* **2003**, 107, 6170-6178.
- (24) Yoshizawa, M.;Xu, W.;Angell, C.A. *J. Am. Chem. Soc.* **2003**, 125, 15411-15419.
- (25) Mclin, M.G.;Angell, C.A. *J. Phys. Chem.* **1991**, 95, 9464-9469.
- (26) Chin, D.;Chang, H. *J. Appl. Electrochem.* **1989**, 19, 95-99.

- (27) Reiche, A.;Cramer, T.;Fleischer, G.;Sandner, R.;Sandner, B.;Kremer, F.;Karger, J. *J. Phys. Chem. B* **1998**, 102, 1861-1869.
- (28) Schuster, M.;Kreuer, K.D.;Steininger, H.;Maier, J. *Solid State Ionics* **2008**, 179, 523-528.
- (29) Olah, G.A.;Prakash, G.K.S.;Sommer, J. *Science (Washington, DC, United States)* **1979**, 206, 13-20.

Supporting Information

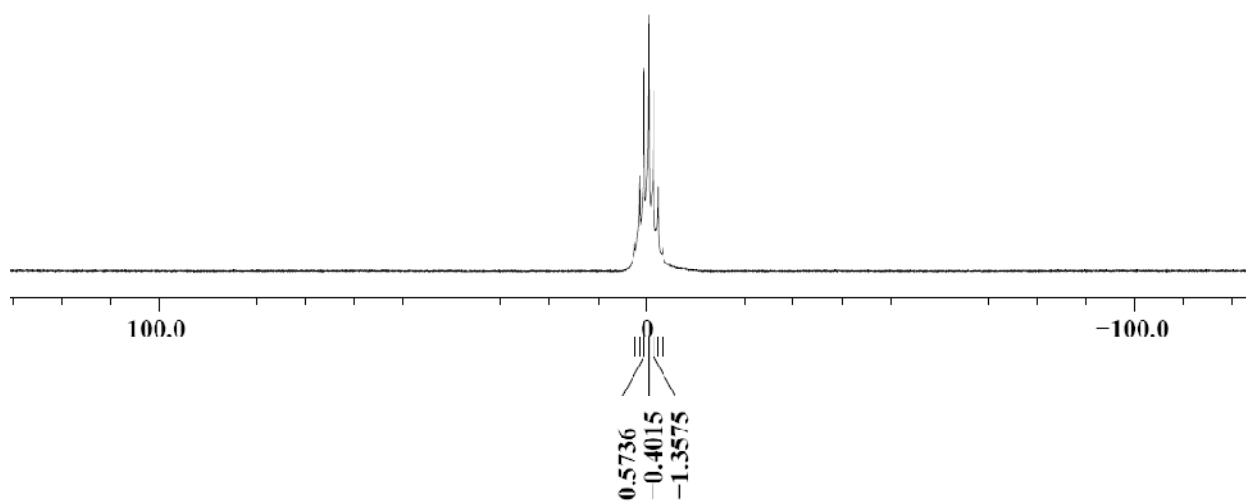


Figure 2.4 ^{31}P NMR spectrum of neat $(\text{CF}_3)_2\text{PO}_2\text{H}$ compound locked with an external lock solvent

CHAPTER THREE

THE EFFECT OF THE PERFLUOROALKYL CHAIN LENGTH ON THE PROTON CONDUCTION OF FLUOROALKYLATED PHOSPHONIC, PHOSPHINIC AND SULFONIC ACIDS

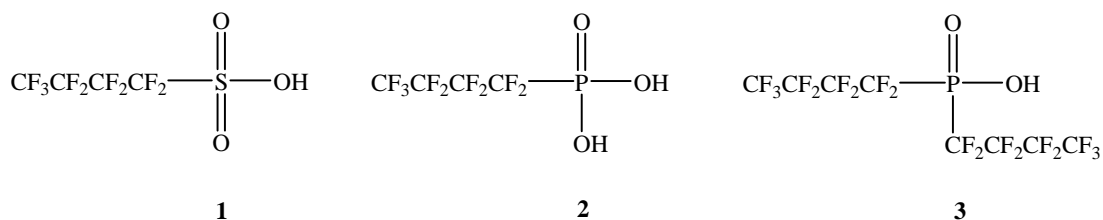
Introduction

The most commonly used proton exchange membrane (PEM) materials for fuel cells are based on a sulfonic acid functionalized polymers such as Nafion, Flemion and or Aciplex.¹ These polymers do not function well at temperatures above 80 °C and at low humidity. Therefore substituting the sulfonic acid group with a phosphonic acid group as an alternative protogenic moiety to construct these polymers have been intensely discussed in the literature.²⁻⁵

We recently reported ⁶ in a model study that involved 1) $\text{CF}_3\text{SO}_3\text{H}$ 2) $\text{CF}_3\text{PO}_3\text{H}_2$, 3) $(\text{CF}_3)_2\text{PO}_2\text{H}$ and 4) CF_3COOH that the two phosphorous based acid compounds shows the highest conductivity under anhydrous conditions at all temperatures ($T < 120$ °C). Further, we showed that both these phosphorous-based model compounds displayed a very high degree of self-dissociation. In addition, the proton conduction in these two model compounds was shown to occur primarily by a Grotthuss-like proton hopping mechanism. In contrast, under anhydrous conditions the sulfonic and carboxylic acid model compounds had a relatively low ionic conductivity and showed relatively little dissociation.

For PEM polymers containing side chains terminating with sulfonic acid, it has been reported^{7,8} that depending on the length of the side-chain these polymers exhibit different macroscopic properties in terms of proton conductivity and membrane morphology. To study the effect of the length of the perfluoroalkyl chain on the type of the protogenic group, the the

trifluoromethyl group of the short chain model compounds of $\text{CF}_3\text{SO}_3\text{H}$, $\text{CF}_3\text{PO}_3\text{H}_2$ and $(\text{CF}_3)_2\text{PO}_2\text{H}$ were replaced with a longer chain perfluorobutyl group. The chemical structures of the model compounds with this longer perfluoroalkyl chain are shown in Scheme 3.1. They are as follows: (1) perfluorobutyl sulfonic acid, (2) perfluorobutyl phosphonic acid and (3) bisperfluorobutyl phosphinic acid. These compounds were investigated for molecular properties such as diffusivity and viscosity that influence proton conductivity as described previously for the short-chain analogs.⁶ In this chapter we discuss the structure-property relationships for the shorter vs. Longer-chain model compounds. This work can help to better understand and develop polymers with optimal conductivities for fuel-cell membrane applications.

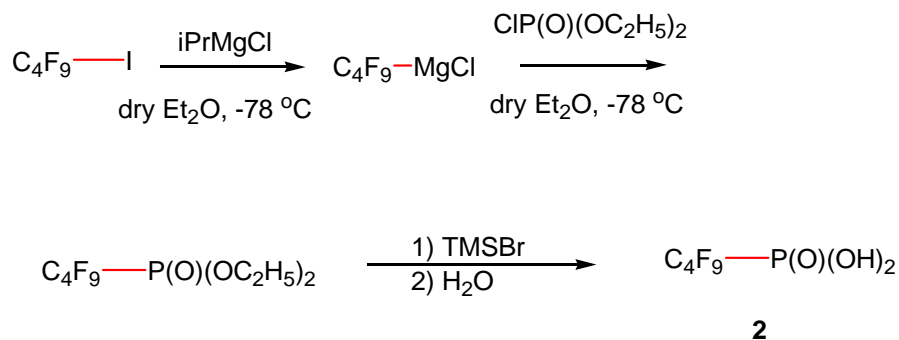


Scheme 3.1 The chemical structures of model acids. **1**-perfluorobutyl sulphonic acid **2**-perfluorobutyl phosphonic acid, **3**-bisperfluorobutyl phosphinic acid

Experimental Section

Materials and reagents: Unless otherwise noted, starting materials were obtained from commercial suppliers and used without further purification. Acetonitrile was dried by storing over KOH overnight and distilling from P_2O_5 . Perfluorobutyl sulfonic acid (1) (Aldrich 98+ %) was obtained from a commercial supplier and used without further purification. ^1H , ^{19}F , and ^{31}P NMR spectra were recorded on a NMR instrument at 300.3, 282.2, and 121.5 MHz respectively, using CD_3CN as the solvent except where noted.

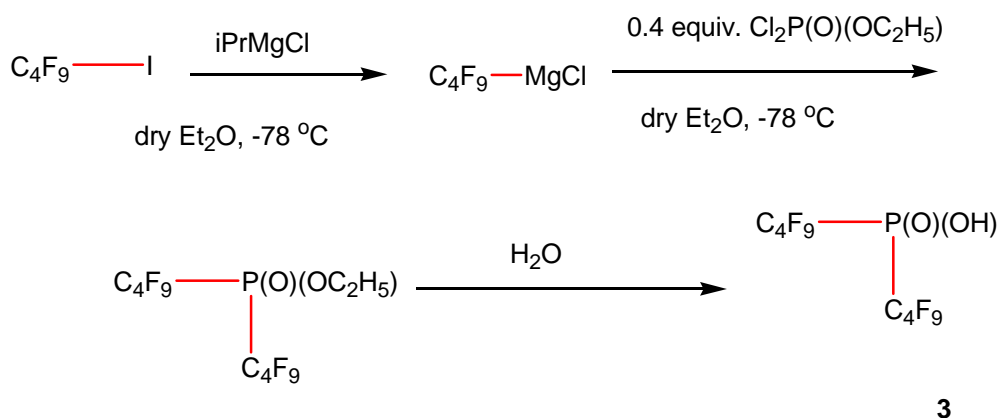
Analytical procedures: Proton conductivity, viscosity, density, pulse field gradient nuclear magnetic resonance (PFG NMR) studies at 85 °C and Hammett acidity measurements were determined as previously described by us in the experimental section of references 6 and in chapter 2 of this dissertation.



Scheme 3.2 Synthesis of *n*-perfluorobutyl phosphonic acid

n-Perfluorobutyl phosphonic acid (**2**): Under an argon atmosphere, isopropyl magnesium chloride (2M in diethyl ether, 5.80 mL, 11.56 mmol) was added dropwise to a perfluorobutyl iodide solution (4.0 g, 11.56 mmol) in dry diethyl ether (20 mL) at -78 °C. The solution was stirred at this temperature for 1 h to allow exchange to take place. Diethyl chlorophosphate (1.80 g, 11.56 mmol) was then added slowly by syringe at -78 °C. The mixture was maintained at -78 °C for 1 h and then allowed to warm to room temperature overnight. The reaction was quenched with 5 mL of 3M ice-cold HCl. The ether layer was separated and dried with Na₂SO₄. The ether was filtered and concentrated on a rotary evaporator. The residue was mixed with excess bromotrimethylsilane (3.72 g, 24.2 mmol) and stirred at room temperature for 12 h. When the reaction was completed the flask was cooled to room temperature and ethyl bromide and excess

silylating reagent were removed by rotary evaporation at reduced pressure. The silylated ester was hydrolyzed with water (10 mL). After hydrolysis 0.1 g of charcoal and water (2 mL) was added and the mixture was stirred for 2 h at room temperature. The charcoal was filtered and filtrate was extracted with ether (3 x10 mL) and dried over Na₂SO₄. The ether was filtered and rotary evaporated to yield colorless oil. The oil was dried at 60 °C under dynamic vacuum for 48 h to yield (2.50 g, 8.33 mmols, 72% based on perfluorobutyl iodide) of perfluorobutyl phosphonic acid. ¹H NMR (300 MHz, CD₃CN): 10.8 (br, 2H, PO₃H₂). ¹⁹F NMR (282.7 MHz, CD₃CN): - 80.7 (s, 3F, CF₃, J_{FCP} = 107.4 Hz), -121.4 (s, 2F, CF₂), -122.9 (d, -CF₂P, J_{PCF} = 81.8 Hz), -125.7 (s, 2F, -CF₂-CF₂P), ³¹P NMR (121.5 MHz, CD₃CN): -1.92 (t, J_{PCF} = 81.8 Hz).



Scheme 3.3 Synthesis of bisperfluorobutyl phosphonic acid

Bis(n-perfluorobutyl)phosphinic acid(3): Under an argon atmosphere, isopropyl magnesium chloride (2M in diethyl ether, 7.2 mL, 14.4 mmol) was added dropwise to a perfluorobutyl iodide solution (4.9 g, 14.4 mmol) in dry diethyl ether (20 mL) at $-78\text{ }^{\circ}\text{C}$. The solution was stirred at this temperature for 1 h to allow exchange to take place. Dichloroethylphosphate (0.94 g, 5.78 mmol) was then added slowly by syringe at $-78\text{ }^{\circ}\text{C}$. The mixture was maintained at $-78\text{ }^{\circ}\text{C}$ for 1 h and then allowed to warm to room temperature overnight. The reaction was quenched by adding 5 mL of 3M ice cold HCl and the mixture was stirred at room temperature for 1 h. After hydrolysis was complete, 0.1 g of charcoal (2 mL) was added and the mixture was further stirred for 2 h at room temperature. The charcoal was filtered and filtrate was extracted with ether (3 x10 mL) and dried over Na_2SO_4 . The ether was filtered and rotary evaporated to yield a colorless oil. The oil was dried at $60\text{ }^{\circ}\text{C}$ under dynamic vacuum for 48 h to yield (2.17 g, 4.32 mmol, 60% based on perfluorobutyl iodide) of bis(n-perfluorobutyl) phosphinic acid. ^1H NMR (300 MHz, CD_3CN): 10.8 (br, 2H, PO_3H_2). ^{19}F NMR (282.7 MHz, CD_3CN): - 81.6 (s, 3F, CF_3), -121.2 (s, 2F, CF_2), -122.0 (d, $-\text{CF}_2\text{P}$, $J_{\text{FCP}} = 81.8\text{ Hz}$), -126.3 (s, 2F, $-\text{CF}_2-\text{CF}_2\text{P}$), ^{31}P NMR (121.5 MHz, CD_3CN): -0.07 (t, $J_{\text{PCF}} = 88.8\text{ Hz}$).

Results and Discussion

Table 3.1 presents a selected set of physical properties of the three model compounds at $25\text{ }^{\circ}\text{C}$. C_0 represents the molar concentration of molecular acids calculated using the measured density and calculated molar mass for the acids.

Table 3.1 Density ρ , Molecular weight MW, Molar concentration C_0 , Viscosity η , and specific conductivity σ of the model acid compounds

	ρ (g cm ⁻³)	MW (g equiv ⁻¹)	C_0 (moles cm ⁻³)	η at 25 °C (cP)	σ at 25 °C (S cm ⁻¹)
C ₄ F ₉ SO ₃ H	1.80	300	6.0x10 ⁻³	21.8	9.20x10 ⁻⁴
C ₄ F ₉ PO(OH) ₂	1.85	300	6.2x10 ⁻³	84.0	7.90x10 ⁻⁴
(C ₄ F ₉) ₂ PO(OH)	1.76	502	3.5x10 ⁻³	198.2	5.86x10 ⁻⁵

Ionic conductivity and fluidity: The conductivity and fluidity data shown in Figure 3.1 (top) and Figure 3.1 (bottom) respectively includes data for the model compounds listed in Table 3.1 and also for those studied in chapter 2. The conductivities and fluidities of all the model compounds, irrespective of their perfluoroalkyl chain length follow Arrhenius behaviour at all investigated temperatures. The best-fit parameters for the model compounds can be found in the supporting information section.

Increasing the perfluoroalkyl chain length of the short-chain model compounds always leads to a decrease in conductivity. The conductivity of longer-chain C₄F₉PO₃H₂ has decreased by approximately an order of magnitude compared to its shorter-chain analog CF₃PO₃H₂ and the conductivity of (C₄F₉)₂PO₂H has decreased by approximately two orders of magnitude compared to (CF₃)₂PO₂H. Figure 3.2 shows the how proton conductivity and fluidity vary with fluorine to proton content (F/H ratio) for the model compounds. All the phosphorous based-acids except for (CF₃)₂PO₂H show a decreasing proton conductivity with increasing ratio of fluorine to

proton content. Figure 3.2 (bottom) shows that the fluidity of phosphorous based compounds is fairly independent of the length of the perfluoroalkyl chain.

However, for sulfonic based acids as Figure 3.2 shows, both the proton conductivity and the fluidity are decreasing with the increasing perfluoroalkyl chain length. In reference 6 we showed that the proton conductivity of sulfonic acid is governed by its fluidity because the charge carriers move by a vehicle mechanism. Increasing the perfluoroalkyl chain length lowers fluidity and therefore we can expect the proton conductivity to decrease by the same factor that was observed for fluidity if the percent dissociation of acid remains the same for both these model compounds. Comparison of the conductivity and fluidity data for the sulfonic acids at 85 °C shows that the fluidity of $C_4F_9SO_3H$ has decreased by about 2.2 times and the conductivity has decreased by about 4.2 times compared to CF_3SO_3H . The greater decrease in conductivity for $C_4F_9SO_3H$ than expected from the change in fluidity could be due to lower mobility of the ions because of the larger size of the anions and/or lower carrier charge concentration, perhaps due to a lower degree of dissociation.

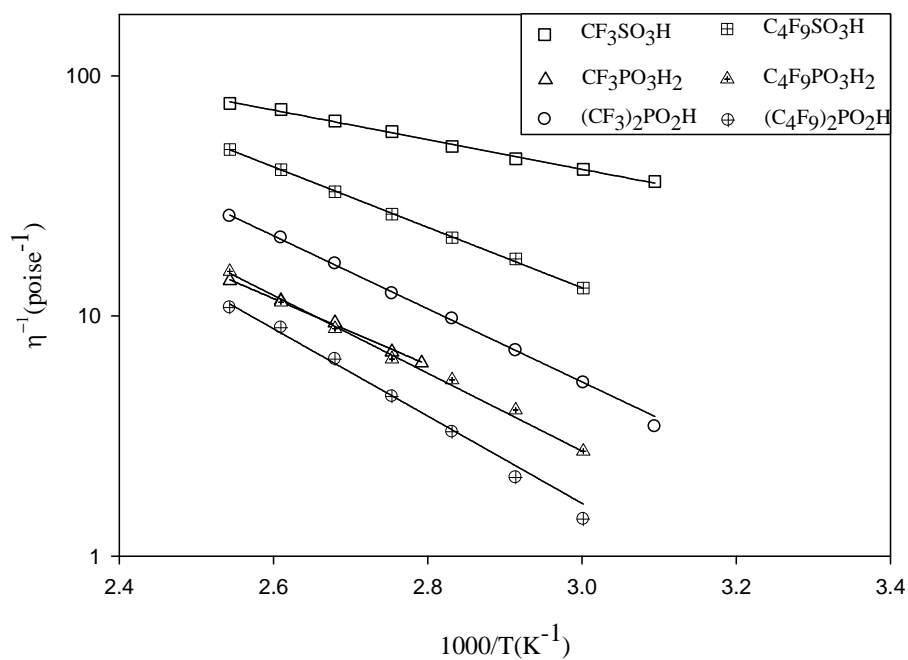
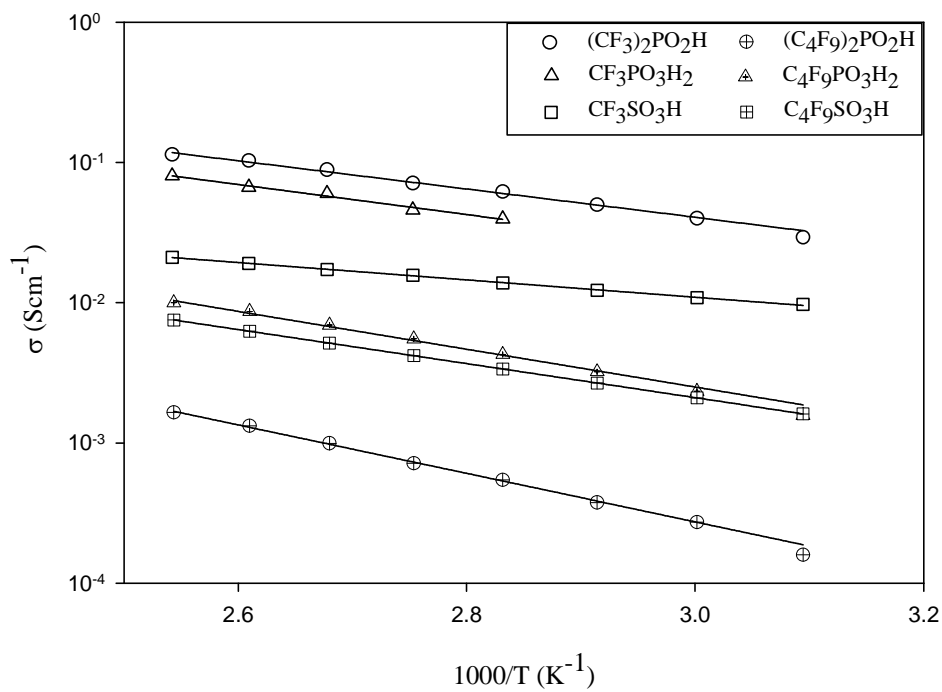


Figure 3.1(top) anhydrous conductivity data as a function of temperature (bottom) fluidity vs temperature studies for the model compounds **1-3** compared with their short chain analogs

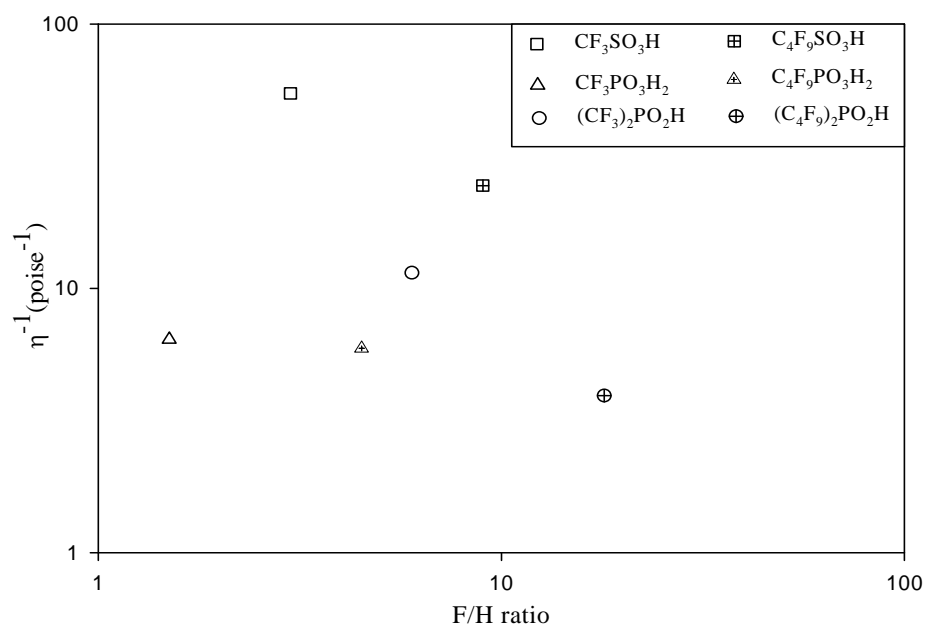
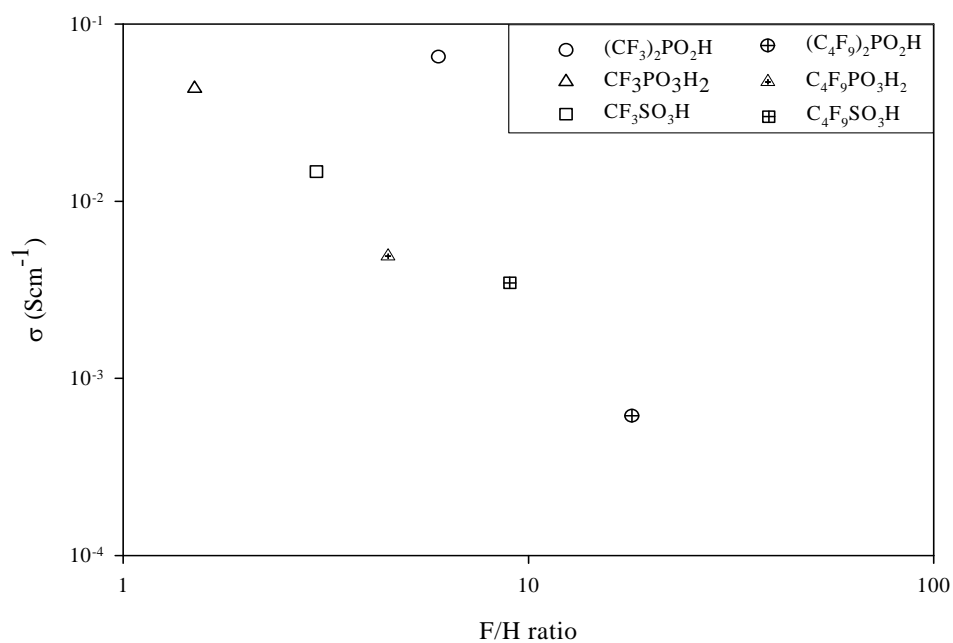


Figure 3.2 (top) conductivity data as a function of F/H ratio (bottom) fluidity vs. F/H ratio; for all the short and longer chain model compounds

Walden Plots: The relationship between conductivity and viscosity may be viewed through the use of the Walden plot. As discussed in reference 6, the Walden plot of a system that obeys Waldens rule ($\Lambda \cdot \eta = \text{constant}$), will have a slope of unity and therefore its Walden plot line will be parallel to the ideal KCl line.

Figure 3.3 presents Walden plot lines for all the short and longer chain model compounds of sulfonic and phosphorous based acids discussed in the previous section.

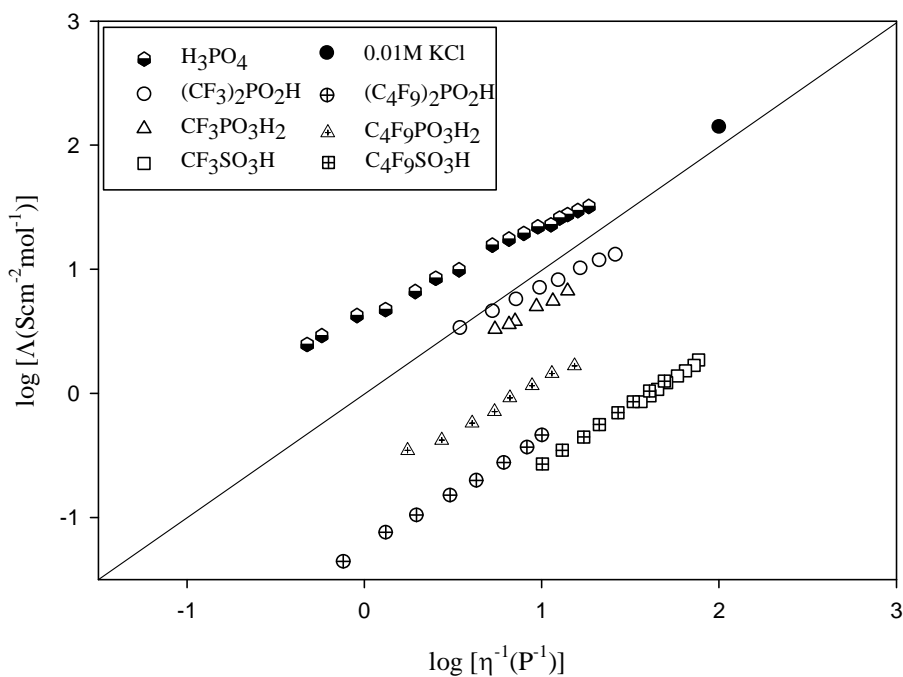


Figure 3.3 Walden plot for the model acids

A slope of unity was found with long chain sulfonic acid, as it was previously found with its short chain analogue in chapter 2 indicating that sulfonic acids obey the classical Walden rule.

A slope less than unity in the Walden line indicates that the system does not obey the classical Waldens rule. A slope of less than unity can also occur if the dissociated carrier concentration changes significantly as a function of temperature. However, previously we showed that the deviations from a slope of unity in Walden plots occurs in perfluorinated phosphorous-based acids because of the special proton transport mechanism (proton hopping/Grotthuss mechanism) present in them and not due to carrier concentration changes as a function of temperature. Specifically Grotthuss-type hopping occurs with a lower activation energy than vehicle transport, so the contribution of proton hopping to transport changes as the temperature changes.

The Walden plots for $C_4F_9PO_3H_2$ and $(C_4F_9)_2PO_2H$ yield slopes of 0.77 and 0.92 respectively. The slope for $C_4F_9PO_3H_2$ is approximately similar to what was observed previously for $CF_3PO_3H_2$ (0.74) and for H_3PO_4 ⁹, which suggests that hopping transport is important for this acid. However, the Walden slope for $(C_4F_9)_2PO_2H$ is significantly higher than what was observed for its short-chain analogue (0.67). A value (0.92) closer to unity for this compound suggests the presence of a significant degree of vehicle transport mechanism.

The position of a Walden line on the Walden plot depends upon the product of the mobility of the charge carriers and their concentrations. Sulfonic acids have the highest mobilities (see Table 3.2 diffusion coefficient data) , but their Walden lines appear all below the phosphorous-based acids suggesting that its conductivity is the lowest. This can be true only if sulfonic acids are the least dissociated of all the model acids studied.

For phosphorous-based acids it can also be shown that the position of the Walden line indicates the percent dissociation of acid. In reference 6 we showed that the ionic conductivity in perfluoroalkyl phosphorous and phosphinic acids occur by proton hopping/structure diffusion

mechanism. Therefore, protons carry most of the charge. Hence the mobility of the protons and the concentration of the protons of a phosphorous based acid become the deciding factor compared to anions in determining the position of the Walden line in the Walden plot.

Comparison of the self-diffusion coefficients of protons of the $\text{CF}_3\text{PO}_3\text{H}_2$, $\text{C}_4\text{F}_9\text{PO}_3\text{H}_2$, and $(\text{C}_4\text{F}_9)_2\text{PO}_2\text{H}$ (see below) indicates that their differences are smaller than the differences in molar conductivities observed in the Walden plot lines. The self-diffusion coefficient of a proton is proportional to the mobility of the proton. So this suggests that the difference in proton mobilities alone can not account for their large differences in conductivities. This observation therefore implies that their ion concentrations must also be involved and must also follow this trend $\text{CF}_3\text{PO}_3\text{H}_2 > \text{C}_4\text{F}_9\text{PO}_3\text{H}_2 > (\text{C}_4\text{F}_9)_2\text{PO}_2\text{H}$ from highly dissociated $\text{CF}_3\text{PO}_3\text{H}_2$ to very low dissociated $(\text{C}_4\text{F}_9)_2\text{PO}_2\text{H}$. In reference 6 we showed that $(\text{CF}_3)_2\text{PO}_2\text{H}$ is less dissociated than $\text{CF}_3\text{PO}_3\text{H}_2$. Thus, the general trend is that acid dissociation is greater in fluoroalkyl phosphonic acids than in bis(fluoroalkyl)phosphinic acids, irrespective of fluoroalkyl chain length.

Pulsed-Field-Gradient Nuclear Magnetic Resonance Spectroscopy Studies: Using ^1H and ^{19}F pulsed field gradient NMR spectra the diffusion coefficients of proton (D_{H}) and its conjugate base (D_{F}) can be measured. PFG-NMR experiments were performed at 85 °C. The results of model acids are listed in Table 3. The decrease in $D_{\text{H}}/D_{\text{F}}$ ratio of the model compounds follows the order $\text{CF}_3\text{PO}_3\text{H}_2 > \text{C}_4\text{F}_9\text{PO}_3\text{H}_2 > (\text{CF}_3)_2\text{PO}_2\text{H} > (\text{C}_4\text{F}_9)_2\text{PO}_2\text{H}_2 > \text{CF}_3\text{SO}_3\text{H} = \text{C}_4\text{F}_9\text{SO}_3\text{H}$. In the Walden plot section we showed that the decrease in percent dissociation follows almost the same order with the exception of $(\text{CF}_3)_2\text{PO}_2\text{H}$; $\text{CF}_3\text{PO}_3\text{H}_2 > \text{C}_4\text{F}_9\text{PO}_3\text{H}_2 > (\text{C}_4\text{F}_9)_2\text{PO}_2\text{H}_2 > \text{CF}_3\text{SO}_3\text{H} = \text{C}_4\text{F}_9\text{SO}_3\text{H}$. Therefore generally we can assume that

the D_H/D_F ratio is indicative of the percent degree of self-dissociation. Based on this assumption the degree of dissociation of $(CF_3)_2PO_2H$ is intermediate to $C_4F_9PO_3H_2$ to $(C_4F_9)_2PO_2H_2$.

Table 3.2 PFG-NMR diffusion coefficients (m^2/s) for the model acids at 85 °C

compound	At 85 °C		
	$10^{10}D_H$	$10^{10}D_F$	D_H/D_F
CF_3SO_3H	10.80	10.70	1.00
$CF_3PO_3H_2$	1.12	4.98×10^{-1}	2.25
$(CF_3)_2PO_2H$	9.47	5.99	1.58
$C_4F_9SO_3H$	4.87	4.87	1.00
$C_4F_9PO(OH)_2$	0.26	0.14	1.85
$(C_4F_9)_2PO(OH)$	0.14	0.12	1.17

Nernst-Einstein Relation and Haven ratio: In the previous section we showed that the higher conductivities of phosphorous-based acids compared to sulfonic based acids is due to the presence of high concentration of self-dissociated ions in them. However, in many cases compounds with high ion concentrations show a significantly lower experimental ionic conductivity (σ_{imp}) than what can be estimated using the Nernst-Einstein relation (σ_{nmr}). This is due to ion-ion correlations (for e.g. some of the ions that diffuse can associate to form uncharged species) that do not contribute to ionic conductivity but do contribute to self-diffusion measurements. Calculation of the Haven ratio (H_R), the ratio of the ionic conductivity estimated from PFG-NMR diffusivity data to that determined by the ac impedance method ($H_R = \sigma_{nmr} / \sigma_{imp}$) allows for estimation of the degree of ion-ion correlations present in these acids. The Nernst-Einstein equation is given as follows.¹⁰

$$\sigma_{\text{nmr}} = \frac{z^2 F^2}{RT} C_0 (\text{H}) [D_{\text{H}} + D_{\text{F}}] \quad \text{Equation 3.1}$$

The terms have the same meanings as in chapter 2. Table 3.1 presents values for σ_{nmr} calculated using Equation 3.1, and also for Haven ratios calculated using σ_{nmr} and σ_{imp} .

Table 3.3 Nernst-Einstein calculated conductivity σ_{cal} (Scm^{-1}), experimental conductivity obtained from Arrhenius plot σ_{meas} (Scm^{-1}), percent dissociation $\sigma_{\text{meas}}/\sigma_{\text{cal}}$ of the model acid compound

compound	At 85 °C		
	σ_{nmr}	σ_{imp}	$H_{\text{R}} = \sigma_{\text{nmr}}/\sigma_{\text{imp}}$
$\text{CF}_3\text{SO}_3\text{H}$	7.62×10^{-1}	1.47×10^{-2}	51.8
$\text{CF}_3\text{PO}_3\text{H}_2$	6.25×10^{-2}	4.33×10^{-2}	1.4
$(\text{CF}_3)_2\text{PO}_2\text{H}$	4.13×10^{-1}	6.53×10^{-2}	6.3
$\text{C}_4\text{F}_9\text{SO}_3\text{H}$	1.83×10^{-1}	3.46×10^{-3}	52.8
$\text{C}_4\text{F}_9\text{PO}(\text{OH})_2$	7.72×10^{-3}	4.90×10^{-3}	1.6
$(\text{C}_4\text{F}_9)_2\text{PO}(\text{OH})$	2.85×10^{-3}	6.14×10^{-4}	4.6

Table 3.3 shows that for both phosphorous-based acids and sulfonic based acids the Haven ratio is approximately independent of the length of the perfluoroalkyl chain. This suggests that the combined effect of percent dissociation and ion-ion correlations is independent of chain length.

Conclusions

Ionic conductivity in perfluorinated phosphorous-based acids depends on the fluorine content of acids. Lower fluorine content is necessary to form a high concentration of hydrogen bonds and for efficient transfer of proton by the Grotthuss mechanism. Perfluoroalkyl phosphonic acids have a higher percent dissociation and give a higher conductivity upon increasing perfluoroalkyl chain length compared to phosphinic or sulfonic acids under anhydrous conditions. The conductivity of perfluorinated sulfonic acids depends on carrier mobility and under anhydrous conditions; they have relatively low carrier concentration due to low degree of acid dissociation.

References

- (1) Li, Q.;He, R.;Jensen, J.O.;Bjerrum, N.J. *Chem. Mater.* **2003**, 15, 4896-4915.
- (2) Kanamura, K.;Tanaka, A.;Gervasio, D.;Kennedy, V.;Adzic, R.;Yeager, E.B. *J. Electrochem. Soc.* **1996**, 143, 2765-2770.
- (3) Kreuer, K.D. *Chem. Mater.* **1996**, 8, 610-641.
- (4) Souzy, R.;Ameduri, B. *Prog. Polym. Sci.* **2005**, 30, 644-687.
- (5) Souzy, R.;Ameduri, B.;Boutevin, B.;Gebel, G.;Capron, P. *Solid State Ionics* **2005**, 176, 2839-2848.
- (6) Herath, M.B.;Creager, S.;Kitaygorodskiy, A.;Desmarteau, D.D. *ChemPhysChem*, submitted.
- (7) Arico, A.S.;Baglio, V.;Di Blasi, A.;Antonucci, V.;Cirillo, L.;Ghielmi, A.;Arcella, V. *Desalination* **2006**, 199, 271-273.
- (8) Miyatake, K.;Yasuda, T.;Hirai, M.;Nanasawa, M.;Watanabe, M. *J. Polym. Sci., Part A: Polym. Chem.* **2007**, 45, 157-163.

- (9) Chin, D.;Chang, H. *J. Appl. Electrochem.* **1989**, 19, 95-99.
- (10) Jost, W.J. Diffusion in solids, Liquids, Gases; Academic Press, NY, **1960**;139.
- (11) Olah, G.A.;Prakash, G.K.S.;Sommer, J. *Science (Washington, DC, United States)* **1979**, 206, 13-20.

Supporting Information

The Arrhenius equations for conductivity and fluidity are given by equations 1 and 2 below

$$\sigma = \sigma_0 \exp(-E_a^\sigma / RT) \quad \text{Equation 3.2}$$

$$\frac{1}{\eta} = \frac{1}{\eta_0} \exp(-E_a^\eta / RT) \quad \text{Equation 3.3}$$

In these equations σ and η are the conductivity and viscosity respectively, σ_0 and η_0 are constants associated with conductivity and viscosity, E_a^σ and E_a^η are activation energies for conductivity and fluidity, R is the universal gas constant, and T is temperature in degrees Kelvin. Best-fit parameters obtained from linear fitting for the conductivity and fluidity Arrhenius plots are listed in Table 3.4.

Table 3.4 Best-fit parameters for temperature-dependent conductivity and fluidity of model acids

	σ_0 (Scm^{-1})	E_a^σ (kJmol^{-1})	η_0 (poise)	E_a^η (kJmol^{-1})
$\text{C}_4\text{F}_9\text{SO}_3\text{H}$	9.3	23.2	1.29×10^{-6}	24.0
$\text{C}_4\text{F}_9\text{PO}_3\text{H}_2$	27.7	25.7	4.74×10^{-6}	31.2
$(\text{C}_4\text{F}_9)_2\text{PO}_2\text{H}$	42.0	33.2	1.87×10^{-6}	35.2

Table 3.5 Hammett acidities of model acids

compound	Hammett Acidity(Exp.)	Hammett Acidity (Lit.)
$\text{C}_4\text{F}_9\text{SO}_3\text{H}$	-11.7	-12.7 ¹¹
$\text{C}_4\text{F}_9\text{PO}(\text{OH})_2$	-4.36	
$(\text{C}_4\text{F}_9)_2\text{PO}_2\text{H}$	-5.34	

The Hammett acidities of the model acids were determined from the method described in reference ⁶.

CHAPTER FOUR

PROTON CONDUCTIVITY OF PHOSPHONIC AND PHOSPHINIC ACIDS UNDER CONDITIONS OF HIGH HYDRATION

Introduction

Some of the proton conductors most commonly discussed in the literature as having the potential to overcome the hydration requirement of Nafion and Nafion-like polymers are imidazole functionalized polysiloxanes¹, bis(trifluoromethanesulfonyl)amide and 4,4'-trimethylenedipyridine combined Brønsted acid-base ionic liquids², salts of inorganic oxo-acids such as CsH_2PO_4 ^{3,4}, phosphoric acid doped polybenzimidazole (PBI)⁵, sulfonated-fluorinated poly(arylene ether) multiblocks by McGrath and coworkers⁶ and polymers comprising graft chains of poly(sodium styrenesulfonate) and a polystyrene (PS) backbone prepared by Holdcroft and coworkers⁷. Some of the common difficulties encountered while these polymers were used as membrane materials for PEMFCs were their poor chemical stability and loss in mechanical strength after absorption of water which turns them into a gel-like material. The acid used in the acid doped PBI membranes and imidazole used in some of these materials could simply get washed away from the liquid water generated during an operation of a fuel cell.

Fluorinated polymers are still preferred today as the best choice for construction of proton exchange membrane materials for PEM fuel cells. Depending on the content of the fluorine and its distribution along the chain of these polymers determine the thermal and chemical stability and water repellent properties. The higher the fluorine content the larger the thermal and chemical stability and better the durability. These properties are a result of the much stronger carbon-fluorine bond compared to the carbon-hydrogen bond.

During the operation of a PEMFC water is generated in liquid and vapor forms. Therefore the inside of a fuel cell will always be humidified during operation. It is important to understand how proton conductivity is affected under hydrated conditions in perfluorinated phosphonic acids compared to perfluorinated sulfonic acids which are now commonly used for construction of PEM materials. This chapter makes a comparison study of the proton conductivity and diffusivity data of $\text{CF}_3\text{PO}_3\text{H}_2$ with $\text{CF}_3\text{SO}_3\text{H}$ under different water contents. Also reported are the proton conductivities under different water contents for $(\text{CF}_3)_2\text{PO}_2\text{H}$ and $\text{C}_4\text{F}_9\text{PO}_3\text{H}_2$. The compound $(\text{C}_4\text{F}_9)_2\text{PO}_2\text{H}$ is immiscible with water so its proton conductivities under different hydration levels could not be determined.

Experimental

Materials and reagents: Unless otherwise noted, starting materials received from commercial suppliers were used without further purification. Trifluoromethyl sulfonic acid (98+ %), nonafluorobutyl sulfonic acid were obtained from Sigma Aldrich. All the perfluoroalkyl phosphonic and phosphinic acids were synthesized as described in chapters 2 and 3. Deionized Millipore Milli-Q water with nominal resistivity of $18 \text{ M}\Omega\cdot\text{cm}$ was used in all experiments. ^1H , ^{19}F , and ^{31}P NMR spectra were recorded at 300.3, 282.7, and 121.6 MHz respectively, using CD_3CN as the solvent.

Acid water mixture preparation: All model acid + water electrolyte mixtures were prepared from weighed amounts of the pure components. The pure acid and distilled water were weighed into a glass vial on a top-loading Mettler P-160 single-pan balance (0.001 gram accuracy) and then transferred into the conductivity cell and to the micro NMR tube for the

measurements. For example the 1:3 molar ratio mixture of trifluoromethylphosphonic acid to water was prepared by weighing 200 mg of solid acid (1.3 mmols) and dissolving it in 72 mg of water (4.0 mmols).

Measurements: All the measurements were done as described in chapters 2 and 3.

Results and discussion

Effect of Addition of water on the ionic conductivity: The water was added as 1, 3 and 20 moles to one mole of neat acid. A solid hydrate was formed as described in literature for $\text{CF}_3\text{SO}_3\text{H}$ with 1 mole of water. However, $\text{CF}_3\text{PO}_3\text{H}_2$ and $(\text{CF}_3)_2\text{PO}_2\text{H}$ did not show formation of solid hydrates with either 1 or 3 mole water mixtures. The conductivity plots of the mixtures of neat acid + waters for different water contents for $\text{CF}_3\text{PO}_3\text{H}_2$ and $\text{CF}_3\text{SO}_3\text{H}$ are shown in Figure 4.1 and Figure 4.2 respectively.

For all of the acids studied, as the water content per mole of acid was increased, the ionic conductivity of the acids also increased. Comparison of the conductivity plots of the different water contents shows that the difference in proton conductivity observed for a mixture with 3 waters to 20 waters at a given temperature is smaller than the conductivity change observed for a mixture with 0 waters to 3 water molecules. Adding 3 water molecules to a neat phosphonic acid causes an order of magnitude increase in conductivity. Adding 17 water molecules to a acid mixture already containing 3 water molecules causes its conductivity to increase by approximately a factor of 2 or 3. For acid : water mixtures of 1:3 ratios, the conductivity of $\text{C}_4\text{F}_9\text{PO}_3\text{H}_2$ reaches close to 1 S/cm at 120 °C. The increase in conductivity with addition of water could be a combined effect of high degree of percent dissociation of the acids which increases the free charge carrier concentration and increase in the mobilities of the charge

carriers as result of decrease in viscosity. Addition of water dilutes the acids leading to a decrease in their viscosities.

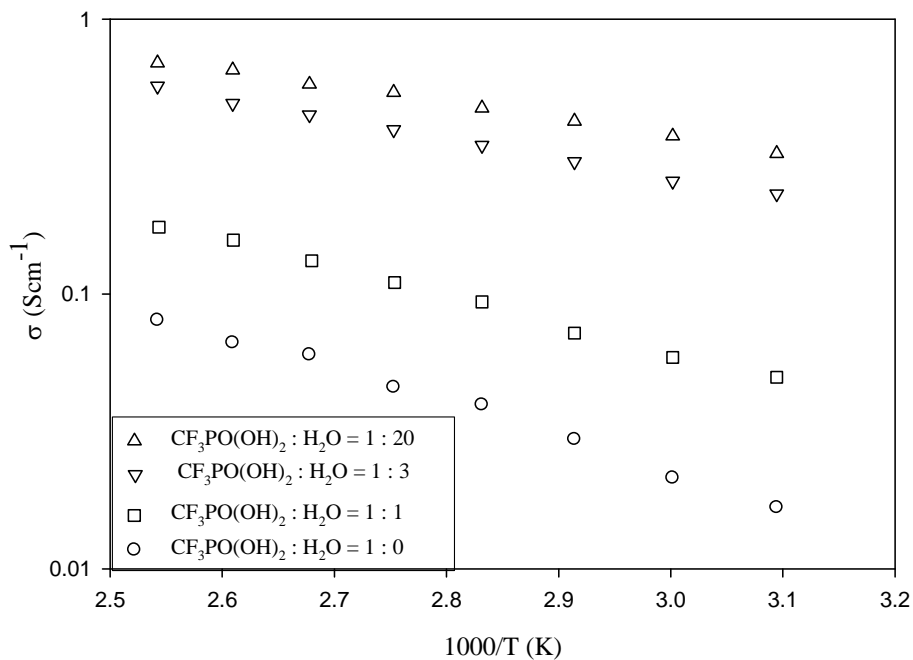


Figure 4.2 Addition of water to perfluoromethyl phosphonic acid

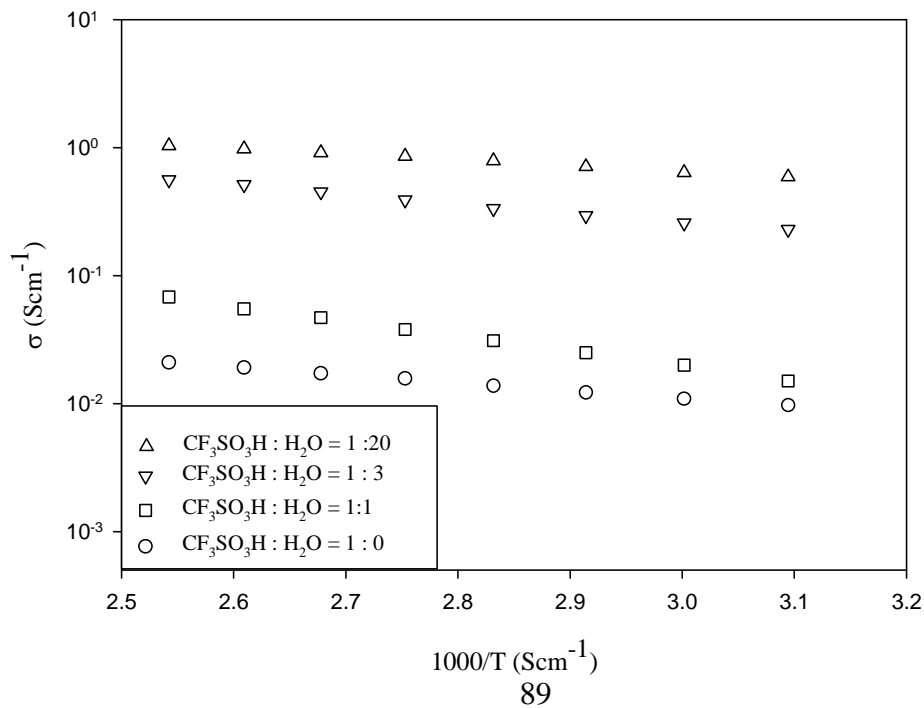


Figure 4.2 Addition of water to perfluorosulfonic acid

PFM NMR Studies: All acid + water mixtures show single peaks in proton and fluorine NMR spectra respectively. The self-diffusion coefficients of protons D_H and its conjugate base D_{CF_3} have been measured at 85 °C for $CF_3PO_3H_2$ and CF_3SO_3H at all their acid + water contents. The results are shown in Table 4.1.

The self-diffusion coefficients of proton and anion increase with addition of water for all acids studied. At acid + water ratio of 1 :3 comparison of the values of proton and anion diffusion coefficients for $CF_3PO_3H_2$ to that for CF_3SO_3H indicates that its proton and anion diffusion coefficients are 3 times less than the sulfonic acid analog. However, at this acid to water ratio the ionic conductivities of CF_3SO_3H and $CF_3PO_3H_2$ at 85 °C are 0.36 Scm^{-1} and 0.37 Scm^{-1} respectively. Despite the lower self-diffusion coefficients of the ions in $CF_3PO_3H_2$ its comparable conductivity to that of CF_3SO_3H must be a direct consequence of the higher degree of proton hopping mechanism present at this concentration. As the water content is increased to 20 and more water molecules, the value of the proton self-diffusion coefficient (D_H) of all the acids approaches the value of self-diffusion coefficient of a neutral water molecule. The literature reported self-diffusion coefficient for pure water at 80 °C is $6.25 \times 10^{-9} \text{ (m}^2/\text{s)}$.⁸ For the $CF_3PO_3H_2$ acid containing 100 water molecules, the D_H value measured at 85 °C in this work is $6.40 \times 10^{-9} \text{ (m}^2/\text{s)}$. At very high water contents (20 or more water molecules per a molecule of acid) the high conductivity in these solutions can be thought of as occurring the same way as it has been shown in literature for dilute aqueous HCl solutions or other strong acids.

Table 4.1 Diffusion coefficients of acid water mixtures

Acid	Acid : water mole	D_H ($\times 10^{10} \text{ m}^2/\text{cm}$)	D_F ($\times 10^{10} \text{ m}^2/\text{cm}$)	D_H/D_F
$\text{CF}_3\text{PO}_3\text{H}_2$	1 : 0	1.12	0.50	2.25
	1:1	2.1	0.91	2.30
	1 :3	12.0	5.17	2.32
	1:20	51.3	17.8	2.86
	1:100	64.0	24.8	2.58
$\text{CF}_3\text{SO}_3\text{H}$	1:0	10.8	10.7	1.00
	1:1	21.9	9.8	2.23
	1:3	39.4	18.3	2.15
	1:20	60.7	28.7	2.11

Proton conductivity in other phosphorous based acids: The following Figures 4.3 and Figure 4.4 show how the proton conductivity changes with addition of water in $(\text{CF}_3)_2\text{PO}_2\text{H}$ and in $\text{C}_4\text{F}_9\text{PO}_3\text{H}_2$. These two acids also, similar to as it was observed with $\text{CF}_3\text{PO}_3\text{H}_2$, show an order of magnitude increase in conductivity with addition of 3 water moles per a mole of neat acid.

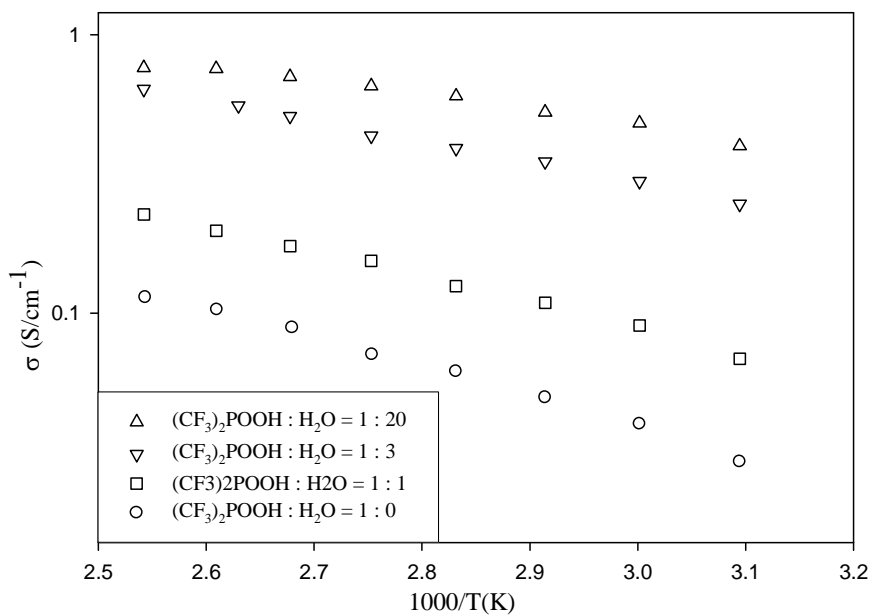


Figure 4.3 Addition of water to bistrifluoromethylphosphonic acid

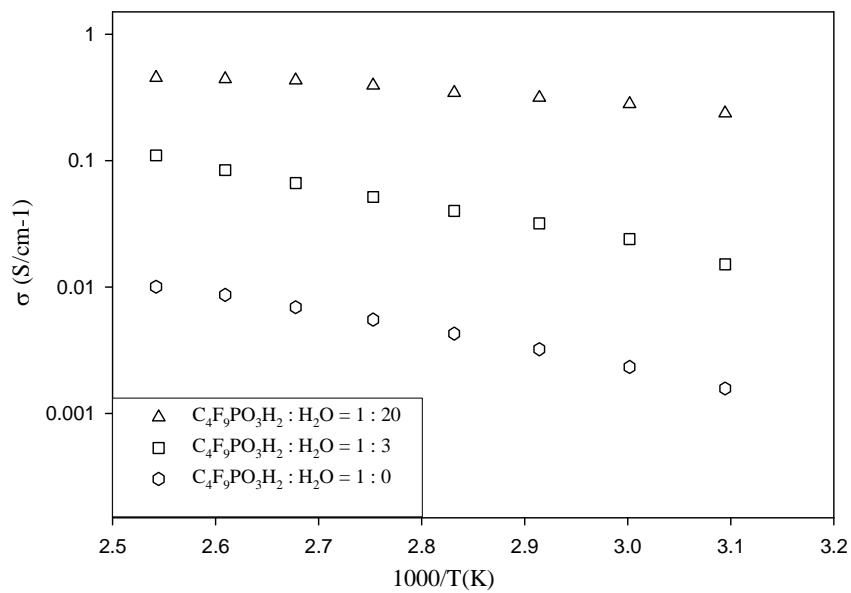


Figure 4.4 Addition of water to perfluorobutylphosphonic acid

Construction of PEM membrane from protogenic groups discussed in chapters 2,3 and 4 requires their immobilization in the polymer membrane. As it was discussed extensively in chapter 1 in the section on phosphonic acid based polymer electrolytes, depending on the flexibility of the spacers covalently linking the protogenic group to the polymer backbone the mobility of the model acids and the protonic charge carriers therein can be lost. However, if same high local mobility as it can be observed with model acids can be guaranteed for these protogenic groups after immobilization in polymers then phosphonic acid based ionomers should show a higher ionic conductivity compared to a sulfonic acid based ionomer designed with a similar concentration of acid groups under low hydration conditions. This is because 1) higher conductivity of phosphonic acids compared to sulfonic acids under anhydrous conditions as seen in chapters 2 and 3 because of the proton hopping mechanism and 2) increase in conductivity upon addition of water as seen in chapter 4, most probably due to the expansion of the hydrogen bonded network of acid groups and water matrix increasing efficiency of transfer of proton between them.

Conclusions

Addition of water increases the conductivity of all the model acid types. An order of magnitude increase in conductivity occurs for the perfluoroalkyl phosphonic and phosphinic acids at low hydration. The proton transport at low hydration in perfluoroalkyl phosphonic acid still appears to be occurring based on proton hopping mechanism. In contrast, sulfonic acid shows high conductivity at low dilution due to acid dissociation and greatly increased ion mobilities compared to phosphonic acid.

References

- (1) Scharfenberger, G.; Meyer, W.H.; Wegner, G.; Schuster, M.; Kreuer, K.D.; Maier, J. *Fuel Cells* **2006**, 6, 237-250.
- (2) Susan, M.A.B.H.; Yoo, M.; Nakamoto, H.; Watanabe, M. *Chem. Lett.* **2003**, 32, 836-837.
- (3) Boysen, D.A.; Uda, T.; Chisholm, C.R.I.; Haile, S.M. *Science (Washington, DC, United States)* **2004**, 303, 68-70.
- (4) Uda, T.; Haile, S.M. *Electrochem. Solid-State Lett.* **2005**, 8, A245-A246.
- (5) Xiao, L.; Zhang, H.; Scanlon, E.; Ramanathan, L.S.; Choe, E.-W.; Rogers, D.; Apple, T.; Benicewicz, B.C. *Chem. Mater.* **2005**, 17, 5328-5333.
- (6) Ghassemi, H.; McGrath, J.E.; Zawodzinski, T.A. *Polymer* **2006**, 47, 4132-4139.
- (7) Ding, J.; Chuy, C.; Holdcroft, S. *Macromolecules* **2002**, 35, 1348-1355.
- (8) Yoshida, K.; Matubayasi, N.; Nakahara, M. *J. Chem. Phys.* **2008**, 129, 214501-214509.

CHAPTER FIVE

IONIC CONDUCTION IN POLYETHER-BASED LITHIUM ARYLFLUOROSULFONIMIDE IONIC MELT ELECTROLYTES

Introduction

The work presented in this chapter was published in *Electrochimica Acta* (Copyright 2009). The citation for this manuscript is:

Herath M.B., Creager S. E., Rajagopal, R.V., Geiculescu, O. E., DesMarteau, D. D. *Ionic conduction in polyether-based lithium arylfluorosulfonimide ionic melt electrolytes*, *Electrochim. Acta* (2009), doi:[10.1016/j.electacta.2009.05.050](https://doi.org/10.1016/j.electacta.2009.05.050)

Cellular phones, laptops, cameras and other portable electronic devices require batteries with high energy density. Lithium ion batteries are attractive because they have higher specific energy than other battery types, for example lead acid and Ni-MH(nickel-metal hydride) batteries. Another important property of lithium ion batteries is the fact that they are able to deliver high power pulses, and therefore are the preferred power alternative¹ for larger battery systems used in Hybrid Electric Vehicles (HEV) and Electric Vehicles (EV).

Because of concerns about safety, the environment, memory effect problems and the relatively short life span associated with conventional lithium batteries which use an organic liquid electrolyte with dissolved lithium salt, there is interest in developing lithium polymer batteries which have the potential to overcome these problems.²

Lithium batteries in all applications must have the ability to charge and discharge quickly while maintaining a low internal resistance during operation. During a rapid charge and discharge cycle of a lithium battery, only lithium ions are released from and absorbed into the electrodes. The ionic conductivity of the cell is due to the migration of the lithium cation and the PF_6^- anion. There is no reaction for anions at the electrodes so they tend to accumulate or become depleted at the electrodes, resulting in a concentration polarization of the electrolyte within the cell. If the salt diffusion coefficient is not sufficiently high for the salt depletion and accumulation layers to relax^{3,4} the internal cell impedance will increase and consequently degrade the power performance of the cell.

One solution to the salt concentration polarization problem is to immobilize the anion. This can be achieved by covalently linking the anion to a large polymeric structure which is immobile on a macroscopic scale. This type of a material is called a single ion conductor because only the lithium ion is macroscopically mobile, so the Li^+ transference number is unity⁵. Previous attempts to design single ion conductors based on immobilization of the anion to the polymer chain have met with limited success. Single ion conductors based on graft polymers of polyacrylate ethers⁶ by Kerr and co-workers, siloxyaluminate polymers^{7,8} by Shriver and co-workers and polyanionic electrolytes based on orthoborate structures synthesized by Angell and co-workers^{9,10} involved multi-step synthetic step reactions and there were issues of isolating the product completely devoid of starting materials. These materials had ionic conductivities ranging from 10^{-7} to 10^{-5} S/cm at room temperature which is on the low side for Li battery applications. The polymers also tend to be difficult to process, especially regarding integration into the electrodes. Even so, salt concentration polarization does not occur in such materials, which is an advantage for high power batteries.

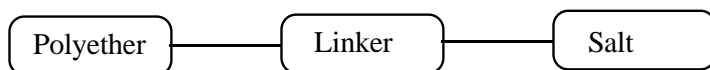
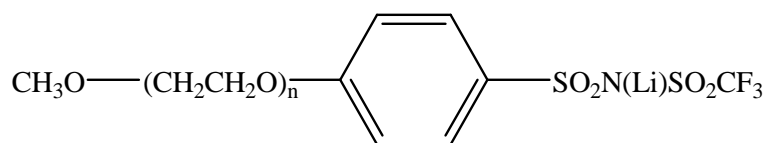
Research groups of Watanabe¹¹ and Sanchez¹² have synthesized lithium salts with large polymeric anions whose negative charges can be well delocalized. These salts minimize ion pairing and increase lithium ion transport. Another approach used by Watanabe and coworkers was to use anion trap sites^{13,14} that decrease the strength of coordination between the anion and the cation of the lithium salt. These salts have also shown an increase in the lithium ion transport rates. But the reported lithium transference number for above described electrolytes was still below unity suggesting that anion was not completely immobile.

One possible solution to the problem of salt concentration polarization in electrolytes involves the use of ionic liquids or melts in which lithium is the only mobile cation. Such materials have been prepared by covalent attachment of anions onto a lithium-solvating material such as an oligomeric polyether¹⁵⁻¹⁹. Bulk salt concentration is fixed in such materials because they contain no non-ionic components to dilute the salt. We recently described one such material consisting of a fluorosulfonimide anion linked to polyether chains of variable length, and we showed that on passage of DC current through such a material, salt concentration gradients did not form, even though the anions are macroscopically mobile¹⁵. Such materials have an attractive combination of relatively high ionic conductivity and high lithium transference number, which could make them attractive for use as battery electrolytes.

In this paper we discuss our research on another example of an ionic melt consisting of a lithium salt of an anion linked to a polyether chain. Figure 5.1 shows the architectures and chemical structures of the ionic melts studied in this work. Two different architectures were studied. In the first as shown in Figure 5.1(a), a single anion is linked to one end of the polyether chain, and in the second, shown in Figure 5.1(b), the anion can be linked at both ends of the polyether chain. These materials were synthesized so that a selected structure from type

5.1(a) had similar EO:Li ratio with a structure from type 5.1(b). This was achieved by choosing a polyether chain two times longer than what was selected for 5.1(a) for that particular chemical structure.

(a)



(b)

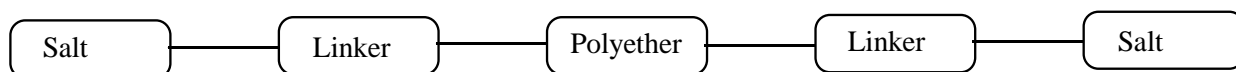
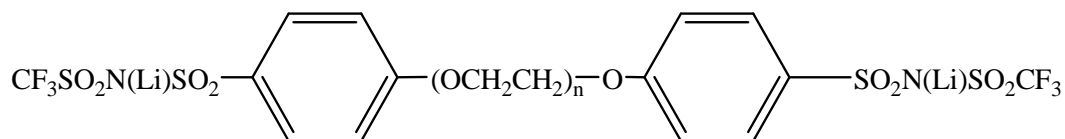


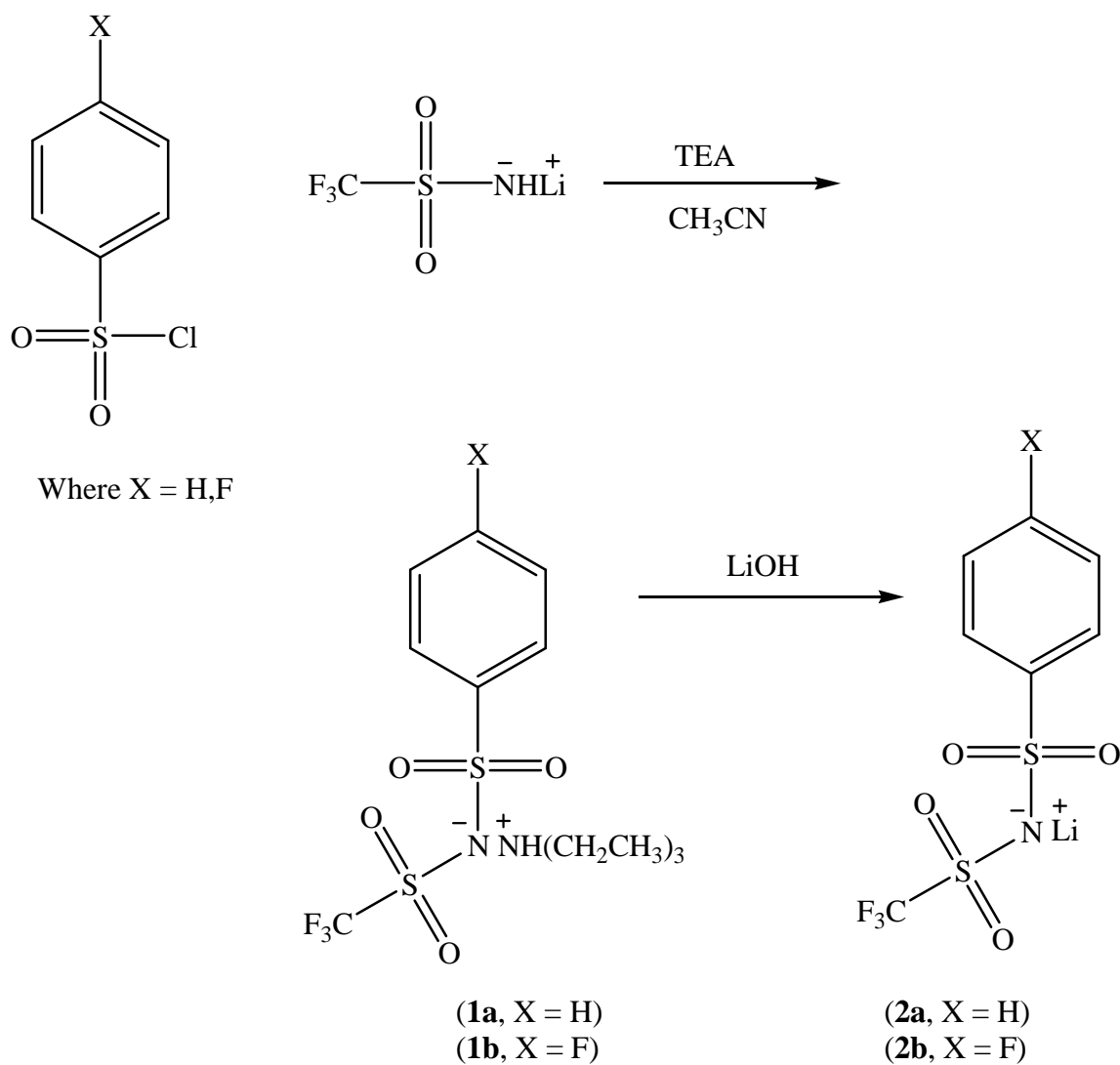
Figure 5.1 Two different architectures of ionic melts based on lithium salts linked to polyether

Lithium phenylsulfonyl(trifluoromethylsulfonyl)imide (LiPSTFSI) was selected as the salt for comparisons with the ionic melt. It is structurally very similar to the ionic melts, which makes comparisons especially significant.

Calculated polydispersities for the selected polyethylene glycols were close to unity (ca. for example mPEG550, it was in the range 0.95 – 1.09) based on the supplier provided data. This was crucial to the study so that we could see clearly the effect of a unique polymer on conductivity. The salt was attached to the polyether via thermally and chemically stable phenyl ether bond. The overall synthesis is simple, involves a low cost and gives a quantitative yield. Therefore these ionic melts could easily be mass produced.

Experimental

Materials and reagents: Samples of polyethylene glycol (PEG) and polyethylene glycol monomethyl ether (mPEG) [mPEG350, mPEG550, PEG600, mPEG750, PEG1000, PEG2000 (polyethylene glycols whose average molecular weight is 350, 550, 600, 750, 1000, 2000, Da respectively)] of various molecular weight were purchased from Aldrich and used as received. Acetonitrile and triethylamine were dried over calcium hydride and distilled over phosphorous pentoxide (P_4O_{10}) prior to use. 4-Fluorobenzenesulfonyl chloride and benzenesulfonyl chloride were obtained from Sigma-Aldrich Company and used as received. Lithium bis[(trifluoromethyl) sulfonyl]imide salt (LiTFSI) was purchased from 3M Company. $CF_3SO_2NH_2$ and CF_3SO_2NHLi were synthesized using a previously published procedure²⁰.

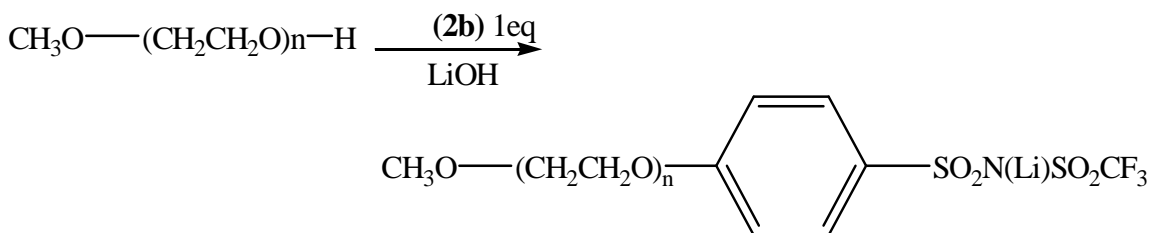


Scheme 5.1 Synthesis of sulfonimide salts

Synthesis of $[\text{XC}_6\text{H}_4\text{SO}_2\text{NSO}_2\text{CF}_3]^- [\text{NH}(\text{C}_2\text{H}_5)_3]^+$ (1a,b; X = H, F): Synthesis of the indicated salt is illustrated in Scheme 1. Details of the synthesis of compound **1b** (X = F) are as

follows. A solution of $\text{XC}_6\text{H}_4\text{SO}_2\text{Cl}$ ($\text{X}=\text{F}$, 1.97 g, 10.2 mmol) in acetonitrile (15 mL) was added under a nitrogen atmosphere to a magnetically stirred solution of $\text{CF}_3\text{SO}_2\text{NHLi}$ (1.58 g, 10.2 mmol) in acetonitrile (15 mL). The compound $\text{CF}_3\text{SO}_2\text{NHLi}$ was synthesized according to the published procedure.²⁰ Triethylamine (3.7 mL, 26.7 mmol) was added dropwise and the resulting mixture was heated at 60- 70°C for 16 hours. ^{19}F NMR was used to monitor the progress of the reaction. Precipitated white LiCl was removed by filtration and the filtrate was concentrated *in vacuo* to give a viscous orange oil. Based on $\text{FC}_6\text{H}_4\text{SO}_2\text{Cl}$, the desired product, $[\text{XC}_6\text{H}_4\text{SO}_2\text{NSO}_2\text{CF}_3]^- [\text{NH}(\text{C}_2\text{H}_5)_3]^+$ was obtained in a high yield (3.92 g, 95%). ^1H NMR (CD_3CN) δ (ppm) 1.26 (t, 9H), 3.07(q, 6H), 7.20 (m, 2H), 7.88 (m, 2H), 8.60 (s,H). ^{19}F NMR(CD_3CN) δ (ppm) -78.92 (s, CF_3), -110.30 (s, F-Ph). A similar procedure gave 4.1 g of compound **1a** in 95% yield.

*Synthesis of $[\text{XC}_6\text{H}_4\text{SO}_2\text{NSO}_2\text{CF}_3]^- [\text{Li}]^+$ (**2a,2b**; $\text{X} = \text{H}, \text{F}$):* To a stirred suspension of **1b** (0.200g, 0.512 mmol) in water (3 mL), LiOH (0.036 g, 1.536 mmol) in water (3 mL) was added and the mixture was stirred at room temperature for 30 min. Water was evaporated and the reaction mixture was dried under dynamic vacuum at 50 °C overnight. The solid was extracted with dry acetonitrile and filtered with 0.2 μm PVDF filter (Whatman) to remove the inorganic salts. Acetonitrile was evaporated to give the desired product as a dark orange solid. Yield (0.143 g, 95%). ^1H NMR (CD_3CN) δ (ppm) 7.45-7.56 (m, 3H). 7.82 (m, 2H) ^{19}F NMR(CD_3CN) δ (ppm) -79.36 (CF_3). -110.30 (F-Ph). A similar procedure gave 0.150 g of compound **2a** 95% yield.



(3a, Mw = 350, n = 7.2)

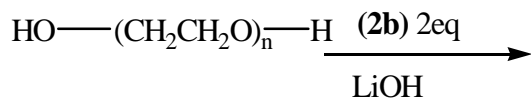
(3b, Mw = 550, n = 11.8)

(3c, Mw = 750, n = 16.3)

(4a, n = 7.2)

(4b, n = 11.8)

(4c, n = 16.3)



(5a, Mw = 600, n = 13.2)

(5b, Mw = 1000, n = 22.2)

(5c, Mw = 2000, n = 45.0)

(6a, n = 13.2)

(6b, n = 22.2)

(6c, n = 45.0)

Scheme 5.2 Synthesis of ionic melts

General Procedure for the Preparation of Lithium Ionic Melts: The following procedure was used for the preparation of the ionic melt **4c**. All the other ionic melts indicated in Scheme 5.2 (**4a,b,c** and **6a,b,c**) were prepared in a similar procedure. In a 50-mL round-bottom flask was placed quantities of **1b** (0.200 g, 0.489 mmol) and mPEG (**3c**) (0.368 g, 0.489 mmol), and solid LiOH (0.035 g, 1.467 mmol) with no solvent. The mixture was heated at 160 °C for 16 hours under vacuum. The progress of the reaction was monitored by ¹⁹F NMR. The complete conversion of the reactant to product was indicated by the disappearance of the ¹⁹F NMR signal from the fluorine atom at the para position of the phenyl ring and the upfield shift of the aromatic proton resonances. The residue was taken up in dichloromethane (30 mL), filtered using a 0.2 μm PVDF filter (Whatman) and concentrated to give a colorless viscous liquid. The sample was dried under vacuum for 4 hours. Yield (0.484 g, 95%). ¹H NMR (CD₃CN): δ (ppm) 3.28 (s, -OCH₃), 3.57(m, -(CH₂CH₂O)₁₃), 3.76(m, -CH₂), 4.14 (m, -CH₂) 6.96 (d, ortho), 7.77(d, meta). ¹⁹F NMR (CD₃CN): δ (ppm) -79.36(s, CF₃)

NMR analysis: ¹⁹F NMR and ¹H NMR spectra were acquired using a JEOL 300 NMR spectrometer (300.5 MHz ¹H, 282.78 MHz ¹⁹F).

Thermal analysis: All measurements were acquired at a heating rate of 10 °C/min using a Perkin Elmer-7 DSC instrument.

HPLC analysis: High performance liquid chromatography(HPLC) analysis was employed to purify and assess the purity of the product. The system (Breeze, Waters) consists of pumps, an auto-injector and a dual-wavelength detector. The column was a C₁₈ analytical column (Symmetry 4.6 x 150 mm, 5 μm particle size, Waters) with a C₁₈ guard-column. The mobile phase uses solvent A (0.1 M ammonium acetate/acetic acid pH 4.0, in water) and solvent B (acetonitrile/methanol, 90/10, v/v) in different ratios. The elution was isocratic with 20% A

and 80% B at a flow rate of 1.5mL/min in 10 min. The detection was by UV absorption at 280 nm. Data were analyzed using the Breeze software (Waters, Milford, MA).

Electrospray Ionization-Mass spectrometric (ESI-MS) measurements: ESI-MS measurements were performed on a tandem (quadrupole-time-of-flight) mass spectrometer (Q-ToF™ *micro*, Waters, Milford, MA). The samples dissolved in methanol were injected directly to the ion source through a capillary LC system (Cap LC, Waters). The flow rate was 1.0 μ L/min. The ESI source voltage was 3000 V in the positive ion mode. The quadrupole mass filter was scanned from 200 to 1200 m/z in 1 s. Methanol was injected between runs to prevent carryovers from previous runs.

Electrochemical impedance spectroscopy: Ionic conductivity of the samples was determined by electrochemical impedance spectroscopy as previously described ²¹. The instrumentation uses a Solatron model 1287 electrochemical interface coupled to a Solatron model 1260 frequency response analyzer in the frequency range of 0.01Hz to 1000 kHz. Measurements were performed over a range of temperatures from 120 °C down to room temperature acquiring spectra every 10 °C decrement using a conductivity cell consisting of two stainless steel blocking electrodes of area 0.196 cm² separated by an annular spacer of thickness 0.023 cm. The resistance of the samples was determined from the Nyquist plot by plotting the imaginary vs. real components of the impedance and extrapolating to the high-frequency limit, where the data intersect the real axis. The specific ionic conductivity, σ , was calculated from the resistance using the equation $\sigma = t/AR$, where t = thickness of the spacer, A = area, and R is the resistance determined from the Nyquist plot.

Results and Discussion

Synthesis and characterization: Compound **1b** was synthesized by reacting $\text{CF}_3\text{SO}_2\text{NHLi}$ with $\text{FC}_6\text{H}_5\text{SO}_2\text{Cl}$ to produce the S-N bond in the bis(sulfonyl)imide functional group. The product was initially isolated as the triethyl ammonium salt, then it was converted to lithium salt by subsequent reaction with LiOH. The progress of the reaction was monitored by ^{19}F NMR whereby completion of the reaction is indicated by the shift of the para-fluorine resonance from δ -101.00 to -110.40 ppm.

Synthesis of the ionic melts was accomplished in quantitative yield by a solvent-free approach that was developed in our laboratory. A mixture of compound **1b** and the selected polyethylene glycol was heated at 160 °C in the presence of LiOH base under vacuum for 16 hours to produce the target ionic melt. The details of the synthesis are shown in Scheme 5.2.

The molecular structures of ionic melts prepared via this approach were confirmed by ^1H NMR and ESI-MS. For ^1H NMR the doublet peaks centered at 7.77 ppm and 6.96 ppm are ascribed to the aromatic protons of the ionic melt. The signal in the region from 3.46 – 4.14 ppm was attributed to the oxyethylene hydrogens of PEO. Four aromatic protons always represent one lithium ion and four oxyethylene hydrogens represent one EO unit. Based on this assumption, EO: Li ratios were calculated for each ionic melt using the following formula:

$$[(\text{Area of EO peaks})/4] / [(\text{Area of aromatic peaks})/4] = \text{EO:Li}$$

Table 5.1 Chemical formula and EO: Li ratio of the ionic melt

Ionic melt	EO:Li*	Exp. EO:Li**
Reference***	11.8	11.8
4a	7.2	7.6
4b	11.8	12.4
4c	16.3	15.2
6a	6.6	6.9
6b	11.1	14.6
6c	22.5	26.2

* Calculated using Mw of PEG provided by supplier

** Obtained from NMR spectra as described in text

*** 1:1 mole mixture of 2a in 3a

Area of the aromatic peaks were obtained by integrating peak intensities in the region around 6.90-7.80 ppm and the area of the EO peaks were obtained by integrating peak intensities in the region around 3.40-4.20 ppm. These experimentally obtained values were compared with expected EO:Li molar ratios calculated from supplier-provided average molecular weights of PEG reactants. Comparisons for compounds **4a-c** and **6a-c** are shown in Table 5.1. A good correspondence was found between the expected and experimentally obtained values for all the ionic melts synthesized in this work.

HPLC studies: Figure 5.2 shows chromatograms for the reactant mPEG550 (compound **3b**, top) and its corresponding ionic melt (compound **4b**, bottom). The ionic melt has a retention time of 2.5 minutes and the reactant mPEG550 has a retention time of 3.5 minutes, which agree with their polarities in partitioning between polar mobile phase and non-polar C₁₈ surfaces. These two peaks were baseline separated by one minute. If there were any residual reactant mPEG present in the ionic melt, then the bottom chromatogram will show two separate peaks corresponding to the retention times discussed. Absence of a peak corresponding to the residual reactant mPEG (peak at 3.5 minutes) in the Figure 5.2 bottom chromatogram suggests that the

ionic melt is free from reactant mPEG. However, we noticed that reactant mPEG has a lower sensitivity to UV-280 nm detection. So this suggests that very low concentrations of reactant mPEG may still be present in the ionic melt but were not detected in this technique. Therefore, in a separate study, two samples, a pure mPEG and an ionic melt sample was analyzed and compared for masses of interest by ESI-MS.

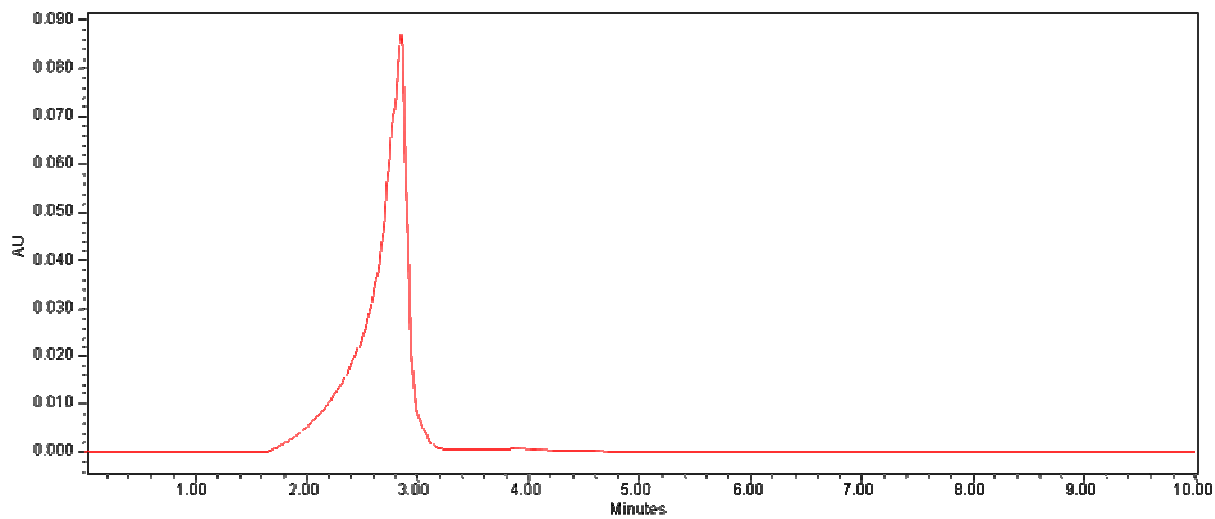
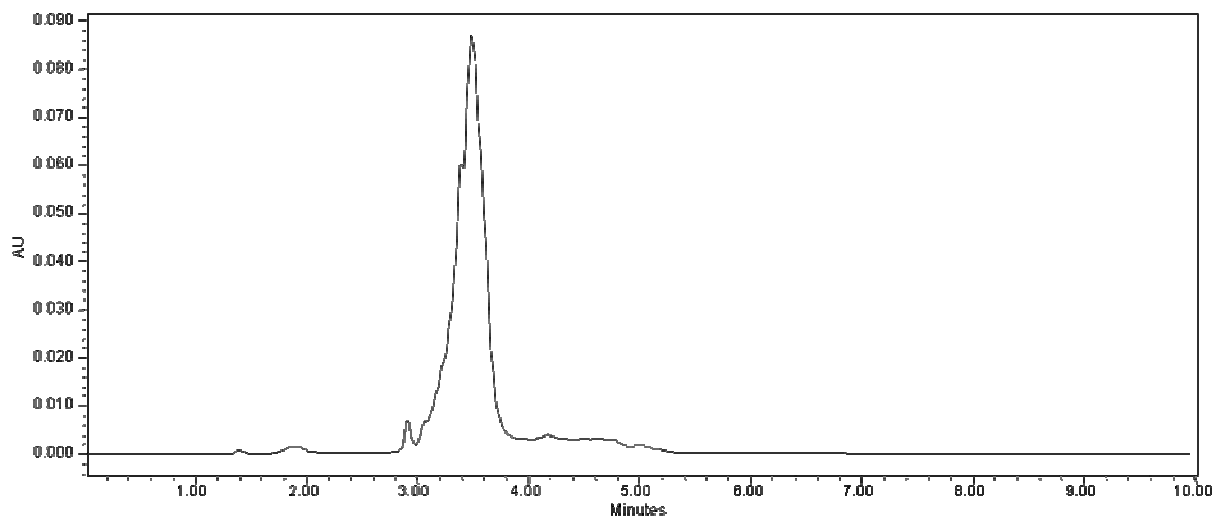


Figure 5.2 HPLC chromatograms for (top) starting polyethylene glycol $\text{CH}_3\text{O}(\text{CH}_2\text{CH}_2\text{O})_{11.8}\text{H}$. (bottom) product ionic melt $\text{CH}_3\text{O}(\text{CH}_2\text{CH}_2\text{O})_{11.8}\text{-C}_6\text{H}_4\text{-SO}_2\text{N}(\text{Li})\text{SO}_2\text{CF}_3$. Absence of a peak near 3.5 minutes in the bottom spectrum indicates the product is free of starting material.

ESI-MS analysis: The mass spectra presented in Figure 5.3 are for the mPEG reactant **3b** (top) and for the ionic melt **4b** (bottom). The most noticeable feature of both mass spectra is the presence of multiple clusters of ions that display a mass unit difference of 44Da between the neighboring peaks, equal to the monoisotopic mass of ethylene oxide unit (-CH₂CH₂O-). The most abundant ion in the reactant mPEG550 spectrum was observed at 517 Da, which corresponds to the protonated structure of [CH₃O(CH₂CH₂O)_nH-H]⁺ that has (n = 11) ethylene oxide units. The corresponding ion in the ionic melt has a mass of 804 Da and corresponds to a protonated structure [CH₃O(CH₂CH₂O)_nC₆H₄SO₂NHSO₂CF₃-H]⁺ that also has 11 ethylene oxide units (n = 11). The ESI spectrum (Figure 3 bottom panel) shows that this is indeed the case. The absence of a peak corresponding the starting material in the region from 400-600Da in the bottom spectrum confirms that no residual mPEG reactant is present in the ionic melt sample.

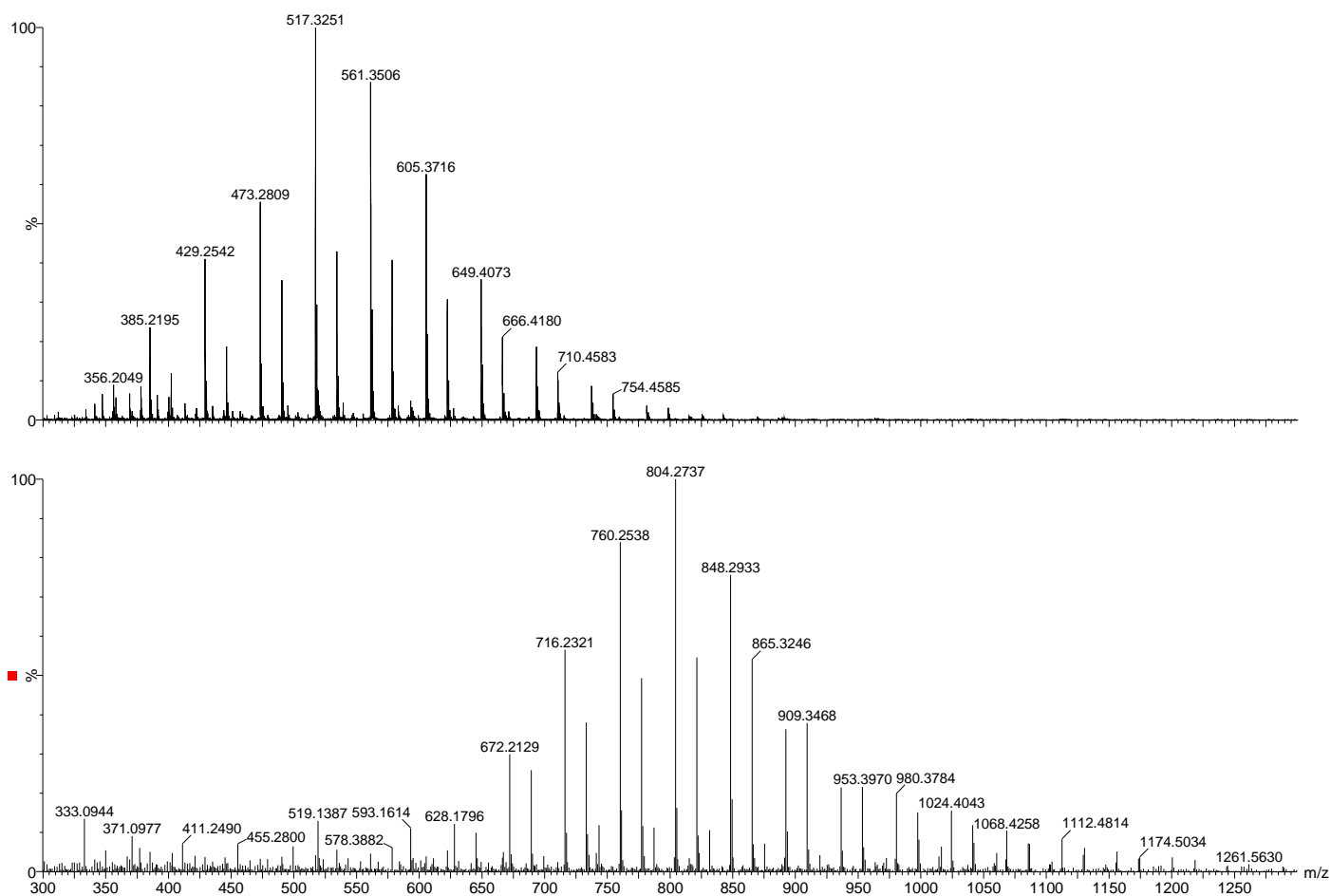


Figure 5.3 Electrospray mass ionization spectra (top) of starting polyethylene glycol $\text{CH}_3\text{O}(\text{CH}_2\text{CH}_2\text{O})_{11.8}\text{H}$. (bottom) Product ionic melt $\text{CH}_3\text{O}(\text{CH}_2\text{CH}_2\text{O})_{11.8}\text{-C}_6\text{H}_4\text{-SO}_2\text{N}(\text{Li})\text{SO}_2\text{CF}_3$. The most abundant peak, 517 Da of top spectra corresponds to the protonated structure $[\text{CH}_3\text{O}(\text{CH}_2\text{CH}_2\text{O})_{11}\text{H-H}]^+$. The most abundant peak, 804 Da of bottom spectra corresponds to the protonated structure $[\text{CH}_3\text{O}(\text{CH}_2\text{CH}_2\text{O})_{11}\text{C}_6\text{H}_4\text{SO}_2\text{NHSO}_2\text{CF}_3\text{-H}]^+$.

Elemental Analysis: Based on the supplier provided $M_n \sim 550$ ($n = 11.8$) data it is possible to calculate the theoretical elemental composition for the ionic melts. Calculated composition for ionic melt **4b**, $[\text{CH}_3\text{O}(\text{CH}_2\text{CH}_2\text{O})_{11.8}\text{-C}_6\text{H}_4\text{-SO}_2\text{NSO}_2\text{CF}_3]^- [\text{Li}]^+$ is as follows: C, 44.95%; H,

6.42%; F, 6.74%; N, 1.66%; S, 7.59%; Found: C, 44.47%; H, 6.82%; F, 6.18%; N, 1.66%; S, 6.91%. This is very good agreement which supports the structural assignment for **4b**.

Ionic conductivity and thermal analysis: Figures 5.4 and 5.5 present the temperature dependence of the ionic conductivity of ionic melts containing different EO:Li ratios derived respectively from the architectures of Figure 5.1(a) and Figure 5.1(b). Conductivity values for 1:1 molar binary mixtures of LiTFSI and mPEG550 polyethylene glycol and LiPSTFSI in mPEG550 are also shown for comparison. The similar conductivities in both samples containing Li salt in mPEG550 show that modification of the LiTFSI with a phenyl linker does not affect its overall transport properties very much. Therefore we used the 1:1 molar binary mixture of LiPSTFSI in mPEG550 as the reference sample to compare with the conductivities of the ionic melts discussed in this paper.

The highest ambient temperature conductivity of 2.7×10^{-6} S/cm was observed for sample **4b** at an optimum EO: Li ratio of 11.8. At 40 and 120°C, the ionic conductivity for **4b** reaches 1.49×10^{-5} and 6.92×10^{-4} S cm⁻¹, respectively. The ionic conductivity required in high performance Li-cells (single ion conductors) sought for applications in electric and hybrid vehicles by the United States Advanced Battery Consortium (USABC) is 10^{-4} S/cm.⁴ The data for ionic melt **4b** shows that this material meets the program conductivity goal above 60 °C.

The samples **4a** and **6a** show the influence of the much lower EO:Li ratios (i.e high salt concentration) on conductivity compared to **4b**. These two samples may be expected to have a higher conductivity because they contain more lithium ions and thus a higher charge carrier concentration. However, the conductivity data in Figures 4 and 5 show lower conductivities for these samples than for sample **4b**. These data suggest a trade-off between the effects of chain flexibility and charge carrier concentration. At higher salt concentrations, there may not be

sufficient number of ethylene oxide units to solvate all the lithium cations, or all the ethylene oxide units have been used in solvating the lithium cation and so there are no left over ethylene oxide units in the polyether chain to allow the lithium cation to move within the ionic melt. These conductivity results for lower EO:Li ratio are consistent with findings reported in a study by Hallac et. al. on some closely related materials. In addition these results extend the previous findings by other researchers on the effect of EO:Li ratios on Lithium-Polyether electrolyte systems.¹⁵⁻¹⁷

At very high EO:Li ratios conductivity decreases due to polyether crystallization and also due to the decrease in charge carrier concentration. The highest EO:Li ratio investigated in this study is for samples **6c** and **4c**. The samples **4c** and **6c** have comparable EO:Li ratios and their carrier concentrations are relatively low compared to other samples. If the ionic conductivity depends only on EO:Li ratios then both samples should have similar conductivities at all temperatures. As expected, both of these samples have comparable conductivities above 30 °C. However, there is a sudden drop in conductivity below 30 °C only for sample **6c**. Thermal analytical data presented in

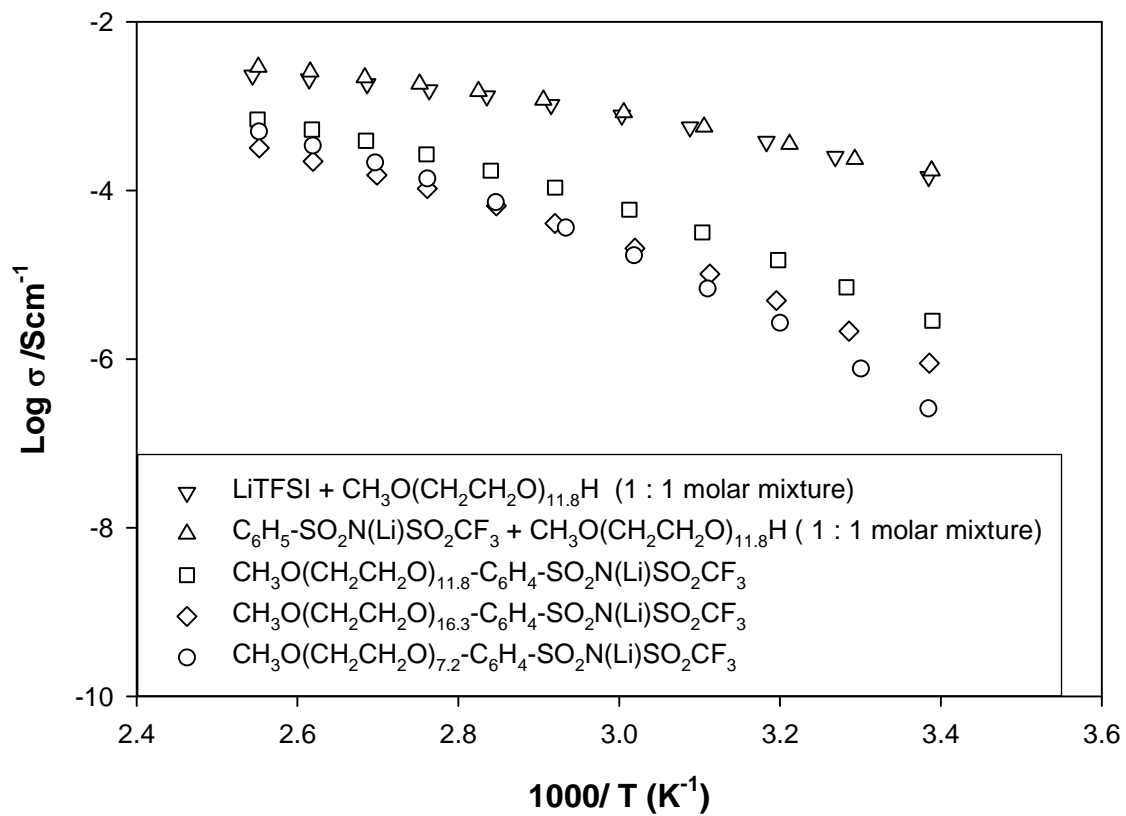


Figure 5.4 Temperature dependence of the conductivity of **polyether-linker-salt** ionic melts, compounds **4a -4c**.

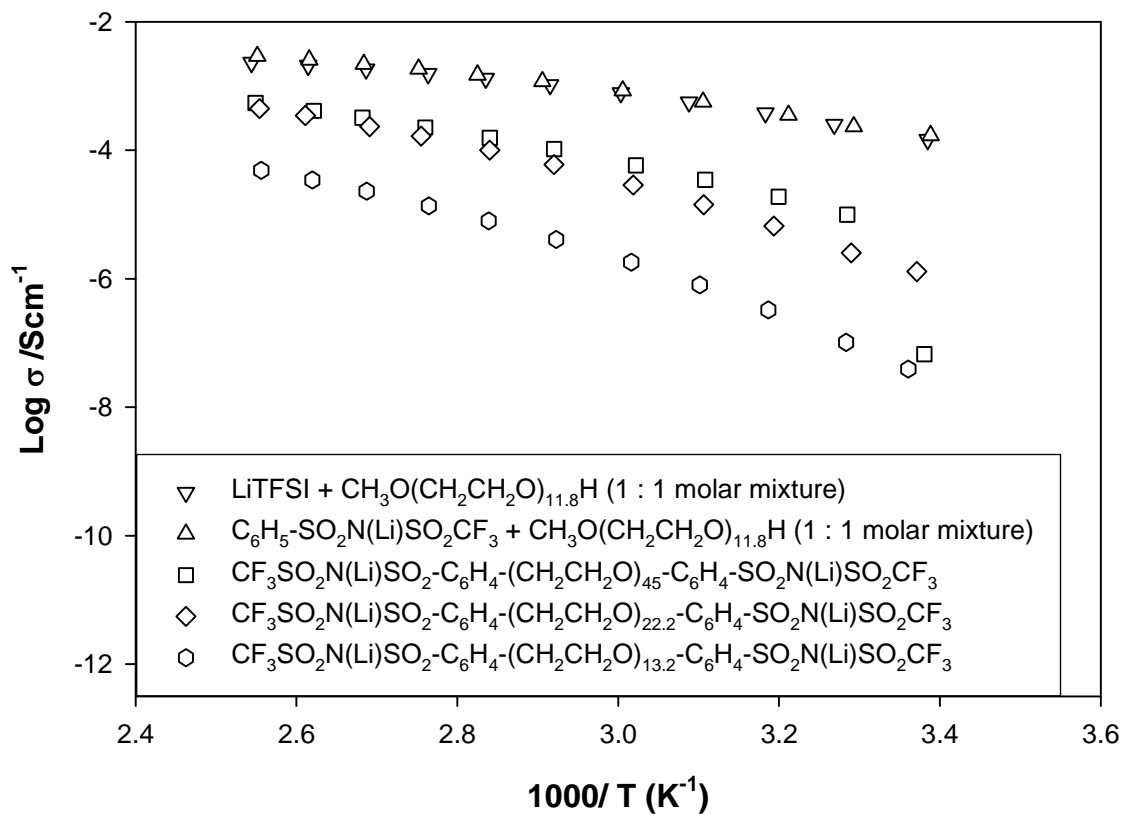


Figure 5.5 Temperature dependence of conductivity of **salt-linker-polyether-linker-salt** ionic melts, compounds **6a -6c**.

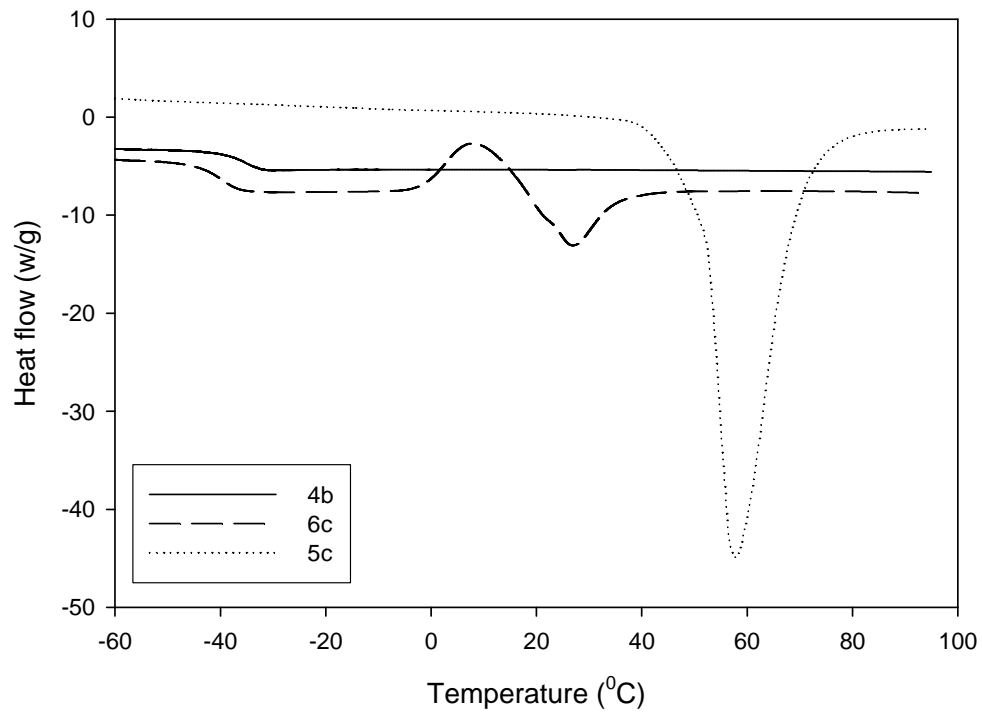


Figure 5.6 DSC traces obtained for ionic melts 4b and 6c and pure PEG 5c.

Table 5.2 DSC results of ionic melts 4b and 6c and pure PEG 5c

material	$\Delta H(\text{J/g})$	$T_m (^{\circ}\text{C})$	$T_g (^{\circ}\text{C})$
4b	-	-	-38
6c	15.7	26	-36
5c	182.8	58	-

Figure 5.6 shows that at this temperature, this sample starts to crystallize. We did not observe crystallization in the other samples. Therefore this suggests that ionic conductivity can be influenced not only by the EO:Li ratio but also by crystallization of the polyether chain.

For this particular series of ionic melts, the shortest polyether chain length that contributes to crystallization can be taken as the length of the polyether chain of the sample **6c**, which has the longest polyether chain length out of all the materials investigated. Previous studies on pure polyethers show that when the chain length gets longer the system is more prone to crystallization²². Crystallization causes the polyether segments to lose the sufficient flexibility to coordinate to and move the lithium cations and thereby decreasing conductivity. Based on observations on crystallization and EO:Li ratio, it can be concluded that any material that falls outside of these limits, (1) longer chain length than **6c** (2) higher EO:Li ratio than **6c**, will have relatively low ionic conductivity at ambient temperature.

The amount of crystallinity that has contributed to the significant lowering of the conductivity of sample **6c** at 30 °C has been calculated as follows:

$$X_c = \Delta H / \Delta H_0 \times 100$$

where X_c is crystallinity, ΔH_0 is the melting enthalpy of the pure PEG²³ (see Table 2, $M_w = 2000$) and ΔH is the melting enthalpy of the **6c** (see Table 5.2). Therefore the crystallinity for **6c** compared to pure PEG is 8.6%.

The highest ionic conductivity in this class of materials occurs at an optimal EO:Li ratio of 12 for ionic melt **4b**. Figure 5.6 shows that no crystallization is associated with this material and it is completely amorphous.

Conclusions

The effect of several factors (e.g. temperature, composition) on ionic conductivity was investigated. The conductivities of ionic melts **4b** and **6b** reached 10^{-4} S cm⁻¹ value above 60 °C. These ionic melt electrolytes are free of non-ionic impurities.

References

- (1) Anderman, M. *J. Power Sources* **2004**, 127, 2-7.
- (2) Gray, F.M. *Solid Polymer Electrolytes. Fundamentals and Technological applications*; VCH Weinheim, Fed. Rep. Ger., **1991**.
- (3) Buriez, O.;Han, Y.B.;Hou, J.;Kerr, J.B.;Qiao, J.;Sloop, S.E.;Tian, M.M.;Wang, S.G. *J. Power Sources* **2000**, 89, 149-155.
- (4) Thomas, K.E.;Sloop, S.E.;Kerr, J.B.;Newman, J. *J. Power Sources* **2000**, 89, 132-138.
- (5) Doyle, M.;Fuller, T.F.;Newman, J. *Electrochim. Acta* **1994**, 39, 2073-81.
- (6) Sun, X.-G.;Reeder, C.L.;Kerr, J.B. *Macromolecules* **2004**, 37, 2219-2227.
- (7) Fujinami, T.;Tokimun, A.;Mehta, M.A.;Shriver, D.F.;Rawsky, G.C. *Chem. Mater.* **1997**, 9, 2236-2239.
- (8) Rawsky, G.C.;Fujinami, T.;Shriver, D.F. *Chem. Mater.* **1994**, 6, 2208-9.
- (9) Xu, W.;Angell, C.A. *Solid State Ionics* **2002**, 147, 295-301.
- (10) Xu, W.;Williams, M.D.;Angell, C.A. *Chem. Mater.* **2002**, 14, 401-409.
- (11) Watanabe, M.;Tokuda, H.;Muto, S. *Electrochim. Acta* **2001**, 46, 1487-1491.

- (12) Ollivrin, X.;Alloin, F.;Le Nest, J.-F.;Benrabah, D.;Sanchez, J.-Y. *Electrochim. Acta* **2003**, 48, 1961-1969.
- (13) Hirakimoto, T.;Nishiura, M.;Watanabe, M. *Electrochim. Acta* **2001**, 46, 1609-1614.
- (14) Tabata, S.-i.;Hirakimoto, T.;Nishiura, M.;Watanabe, M. *Electrochim. Acta* **2003**, 48, 2105-2112.
- (15) Hallac, B.B.;Geiculescu, O.E.;Rajagopal, R.V.;Creager, S.E.;DesMarteau, D.D. *Electrochim. Acta* **2008**, 53, 5985-5991.
- (16) Hamaide, T.;Le Deore, C. *Polymer* **1993**, 34, 1038-46.
- (17) Ito, K.;Nishina, N.;Ohno, H. *J. Mater. Chem.* **1997**, 7, 1357-1362.
- (18) Ito, K.;Nishina, N.;Tominaga, Y.;Ohno, H. *Solid State Ionics* **1996**, 86-88, 325-328.
- (19) Nakai, Y.;Ito, K.;Ohno, H. *Solid State Ionics* **1998**, 113-115, 199-204.
- (20) Geiculescu, O.E.;Xie, Y.;Rajagopal, R.;Creager, S.E.;DesMarteau, D.D. *J. Fluorine Chem.* **2004**, 125, 1179-1185.
- (21) Geiculescu, O.E.;Yang, J.;Blau, H.;Bailey-Walsh, R.;Creager, S.E.;Pennington, W.T.;DesMarteau, D.D. *Solid State Ionics* **2002**, 148, 173-183.
- (22) Takahashi, Y.;Tadokoro, H. *Macromolecules* **1973**, 6, 672-5.
- (23) Hager, S.L.;Macrury, T.B. *J. Appl. Polym. Sci.* **1980**, 25, 1559-71.

CHAPTER SIX

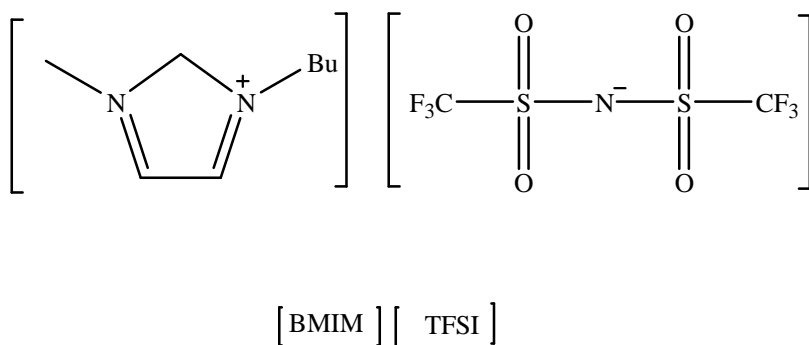
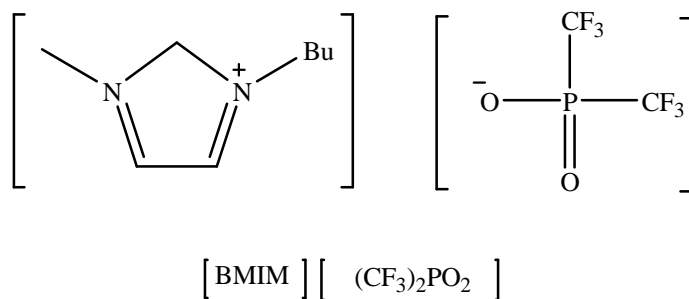
NEW ANION FOR ROOM-TEMPERATURE IONIC LIQUIDS

Introduction

There is great interest in ionic liquids as alternative electrolytes for replacing conventional salt-in-solvent liquid electrolytes used in some electrochemical applications. This is due to their significant differences in physical and chemical properties compared to the conventional electrolytes. They are non-volatile and non-flammable and have a high thermal stability ($>300\text{ }^{\circ}\text{C}$). Other properties such as high ion content and wide electrochemical window ($> 4\text{V}$) are also considered advantageous for electrochemical applications.^{1,2}

Although a large number of ionic liquids have been synthesized, most of them are not suitable for electrochemical application because of the poor conductivity ($< 1\text{ mS}$) and very high viscosity ($> 100\text{ cp}$) at room temperature. However, it has been reported widely that the ionic liquids formed from the combination of a fluoro anion with a cation such as alkylimidazolium have resulted in ionic liquids that display relatively low viscosities and high conductivities favorable in electrochemical applications³. Examples for such fluoro anions are $[\text{PF}_6]^-$, $[\text{BF}_4]^-$, $[(\text{CF}_3\text{SO}_2)_2\text{N}]^-$ and $[\text{CF}_3\text{SO}_3]^-$ anions.

In this paper we report the synthesis, characterization and properties of a new room-temperature ionic liquid based on the fluoro anion, bis(trifluoromethyl)phosphinate ($[(\text{CF}_3)_2\text{PO}_2]^-$). Some of the key physical and chemical properties of ionic liquids based on this anion are compared with those for ionic liquids based on the bis(trifluoromethylsulfonyl)imide-anion (TFSI). The chemical structures of the new IL and the TFSI anion based ionic liquid are shown in Scheme 1 below. The common cation found in these two ionic liquids is methybutylimidazole ([BMIM]).



Scheme 6.1 chemical structures of (top) [BMIM] [(CF₃)₂PO₂]⁻ and (bottom) [BMIM][TFSI]⁻

Experimental

Chemicals: Imidazolium bromide⁴ and bis(trifluoromethyl)phosphonic acid⁵ were prepared by procedures described in literature. Butylmethylimidazolium bis(trifluoromethyl)sulfonyl)imide [BMIM][TFSI] ionic liquid was purchased from Sigma-Aldrich.

Analytical procedures: ^1H , ^{19}F and ^{31}P NMR spectra were measured on a JEOL 300 (300.13 MHz for ^1H , 282.40 for ^{19}F and 121.5MHz for ^{31}P) and Bruker Avance 300 in acetonitrile-D₃ except where noted. ^{19}F chemical shifts were referenced to internal standard CFCl_3 . ^1H chemical shifts were referenced to lock solvent CD_3CN . The external reference for ^{31}P NMR, 85% H_3PO_4 was positioned at 0 ppm. Infra-red spectra were obtained using a Perkin-Elmer 1600 series FTIR spectrometer. Energy dispersive X-ray (EDX) spectra were recorded by a SiLi detector (Oxford) attached to a SEM (S-3400N, Hitachi). Thermogravimetric analyses (TGA) were recorded on a Perkin-Elmer TGA 7 under N_2 (g). Ionic conductivities were measured as a function of temperature by electrochemical impedance spectroscopy (EIS). Data were collected using a Solatron model SI 1286 electrochemical interface coupled to a Solatron model 1254 frequency response analyzer. The conductivity experiments were carried out inside of a stainless steel apparatus using a conductivity cell constructed from PEEK (polyether etherketone) material and under a nitrogen atmosphere as previously described by us in reference [3]. The conductivity was calculated by dividing the cell constant value by the impedance value extracted from a Nyquist plot. Viscosities were measured using a set of calibrated Cannon-Manning Semi-Micro Extra-Low-Charge capillary viscometers. Densities were determined from measuring the weight of the 1mL volume dispensed by an Eppendorf micropipette. Cyclic voltammograms were recorded on neat ionic liquids using a platinum (Pt) working electrode and a Pt auxiliary electrode and silver (Ag) wire as a reference electrode on CH 660 A (CH instruments) instrument.

Synthesis: In water (2 mL), solid Ag_2O (1.1g, 4.9 mmol) and $(\text{CF}_3)_2\text{PO}_2\text{H}$ (2.0 g, 9.9 mmol) prepared as described in reference 5 were stirred until the Ag_2O had reacted completely giving a clear solution. 1-Butyl-3-methyl-imidazolium bromide (2.2g, 9.9 mmol) dissolved in

water was then added to this solution. After 1 h of stirring, the AgBr precipitate was filtered off, and the filtrate was concentrated on a rotary evaporator. The resulting slightly yellow color liquid was further dried overnight in a vacuum oven at 120 °C to give 2.9g of [BMIM][(CF₃)₂PO₂] (85% yield). ¹H NMR (CDCl₃, 300.13 MHz): δ = 0.91 (t, 3H, -CH₃), 1.26 (m, 2H, -CH₂), 1.78 (m, 2H, -CH₂), 3.8 (s, 3H, -CH₃), 4.10 (t, 2H, -CH₂), 7.35 (d, 2H, -CH), 8.59 (s, 1H, -CH). ¹⁹F NMR (CDCl₃, 282.40 MHz): δ = -72.73 (d, 6F, -CF₃). ³¹P NMR (CDCl₃, 121.5MHz): δ = -6.10 (septet, -(CF₃)₂P).

Elemental Analysis: Anal. Calculated for C₁₀H₁₅F₆N₂O₂P : C, 35.3; H, 4.44; F, 33.5; N, 8.2; O, 9.4 %. Found C, 34.85; H, 4.73; F, 33.49; N, 8.0; Br, 0.0; O, 12.5%,

Results and discussion

Synthetic aspects: [BMIM][(CF₃)₂PO₂] was prepared by a metathesis reaction of 1-butyl-3-methylimidazolium bromide, [BMIM]Br, with an equimolar amount of Ag[(CF₃)₂PO₂] as described in detail in the synthesis section. ¹H, ¹⁹F and ³¹P NMR spectra did not show any signals of impurities and were in agreement with the expected chemical structure. Chemical composition analysis by elemental analysis (see synthesis section) gave results that agree with the chemical formula of [BMIM][(CF₃)₂PO₂]. Energy-dispersive X-ray (EDS) spectral analysis (see supporting information) did not indicate the presence of bromide or any other inorganic impurities. Comparison of the FT-IR spectra of [BMIM][TFSI] and [BMIM][(CF₃)₂PO₂] over time in air indicate that [BMIM][TFSI] saturates quickly with a smaller amount of water uptake from air whereas [BMIM][(CF₃)₂PO₂] appears to be more hydrophilic and therefore the water uptake from air is much greater. By placing a drop of ionic liquid on the inside surfaces of one of

the KBr windows at the ends of a FT-IR glass cell for gas analysis, and after evacuating the inside air for 30 min using dynamic vacuum system, we recorded an FT-IR spectrum for [BMIM][(CF₃)₂PO₂] (see Figure 6.7 in supporting information section). Absence of the –OH stretching band in the 3200-3800 cm⁻¹ region in the recorded spectrum showed that absorbed moisture in [BMIM][(CF₃)₂PO₂] can be completely removed by thus drying in vacuum for 30 m. All relevant FT-IR spectra are provided in the supporting information section.

Thermal properties: Table 6.1 shows glass transition temperatures, melting points and thermal decomposition temperatures for the investigated ionic liquids. The glass transition temperature for [BMIM][(CF₃)₂PO₂] was obtained from the differential scanning calorimetry (DSC) curve recorded in the temperature range -100 to 100 °C at a heating rate of 5 °Cmin⁻¹. Compared to the [BMIM][TFSI], the new ionic liquid did not show a melting point suggesting that it has a weaker tendency than TFSI based ionic liquid for crystallization. The absence of a melting point and roughly a same low glass transition temperature of [BMIM][(CF₃)₂PO₂] compared to [BMIM][TFSI] indicate that this new ionic liquid is a good glass former. TGA data were recorded with similar sample sizes, near 12 mg, and at sample heating rate of 20 °C min⁻¹. Figure 6.1 shows the TGA curves recorded for these two ionic liquids. [BMIM][(CF₃)₂PO₂] shows some minor weight loss, < 1%, below 200 °C. [BMIM][(CF₃)₂PO₂] appears to be somewhat less thermally stable than its TFSI analog; thermal decomposition temperature of the new ionic liquid is somewhat lower than TFSI analog (see Table 6.1).

Table 6.1 Physical parameters determined for ionic liquids

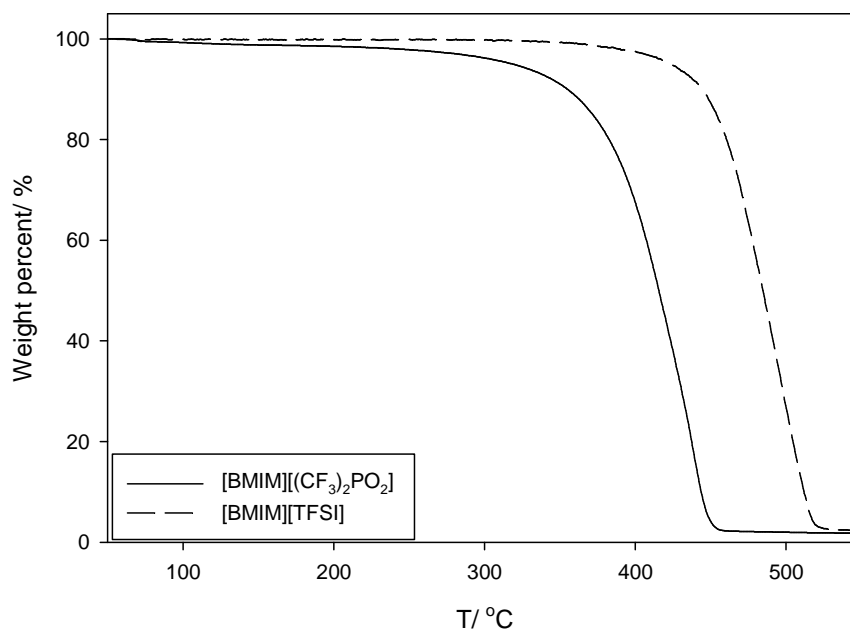
IL	MW (g mol ⁻¹)	ρ (g ml)	T _g (°C)	T _m (°C)	T _d (°C)	η (cp)	σ (mS cm ⁻¹)
[BMIM][TFSI]	419.4	1.45	-84	-3	459 ^c	49.7	3.7
[BMIM][(CF ₃) ₂ PO ₂]	340.2	1.35	-88 ^b	a	380 ^c	101.8	2.4

Molecular weight (MW), density (ρ), glass transition temperature (T_g), melting point (T_m), decomposition temperature (T_d) and dynamic viscosity (η), specific conductivity (σ) are given. T = 25 °C.

^a melting point was not observed

^b determined by DSC exotherm

^c determined by TGA analysis

**Figure 6.1** TGA results for [BMIM][(CF₃)₂PO₂] and [BMIM][TFSI]

Fluidity and Conductivity: The fluidity (inverse of viscosity) and the conductivity of the [BMIM][TFSI] and [BMIM][(CF₃)₂PO₂] samples strongly depend on the temperature used for the measurement. The behavior of viscosity (Figure 6.2) and conductivity (Figure 6.3) over the temperature range between 25 °C and 100 °C does not follow the Arrhenius law, but can be best described by the the Vogel–Fulcher–Tammann equations. The Vogel–Fulcher–Tammann equations for viscosity and conductivity are given by equations 6.1 and 6.2 below.

$$\sigma = \sigma_0 \exp[-B_\sigma / (T - T_0)] \quad \text{Equation 6.1}$$

$$\frac{1}{\eta} = \frac{1}{\eta_0} \exp[-B_\eta / (T - T_0)] \quad \text{Equation 6.2}$$

In these equations σ and η are the conductivity and viscosity respectively, σ_0 (Scm⁻¹) and η_0 (P) are constants associated with conductivity and viscosity, B_σ (K) and B_η (K) are pseudo activation energies for conductivity and fluidity, and T_0 (K) is a characteristic temperature corresponding to the freezing of the liquid within the VTF theory. The values for these parameters are obtained by non-linear fits of Eq.(1) and Eq.(2) to η^{-1} -T and σ -T datasets and are given in Table 6.2 and Table 6.3 respectively.

The conductivity is defined as the product of the ion concentration times the mobility of the ions. It has been discussed in the literature^{6,7} that the glass transition temperature T_g is a measure of the mobility of the ions and the pseudo activation energy B_σ is a measure of the degree of dissociation of the ionic liquid. The lower the T_g value, the higher the mobility of the ions and thus the conductivity. Lower the B_σ value, the weaker the temperature dependency of ion transport of the ionic liquid. In the thermal properties section we observed that the T_g values

of both these ionic liquids are similar. However, the VTF fits show that the B_σ value of $[\text{BMIM}][(\text{CF}_3)_2\text{PO}_2]$ is less than the B_σ value of $[\text{BMIM}][\text{TFSI}]$ suggesting that $[\text{BMIM}][(\text{CF}_3)_2\text{PO}_2]$ is less ion-paired than $[\text{BMIM}][\text{TFSI}]$. This result is further supported by the fact that the difference between ionic conductivity of $[\text{BMIM}][(\text{CF}_3)_2\text{PO}_2]$ and $[\text{BMIM}][\text{TFSI}]$ is smaller than the difference between the viscosities of these two ionic liquids.

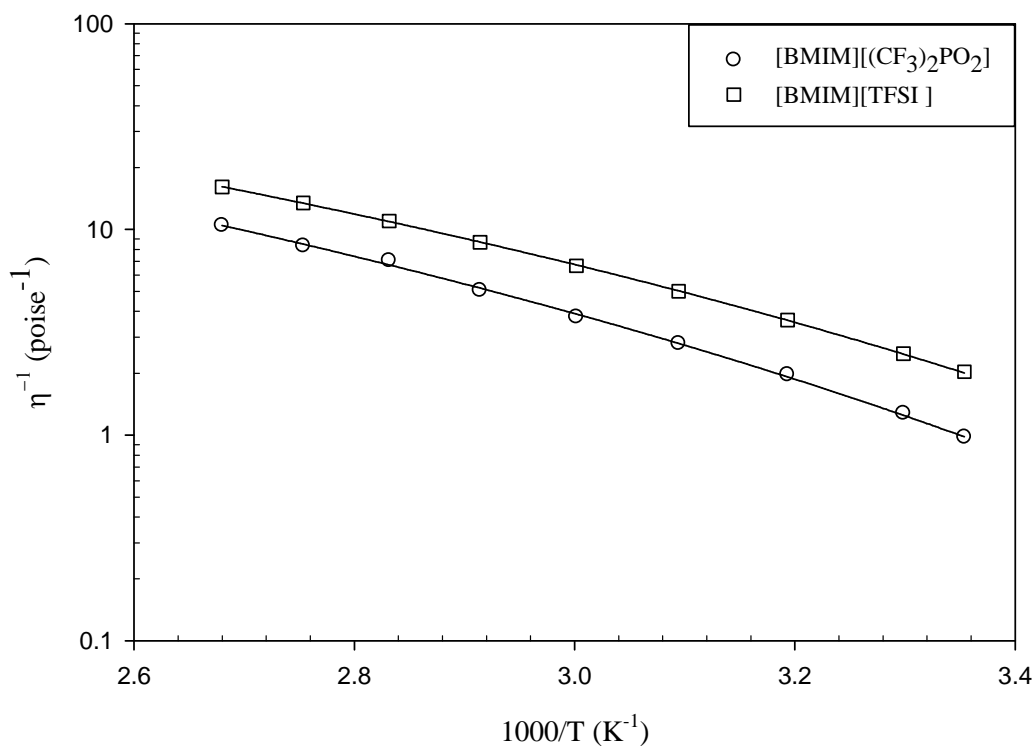


Figure 6.2 Fluidity data for $[\text{BMIM}][(\text{CF}_3)_2\text{PO}_2]$ in comparison with $[\text{BMIM}][\text{TFSI}]$

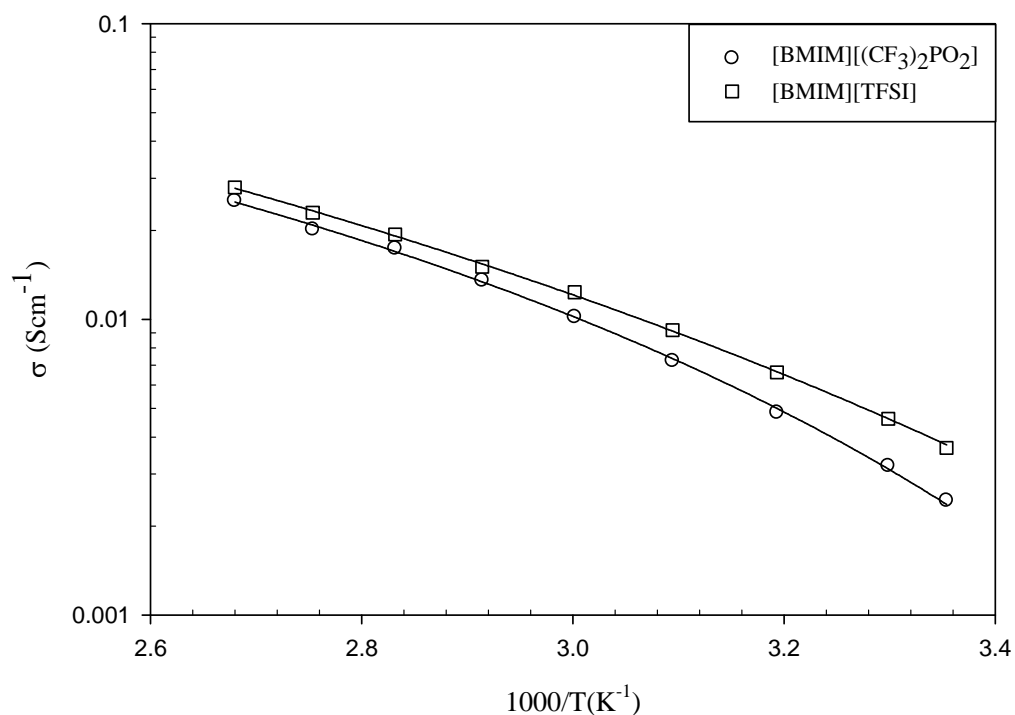


Figure 6.3 Ionic conductivity of data for [BMIM] [(CF₃)₂SO₂N] in comparison [BMIM][(CF₃)₂PO₂] conductivity values.

Table 6.2 The best fit parameters for the fluidity data

	η_0 (P)	B_η (K)	T_0 (K)
[BMIM][(CF ₃) ₂ PO ₂]	0.00164	827.7	169.4
[BMIM] [TFSI]	0.00167	740.5	168.2

Table 6.3 The best fit parameters for conductivity data

	σ_0 (S cm ⁻¹)	B_σ (K)	T_0 (K)
[BMIM][(CF ₃) ₂ PO ₂]	0.382	442.6	211.1
[BMIM][TFSI]	0.800	678.8	171.7

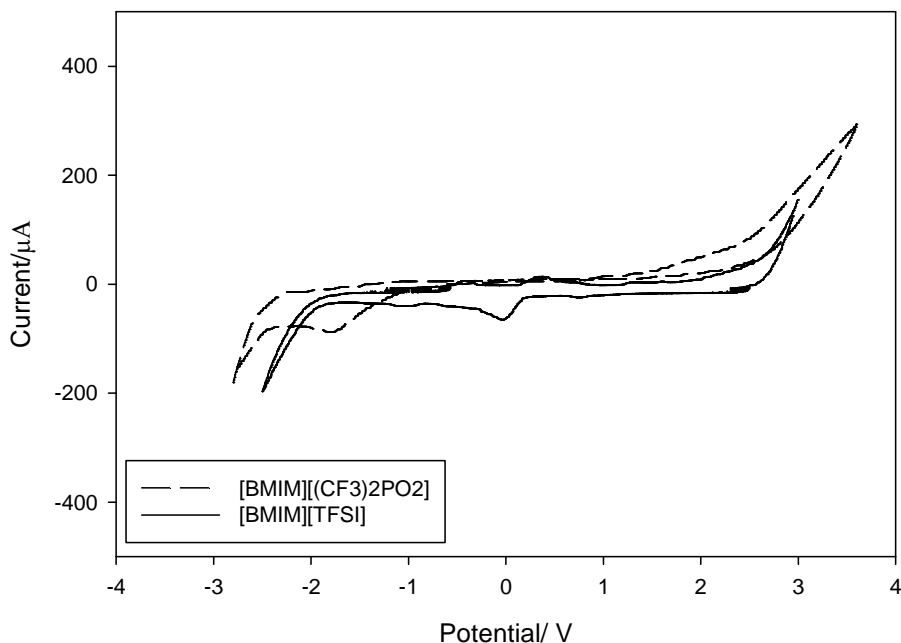


Figure 6.4 Cyclic voltammetry of neat [BMIM][(CF₃)₂PO₂] and neat [BMIM][TFSI] at 23 °C , on a platinum electrode, with a platinum counter electrode and Ag/Ag⁺ pseudo reference electrode with a sweep rate of 100mV/s.

Electrochemical stability: The electrochemical stabilities were determined for both ionic liquids using cyclic voltammetry (CV) at platinum electrodes vs. a silver quasi-reference electrode in their neat liquids. CV scans were always first recorded from positive to negative direction. Cyclic Voltamgrams for the ionic liquids are shown in Figure 6.5. For [BMIM][(CF₃)₂PO₂] an electrochemical window of 4.5 V was determined. The electrochemical window of [BMIM][TFSI] was about 4.2V. This suggests that [BMIM][(CF₃)₂PO₂] is somewhat more electrochemically stable than [BMIM][TFSI]. The small additional reduction peaks at -2V and -1V could be due to reduction of absorbed H₂O or dissolved O₂.

Conclusions

A new ionic liquid [BMIM][$(\text{CF}_3)_2\text{PO}_2^-$] based on a new fluoro anion $(\text{CF}_3)_2\text{PO}_2^-$ is reported. Its chemical and physical properties were investigated, including thermal stability, viscosity, voltage window, and conductivity. This substance may be useful as an electrolyte in batteries.

References

- (1) Fuller, J.;Carlin, R.T.;Osteryoung, R.A. *J. Electrochem. Soc.* **1997**, 144, 3881-3886.
- (2) McEwen, A.B.;Ngo, H.L.;LeCompte, K.;Goldman, J.L. *J. Electrochem. Soc.* **1999**, 146, 1687-1695.
- (3) Hagiwara, R.;Ito, Y. *J. Fluorine Chem.* **2000**, 105, 221-227.
- (4) Bonhote, P.;Dias, A.P.;Papageorgiou, N.;Kalyanasundaram, K.;Gratzel, M. *Inorg. Chem.* **1996**, 35, 1168-1178.
- (5) Herath, M.B.;Creager, S.;Kitaygorodskiy, A.;Desmarteau, D.D. *ChemPhysChem*, submitted.
- (6) Hirao, M.;Sugimoto, H.;Ohno, H. *J. Electrochem. Soc.* **2000**, 147, 4168-4172.
- (7) Ohno, H.;Yoshizawa, M. *Solid State Ionics* **2002**, 154, 303-309.

Supporting Information

FT-IR spectra: Figures 6.5, 6.6, 6.7 and 6.8 shows the FT-IR spectra of the compounds [BMIM][(CF₃)₂PO₂], [BMIM][TFSI], [BMIM]Br and (CF₃)₂PO₂K. It should be noted that the only the FT-IR spectra given in Figure 6.7 is recorded under vacuum conditions so that we could find out if we can get rid of all the moisture present in the sample. The vibrational bands appearing in the all these FT-IR spectra can be assigned as follows.

FT-IR (Thin film, cm⁻¹) : 3200-3500 (-OH stretch, H-bonded), 3000-3155 (=C-H stretch, aromatic), 2800-3000 (-C-H stretch, alkanes), 1574 (-C=C- stretch, aromatic), 1466 (-C-H bending, methyl), 1168 (-C-N stretch, amines), 1133 (-C-F stretch, alkanes), 1280-1340 (-P=O stretch)

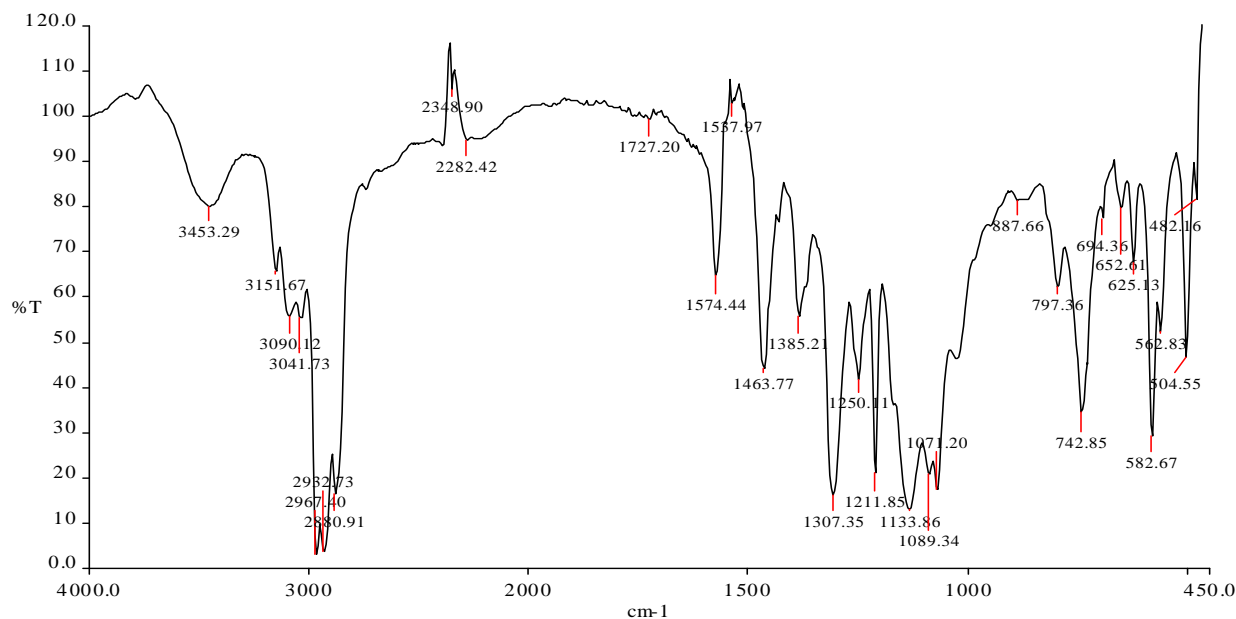


Figure 6.5 FT-IR spectrum of the [BMIM][(CF₃)₂PO₂] ionic liquid

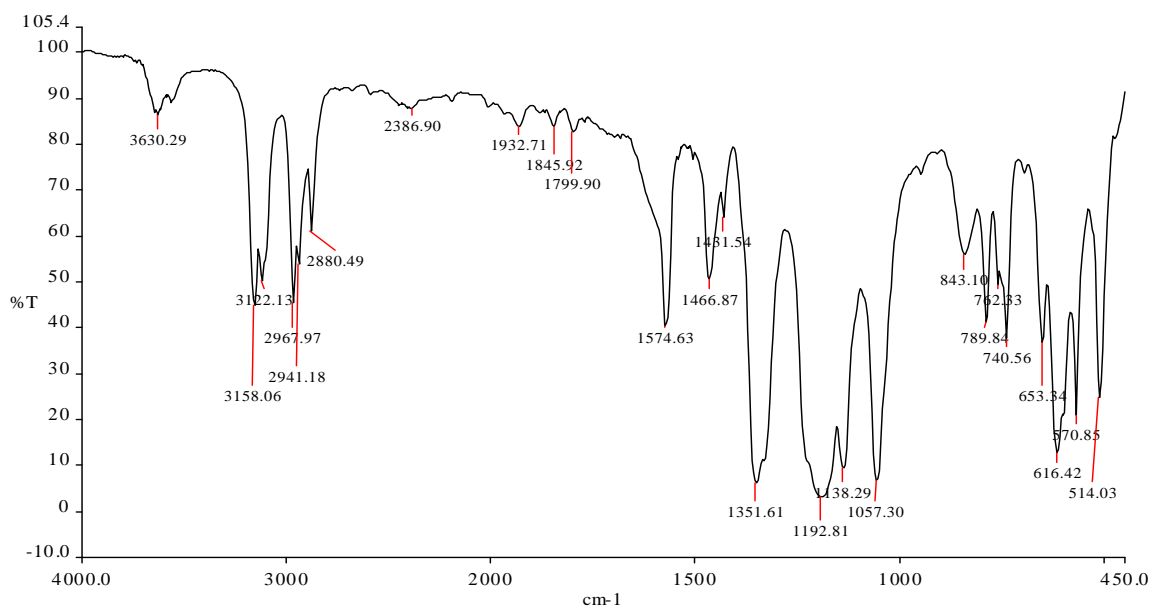


Figure 6.6 FT-IR spectrum of the [BMIM][TFSI]

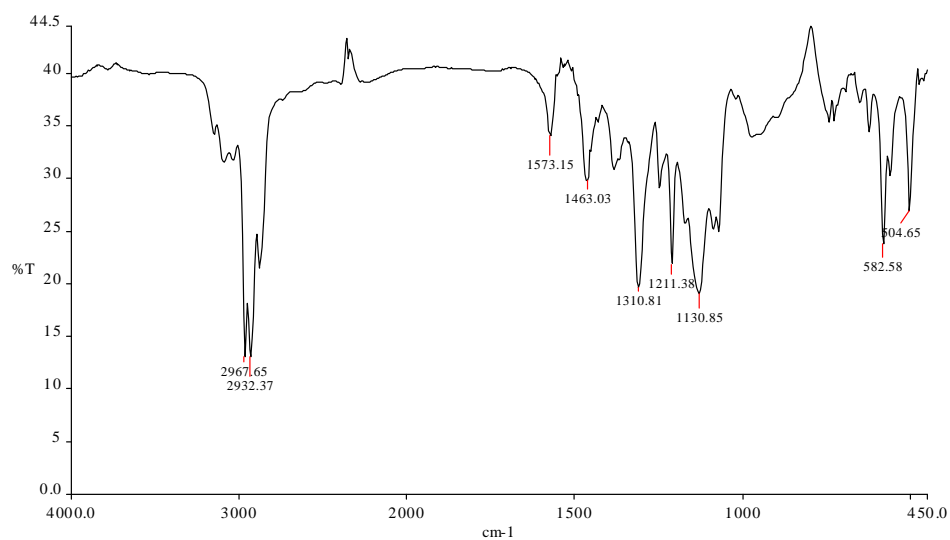


Figure 6.7 FT-IR spectrum of the [BMIM][(CF₃)₂PO₂] ionic liquid obtained under vacuum conditions. Note the absence of the –OH stretch that appears at 3200-3500 cm⁻¹ that appeared in Figure 6.5.

DSC data: The DSC curve of $[\text{BMIM}][(\text{CF}_3)_2\text{PO}_2]$ is shown in Figure 6.8.

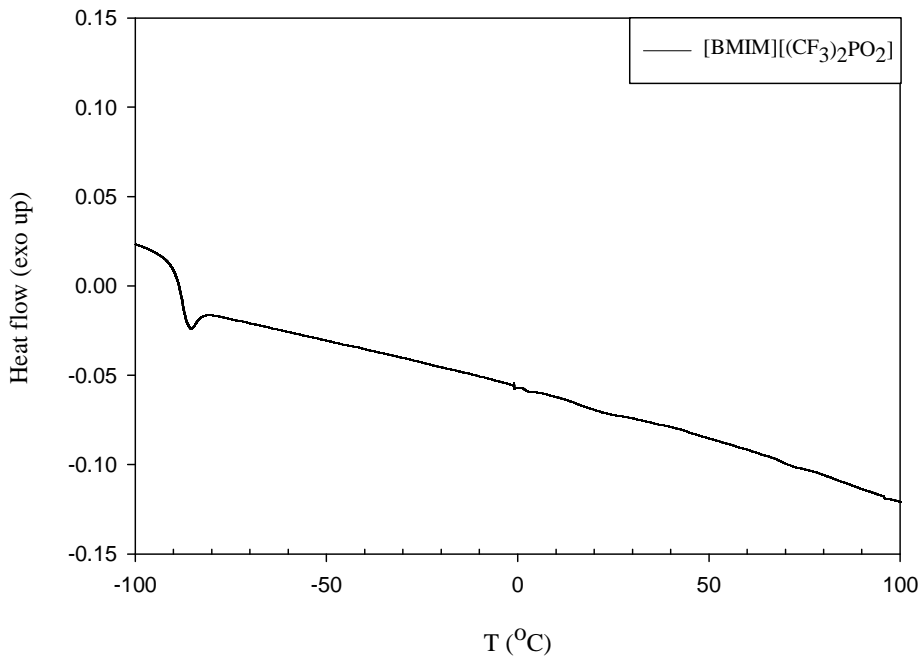


Figure 6.8 DSC spectrum of the $[\text{BMIM}][(\text{CF}_3)_2\text{PO}_2]$ ionic liquid

EDX data: Energy dispersive X-ray spectrum of $[\text{BMIM}][(\text{CF}_3)_2\text{PO}_2]$ is shown below in Figure 6.7. Indicates that there no peaks can be detected corresponding to elements other than what constituted the material.

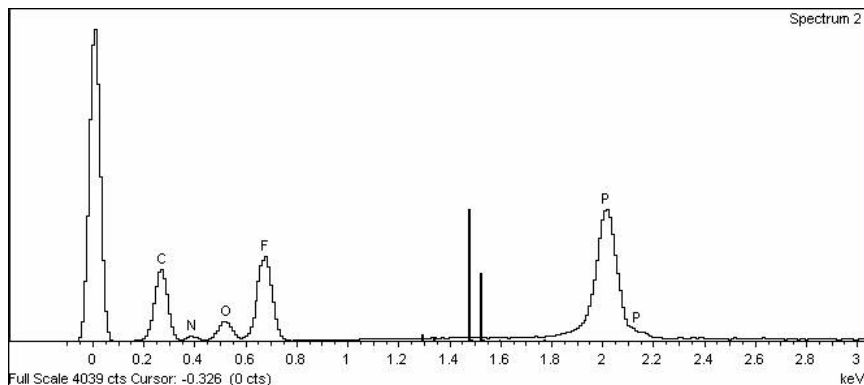


Figure 6.9 EDX spectrum of the the $[\text{BMIM}][(\text{CF}_3)_2\text{PO}_2]$ ionic liquid. The two K_α lines centered at 1.5 kv shows the where a peak for Br is expected

Table 6.4 The self-diffusion coefficients of cation (D^+ , cm^2s^{-1}) and anion (D^- , cm^2s^{-1}) of the ILs

Compound	At 25 °C		At 60 °C	
	$D^+/10^{-7}$	$D^-/10^{-7}$	$D^+/10^{-7}$	$D^-/10^{-7}$
[BMIM] $[(\text{CF}_3)_2\text{PO}_2]$	1.1	0.9	4.9	4.1
[BMIM] $[(\text{CF}_3)_2\text{SO}_2\text{N}]^*$	2.8	2.2	9.0	7.5

* the diffusion data were obtained from ref ⁶

Activation Energy Calculation:

The tangent line to the curve $y = f(x)$ at $x = x_1$ has a slope $f'(x_1)$ and passes through the point $[x_1, f(x_1)]$. The equation of the line with that slope passing through that point is

$$y = f(x_1) + (x - x_1) * f'(x_1)$$

This can be rearrange to give $y = f'(x_1) * x + C$ where $C = f(x_1) - x_1 * f'(x_1)$

Taking $f(x) = y = \log \sigma$ and $x = 1/T$ and substituting these values in eq 1 and taking the derivative of eq 1 with respect to $1/T$, we get

$$\frac{d(\log \sigma)}{d(1/T)} = \frac{-B_\sigma}{(1 - T_0 * x)^2}$$

Therefore the equation of the tangent at $x = x_1 = 1/T_1$

$$\log \sigma = C - \frac{B_\sigma}{(1 - T_0 * x_1)^2} \left(\frac{1}{T} \right)$$

The equation of this line is parallel to following Arrhenius equation

$$\log \sigma = - \frac{E_a}{R} \left(\frac{1}{T} \right)$$

Therefore the Arrhenius activation energy at a given temperature T can be calculated from VTF equation and it is equal to,

$$E_a^\sigma = \frac{R * B_\sigma T^2}{(T - T_0)^2}$$

Additional FT-IR spectra:

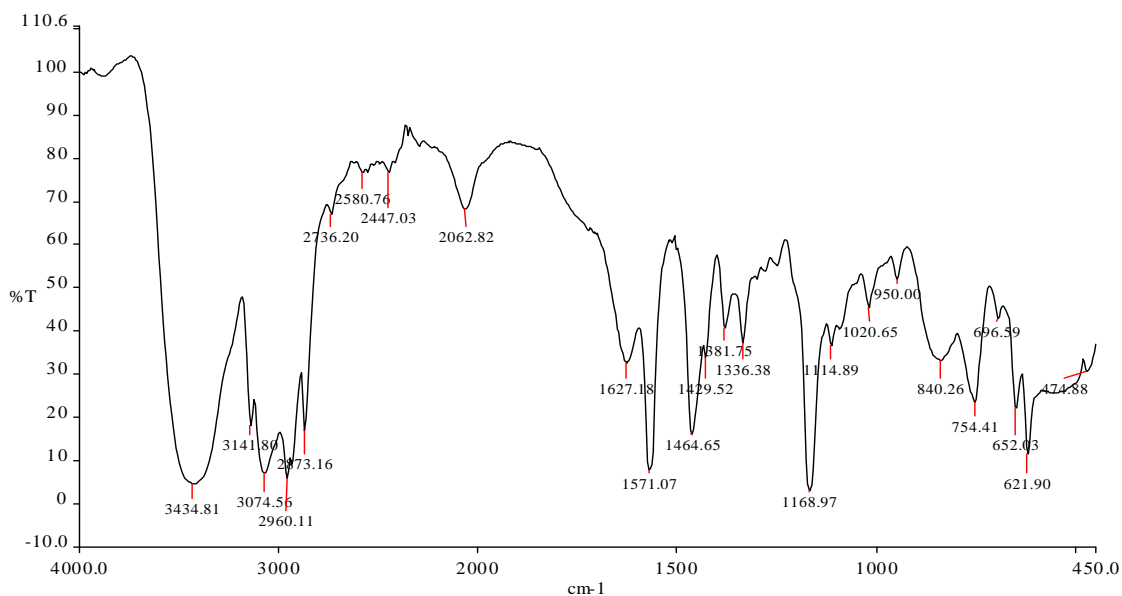


Figure 6.10 FT-IR spectra of [BMIM]Br

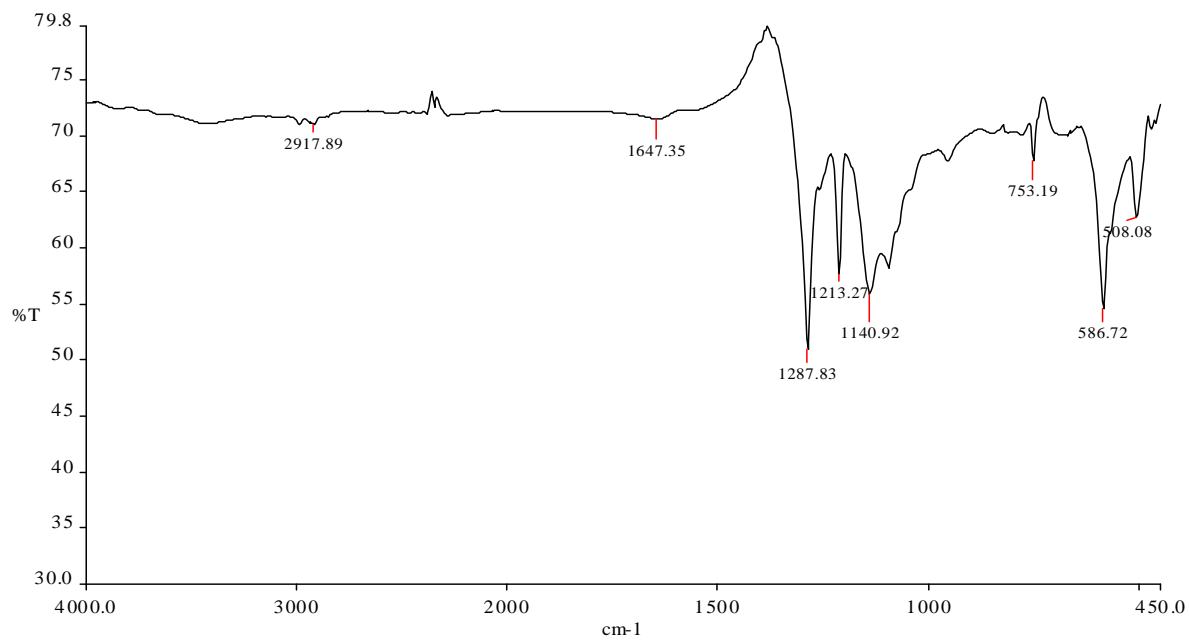


Figure 6.11 FT-IR spectra of $(CF_3)_2PO_2K$

CHAPTER SEVEN

CONCLUSIONS AND OUTLOOK

Introduction

Chapters 2 discussed the synthesis and characterization of short chain perfluorinated model compounds functionalized with phosphonic, phosphinic, sulfonic and carboxylic acid protogenic groups. The model compounds were characterized with respect to proton conductivity, viscosity, proton and anion (conjugate base) self-diffusion coefficients, and Hammett acidity. The results of the study collectively supported the hypothesis that anhydrous proton transport in the phosphonic and phosphinic acid model compounds occurs primarily by a structure diffusion/ proton hopping based mechanism rather than a vehicle mechanism. Further analysis of ionic conductivity and ion self-diffusion rates using the Nernst-Einstein equation reveals that the phosphonic and phosphinic acids are relatively highly dissociated even under anhydrous conditions. In contrast, sulfonic and carboxylic acid-based systems exhibit relatively low degrees of dissociation under anhydrous conditions.

Chapter 3 discussed the effects of increasing the perfluoroalkyl chain length on the molecular properties of viscosity, diffusivity and proton conductivity of phosphonic, phosphinic and sulfonic acid model compounds discussed in chapter 2. The results of the study concluded that proton conductivity of the phosphorous based acids is dependent on the fluorine to proton content. Perfluorinated phosphonic acids show much higher conductivity (by an order of magnitude) than perfluoroalkyl phosphinic acids when the perfluoroalkyl chain length is increased. The proton conductivity of sulfonic acid decreases with the increasing perfluoroalkyl chain length. The decrease in proton conductivity in sulfonic acids was proportional to the decrease in viscosity observed with the increasing perfluoroalkyl chain length. This observation

was in contrast with the relation observed phosphorous based acids on viscosity and conductivity.

Chapter 3 discussed the effect of addition of water to pefluorinated phosphonic, phosphinic, and sulfonic acids. An order of magnitude increase in proton conductivity was observed with phosphonic and phosphinic based acids. The proton conduction mechanism at low hydration in phosphonic acids appears to be predominantly based on the structure diffusion/proton hopping mechanism. In contrast, the conductivity increase with addition of low content of water in sulfonic acids appear to be based on vehicle mechanism as it indicated by the high mobilites of the charge carriers.

Most of the polymeric materials discussed in the chapter 1 as proton exchange membrane materials are random copolymers constituting a hydrophobic fraction and a hydrophilic fraction. Hydrophilic fraction contains the protogenic groups such as phosphonic or sulfonic acid groups that provide conductivity. Hydrophobic fraction offers the mechanical strength. Mixing of hydrophilic and hydrophobic content in a copolymer leads to isolated morphological domains. Depending on the preparation methods a copolymer containing hydrophobic and hydrophilic fractions can exhibit different morphologies and therefore can influence the resulting proton conductivities. High proton conductivity can be achieved only if a highly percolated morphology of hydrophilic domains is ensured within the copolymer system. Poor conductivities of fluorinated phosphonic and phosphinic acid based membranes discussed in chapter 1 were speculated most probably due to a poorly percolated morphology. While there are many papers available that discuss how to synthesize phosphonated membranes for PEMFCs, scientific papers that discuss the transport properties of a phosphonated membrane in terms of its distinct differences in microstructure are still lacking in literature.

The model compound study does not take into consideration how the immobilization of the phosphonic and phosphinic protogenic groups will affect the transport properties of comb-branch ionomers. Immobilization limits the translational motion of the protogenic groups. However, since the proton transport of the phosphorous based acids are predominantly rely on structure diffusion mechanism, where protons are transferred via the formation and breaking of hydrogen bonds between the acid groups, the phosphonated polymers must show high transport properties as model compounds. However, it should also be noted that depending on the flexibility of the spacers that are used to covalently link the protogenic group to the polymer backbone the mobility of the protogenic group and the protonic charge carriers therein can be lost. Therefore it is important to guarantee the same flexibility for the spacers as in model acids to avoid any loss in conductivity that can incur after immobilization in a polymer.

The polymer membranes must also possess good thermo-mechanical properties for use in high temperature operation fuel cells. For example the Nafion membrane is mechanically unstable at temperatures above 100 °C due to its low glass-transition (T_g) temperature (T_g for Nafion[®]-112 is 110 °C). We showed in chapters 2 and 3 that how the length of the spacer group affect the proton conductivity. It may be also be possible that depending on the length of the spacer connected to the phosphorous-based acid group the T_g value of the polymer to increase or decrease. While it is possible to predict the conductivity depending on the spacer length, it is not possible to predict the T_g values of polymers or how the T_g values are going to be affected based on the model acids investigated in this study. For example with a shorter spacer group the polymer may exhibit a lower T_g and high conductivity and with a longer spacer group the polymer may exhibit a higher T_g and poor conductivity. A membrane with a higher T_g (above 120 °C) is thought to have good thermo-mechanical properties for PEMFCs that operates at or

below 120 °C. A higher T_g shows that the polymer is more elastic and therefore can withstand higher temperatures.

It was discussed in chapter 1 that the ionic conductivity of the polymer membranes depends on its ion exchange capacity (IEC) values. The higher the IEC value of a polymer the higher the expected conductivity. Based on the densities it can be shown that for the phosphorous-based model acids investigated here have IEC values of close to 10 meq/g. In chapter 1, we saw that for all the phosphonic and phosphinic acid based polymers, their IEC values did not exceed much above 3 meq/g. This suggests that there must be some technical difficulties in achieving very high concentrations of phosphorous-based acid groups during the immobilization process. Most probably increasing the IEC values close to 10 can result in membranes with compromised mechanical properties. Membranes with poor mechanical properties can either swell too much or can leach out easily from the PEM.

The chapter 5 describes the synthesis, characterization and ion transport of lithium polymer electrolytes that can provide rechargeable lithium batteries with high power/ high rate capabilities by overcoming concentration polarization. Investigation of the purity of the ionic-melt by HPLC analysis and electrospray ionization mass spectrometry indicated that the ionic-melt is free of non-ionic impurities. The highest ionic conductivity of 7.1×10^{-6} S/cm at 30 °C was obtained for the sample consisting of a lithium salt of an arylfluorosulfonimide anion attached to a polyether oligomer with an ethyleneoxide (EO) to lithium ratio of 12. The conductivity order of various ionic melts having different polyether chain lengths suggests that at higher EO:Li ratios the conductivity of the electrolytes at room temperature is determined in part by the amount of crystallization of the polyether portion of the ionic melt.

The chapter 6 describes the synthesis and characterization of a new room-temperature ionic liquid based on a alkyimidazolium cation and new fluoro anion $[(CF_3)_2PO_2^-]$. Investigation of its thermal stability, viscosity, voltage window, and conductivity suggests that it may be a useful as an electrolyte in batteries.

Appendix A

Conductivity Cell

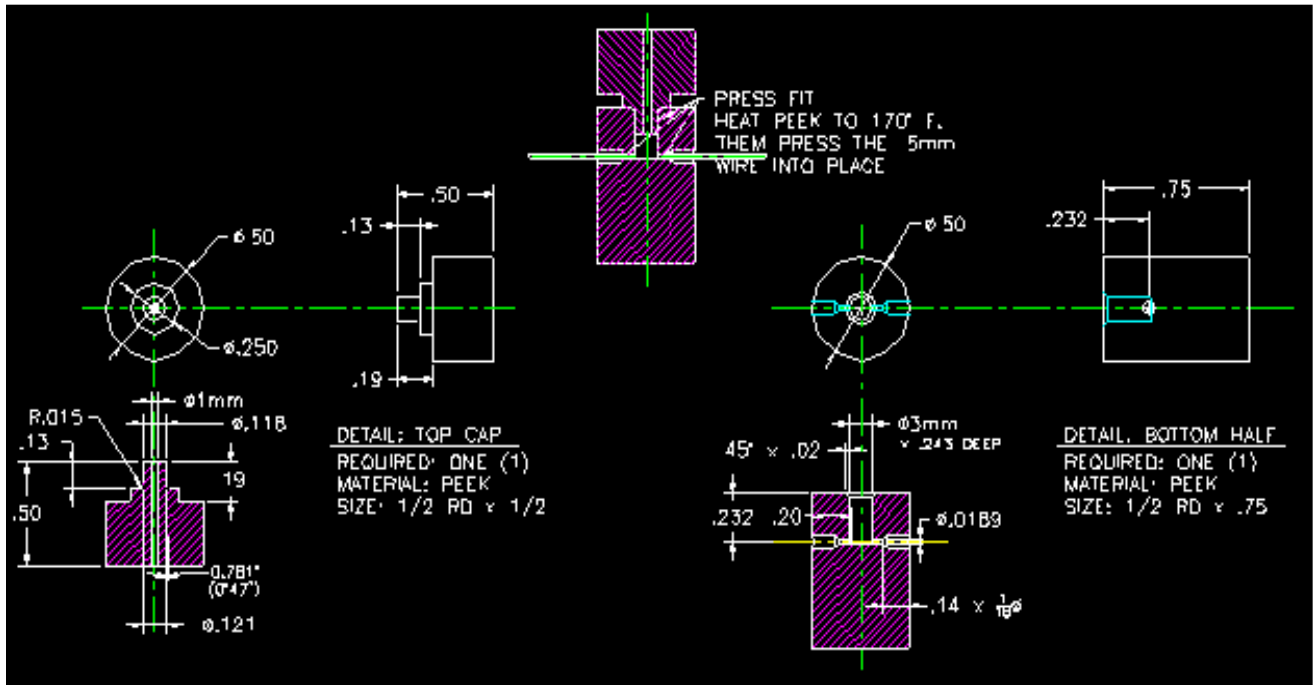
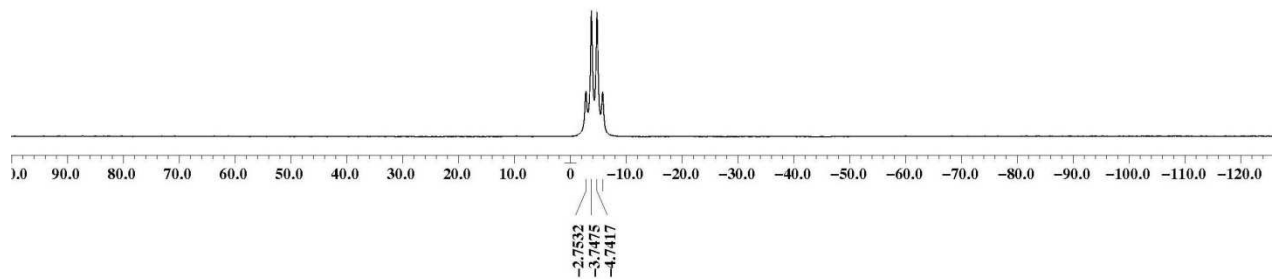


Figure A-1: PEEK conductivity cell

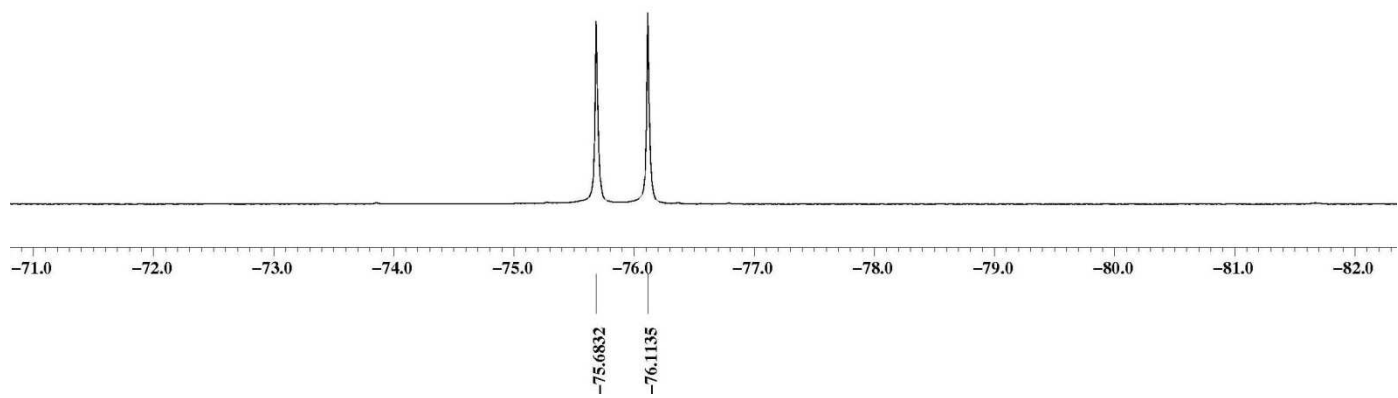
Appendix B

NMR spectra for the phosphonic acids

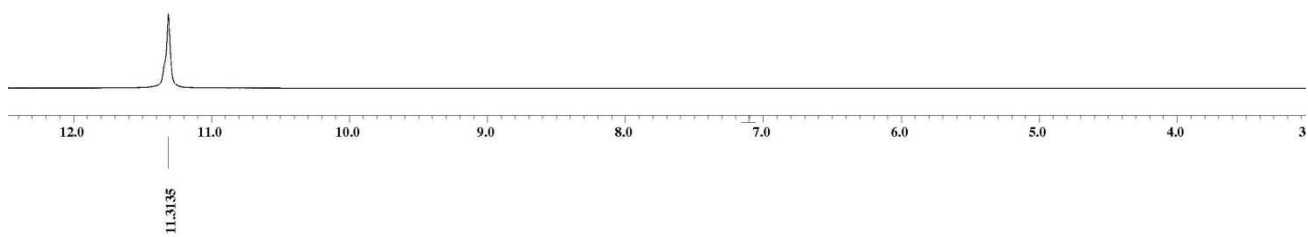
^{31}P NMR spectra of $\text{CF}_3\text{PO}_3\text{H}_2$



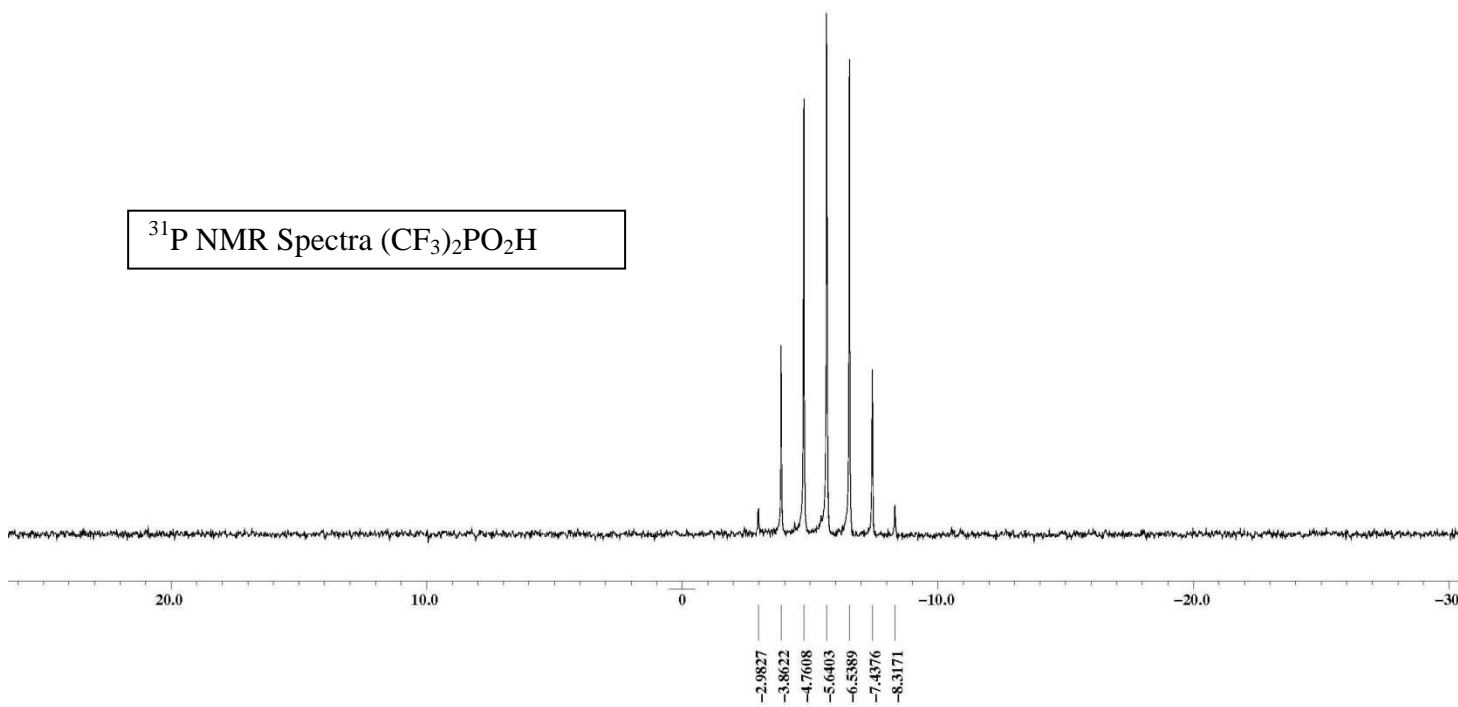
^{19}F NMR spectrum of $\text{CF}_3\text{PO}_3\text{H}_2$



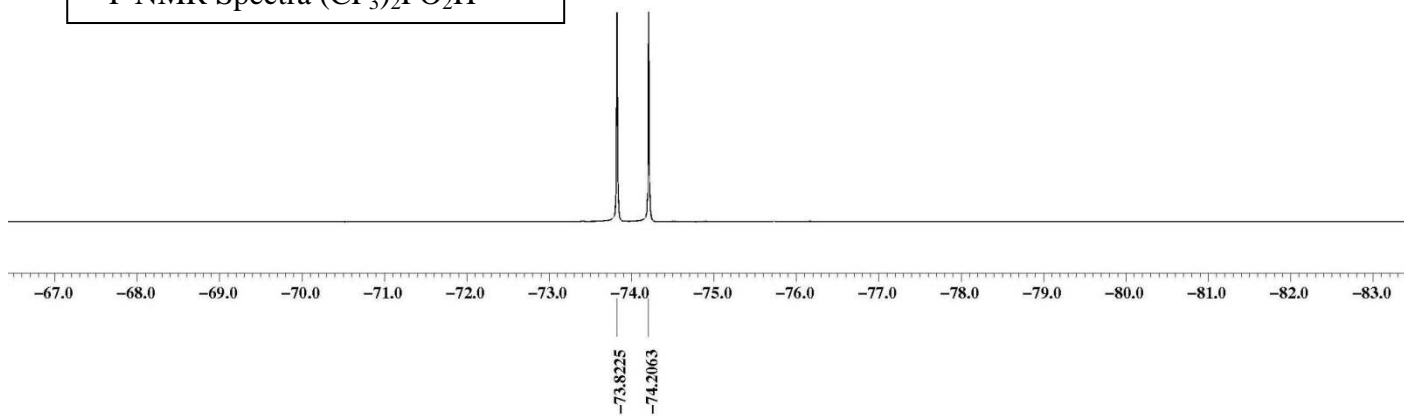
^1H NMR spectrum of $\text{CF}_3\text{PO}_3\text{H}_2$



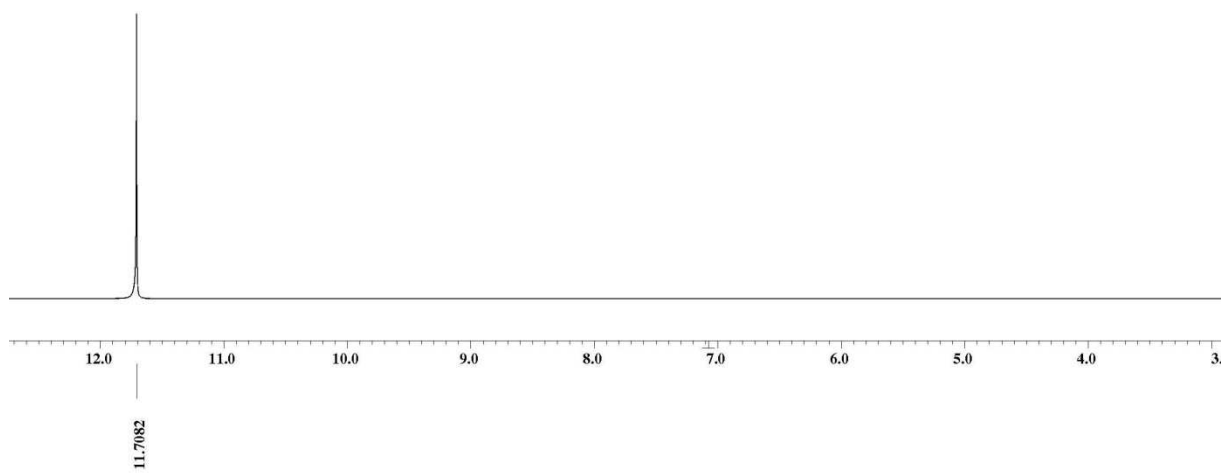
^{31}P NMR Spectra (CF_3) $_2\text{PO}_2\text{H}$



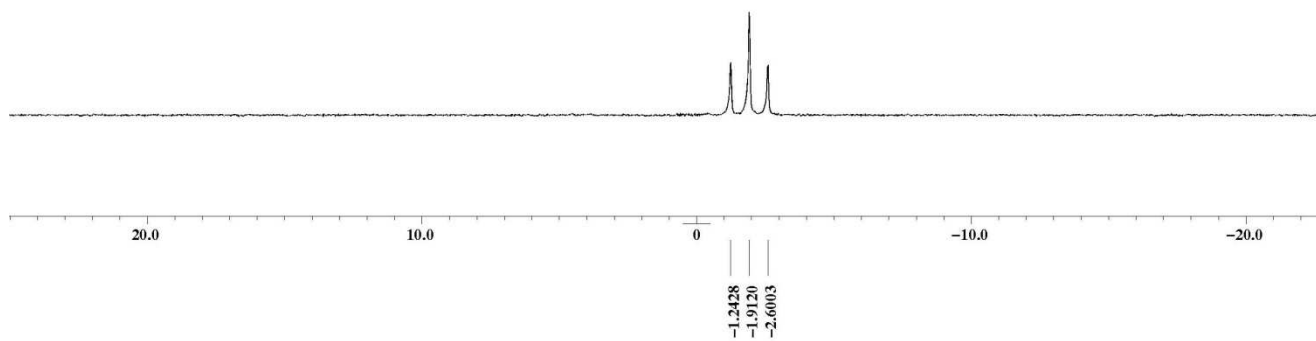
^{19}F NMR Spectra $(\text{CF}_3)_2\text{PO}_2\text{H}$



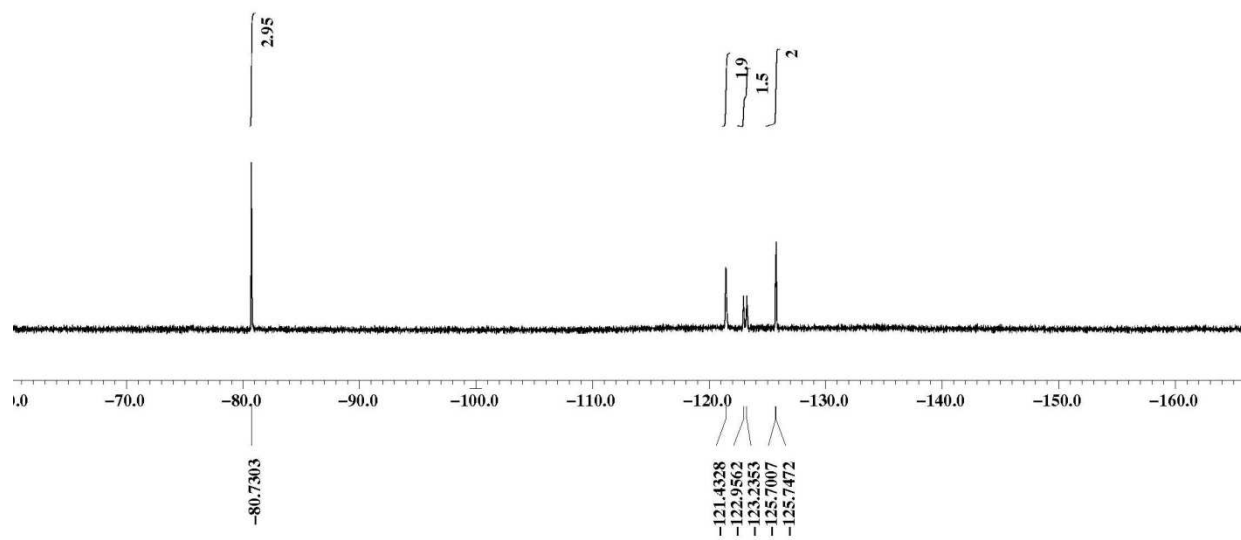
^1H NMR Spectra $(\text{CF}_3)_2\text{PO}_2\text{H}$



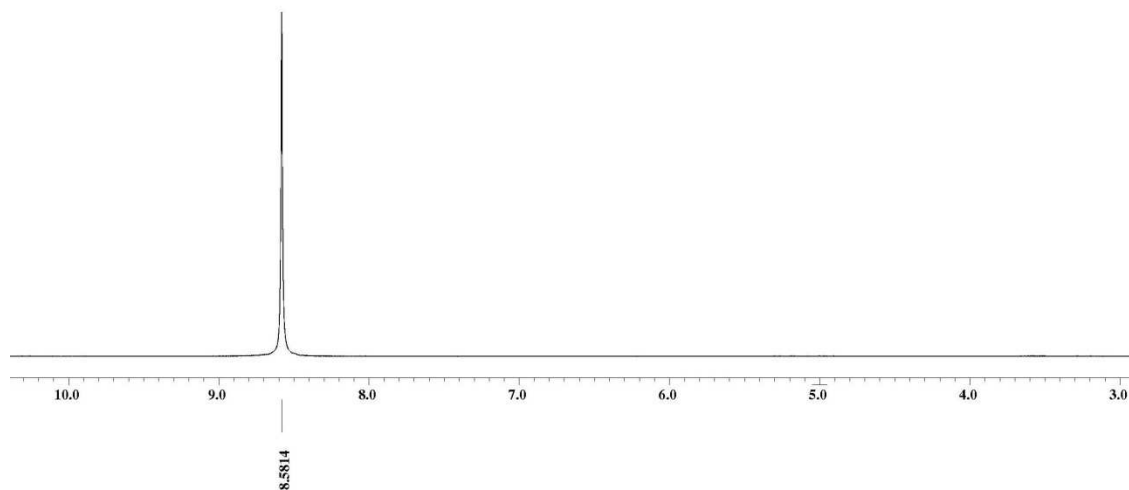
^{31}P NMR Spectra $\text{C}_4\text{F}_9\text{PO}_3\text{H}_2$



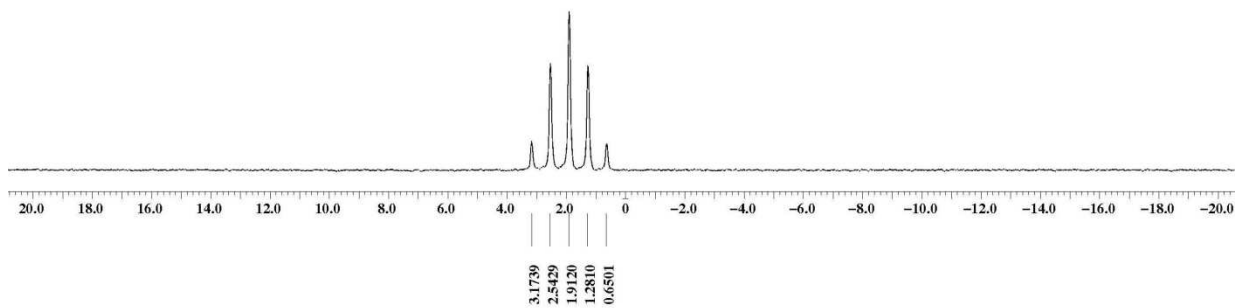
^{19}F NMR Spectra $\text{C}_4\text{F}_9\text{PO}_3\text{H}_2$



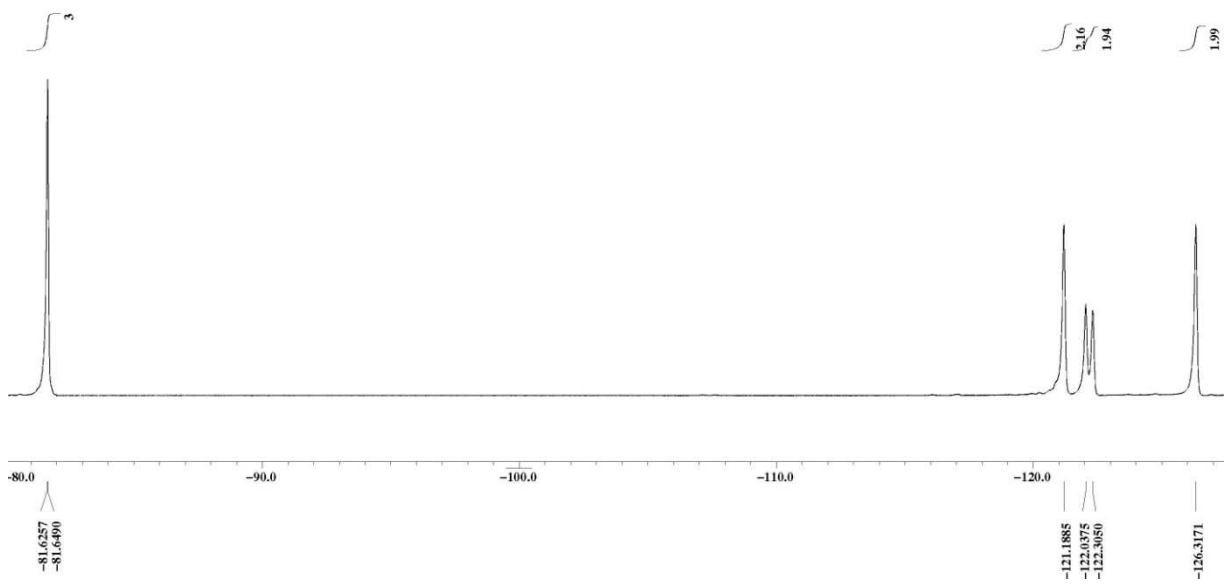
^1H NMR Spectra $\text{C}_4\text{F}_9\text{PO}_3\text{H}_2$



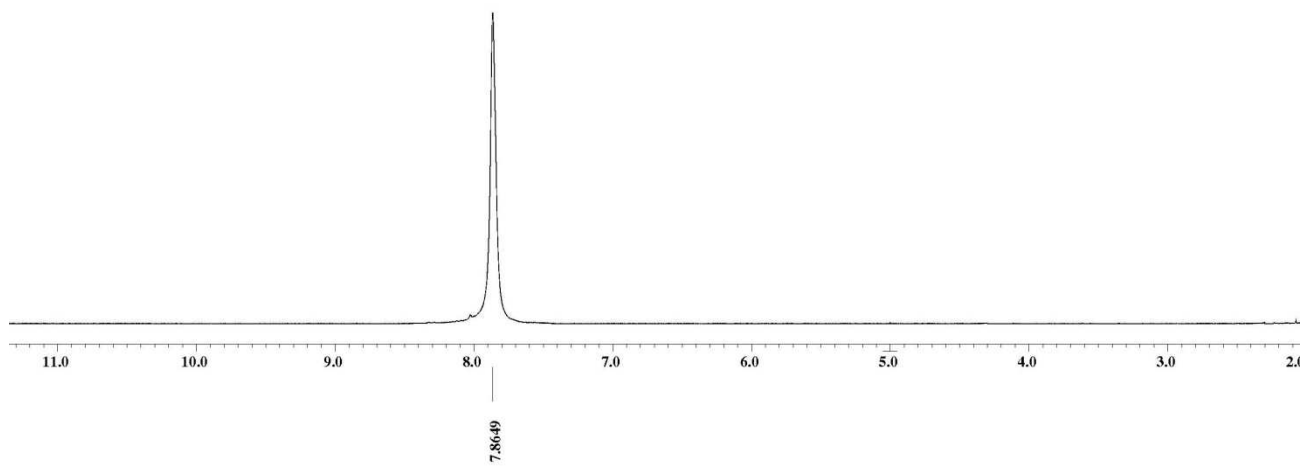
^{31}P NMR Spectra $(\text{C}_4\text{F}_9)_2\text{PO}_2\text{H}$



^{31}F NMR Spectra $(\text{C}_4\text{F}_9)_2\text{PO}_2\text{H}$



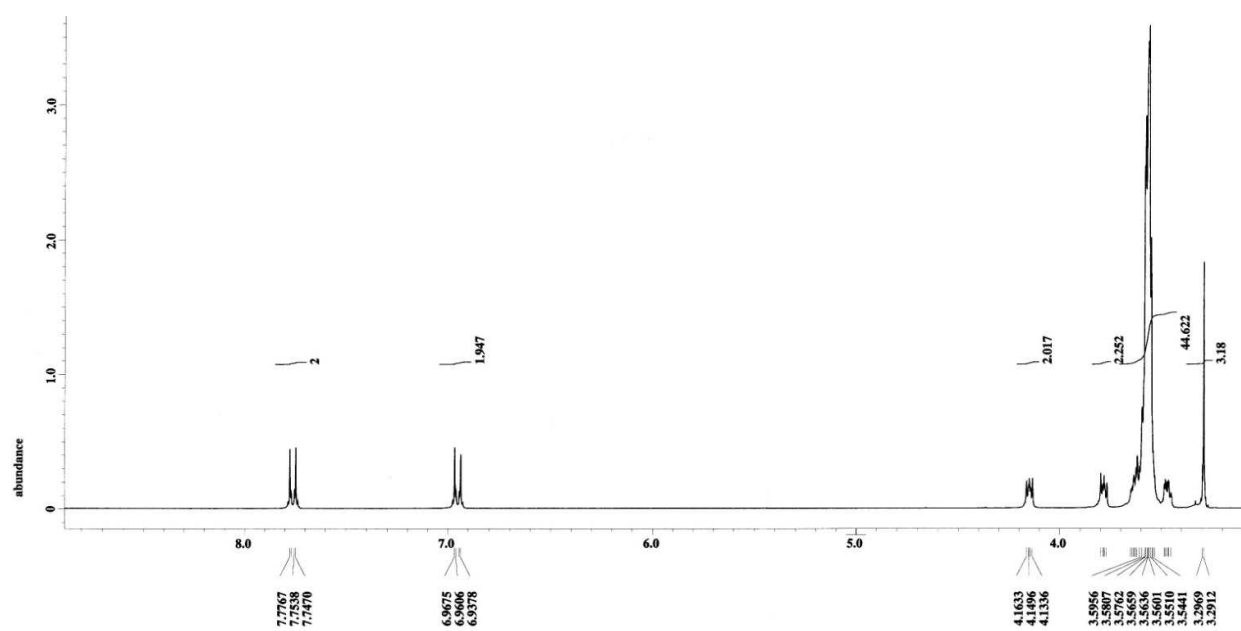
^1H NMR Spectra $(\text{C}_4\text{F}_9)_2\text{PO}_2\text{H}$



Appendix C

Ionic melt

$^1\text{H NMR}$: $\text{CH}_3\text{O}-(\text{CH}_2\text{CH}_2\text{O})_{11.8}-\text{Ph}-\text{SO}_2\text{N}(\text{Li})\text{SO}_2\text{CF}_3$



$^1\text{H NMR}$: $\text{CH}_3\text{O}-(\text{CH}_2\text{CH}_2\text{O})_{11.8}-\text{Ph}-\text{SO}_2\text{N}(\text{Li})\text{SO}_2\text{CF}_3$

